Simulative Investigation on Pre-turbine Exhaust Gas Aftertreatment Systems of Diesel Engines with Dynamic Compensation

Von der Fakultät Konstruktions-, Produktions- und Fahrzeugtechnik der Universität Stuttgart zur Erlangung der Würde eines Doktor-Ingenieurs (Dr.-Ing.) genehmigte Abhandlung

Vorgelegt von

Martin Angerbauer
aus Stuttgart

Hauptberichter:	Prof. Dr.-Ing. M. Bargende
Mitberichter:	Prof. Dr.-Ing. P. Eilts
Tag der mündlichen Prüfung:	27.07.2021

Institut für Fahrzeugtechnik Stuttgart
der Universität Stuttgart

2021

Preface

This work was realized during my tenure as a research associate at the Institute of Internal Combustion Engines and Automotive Engineering (IVK)/Institute of Automotive Engineering (IFS) the at the University of Stuttgart under the supervision of Prof. Dr.-Ing. M. Bargende.

My deep gratitude goes to Prof. Dr.-Ing. M. Bargende for his support and guidance. I want to thank Prof. Dr.-Ing. P. Eilts for his interest in this work and for joining the doctoral committee.

I am extremely grateful to all my colleagues from the Institute of Automotive Engineering for their collaboration, inspiration and discussion. My special thank goes to my supervisor Dr.-Ing. Michael Grill for his professional support and guidance.

I would also like to express my gratitude to the working group led by Dr. Frank Bunar and all the companies that supported the research tasks within the project "Abgasnachbehandlung vor Abgasturbine" defined and financed by the Research Association for Combustion Engines (FVV) e.V. My very sincere thanks also goes to my project partner Ferhat Inci from Chair of Powertrain Technologies (FZA) of TU Berlin for providing the experimental work.

Furthermore, I want to thank my family, friends and everybody who supported me during the last three years.

Stuttgart, July 27, 2021 Martin Angerbauer

Contents

Figures

Tables

Abbreviations

ANN	Artificial neural network
BMEP	Brake mean effective pressure
CFD	Computational fluid dynamics
CRFD	Computational reactive fluid dynamics
DEF	Diesel emission fluid
DF	Diesel fuel
DOC	Diesel oxidation catalyst
DOE	Design of Experiment
DPF	Diesel particulate filter
EAT	Exhaust gas aftertreatment
EATC	Electrically assisted turbocharger
ECU	Electronic control unit
EDB	Electrically driven booster
EGR	Exhaust gas recirculation
HC	Hydrocarbons
ICE	Internal combustion engine
IMEP	Indicated mean effective pressure
ISG	Integrated starter generator
MFB	Mass fraction burned
NEDC	New European driving cycle
PAH	Polycyclic aromatic hydrocarbons
PHEV	Plug-in hybrid electric vehicle

PM	Particulate matter
PMEP	Pumping mean effective pressure
PTS	Pre-turbine system
QDM	Quasi-dimensional model
QS	Quasi-steady
RDE	Real driving emission
SCR	Selective catalytic reaction
TDC	Top dead centre
THC	Total hydrocarbons
TPO	Temperature programmed oxidation
VGT	Variable geomatry turbine
WLTC	Worldwide harmonized light vehicles test cycles

Symbols

	Latin Letters	
c_p	Specific heat capacity	J/(kg K)
k	Equilibrium constant	-
m	Mass	kg
$\dot{m}$	Mass flow rate	kg/s
P	Power	W
p	Pressure	bar
T	Temperature	K
t	Time	s
V	Volume	m^3

	Greek Letters	
η	Efficiency	%
κ	Heat capacity ratio	-
λ	Air–fuel equivalence ratio	-
π	Pressure ratio	-
ρ	Density	kg/m^3

	Indices
1	Thermodynamic state upstream of the compressor
2	Thermodynamic state downstream of the compressor
3	Thermodynamic state upstream of the turbine
4	Thermodynamic state downstream of the turbine
C	Compressor
T	Turbine
TC	Turbocharger

Abstract

Most pollutants formed during diesel combustion are transformed into harmless substances by catalysts in the exhaust tract. Together with the diesel particulate filter (DPF), they form the exhaust gas aftertreatment (EAT) system. The catalytic surface needs to be within a certain temperature range to lower the required activation energy for the corresponding reactions. The catalysts are heated-up by the exhaust gas to reach a temperature level, at which, the pollutant conversion works reliably. The challenge is to ensure that the exhaust gas aftertreatment system warms-up quickly, even under demanding conditions. In nowadays common turbocharged diesel engines, the turbine inhibits the heating of the exhaust gas aftertreatment components. On the one hand, their thermal mass acts as a heat sink during warm-up. On the other hand, the exhaust gas temperature drops due to the expansion over the turbine. One possibility to overcome this is the positioning of the exhaust gas aftertreatment upstream of the turbine. In this way, the warm-up of the aftertreatment system is improved without using possible fuel-intensive heating measures.

Since this impairs the dynamic response of the turbocharger, the dynamics of the engine is limited. Thus, pre-turbine exhaust gas aftertreatment has so far mostly been investigated for use in stationary large engines or commercial vehicles. Engines for passenger cars are usually expected to have a strong dynamic response. Only the increasing proportion of hybrid vehicles makes the application of pre-turbine exhaust gas aftertreatment systems for passenger vehicles interesting. The electric assistance is necessary for counteracting the disadvantage of the increased turbo lag caused by the PTS.

In this work, different configurations with a pre-turbine exhaust gas aftertreatment are examined. The series catalysts of the reference system are placed in their new position in front of the turbine without further adaptions. The examined systems differ in the type and number of components that are placed in front of the turbine and their sequence is varied. The investigations are carried out using 0d/1d simulation on a representative four-cylinder diesel engine. The reference exhaust gas aftertreatment system consists of a diesel oxidation

catalyst (DOC), a catalytic diesel particulate filter (cDPF) and selective catalytic reaction (SCR) system. The simulation model for this configuration is calibrated and validated using test bench data. The 0d/1d simulation offers the possibility to compare several configurations under exactly the same conditions within a short time. Furthermore, components can be examined without the need for them to be in physical form, which facilitates the analysis of a variety of measures to increase dynamic performance.

A neural network with several input parameters is used for emission prediction. This multidependent neural network predicts the emissions well under transient conditions because the boost pressure is one of the input variables. Since pre-turbine components influence the boost pressure development, such a model is necessary for the overall evaluation of the configurations. In addition to the reduction of emissions through the catalytic converters, this also includes the change in emission formation.

Test scenarios are defined to compare the pre-turbine systems (PTS) with the reference configuration. In the first one, the engine with EAT system is analysed in isolation at stationary, steady-state operating points. The focus is set on the influence of the pre-turbine components of the turbine, which attenuate the pressure pulsations from the exhaust manifold. In addition, the pressure loss of the entire exhaust tract is influenced, which causes fuel consumption advantage for the PTS of up to 1.6 %.

During a load step at a constant speed, the torque build-up is slowed down in correlation with the thermal mass in front of the turbine. In the extreme case, the delay is greater than 109 s compared to the reference system. This is not acceptable for use in passenger vehicles that have a dynamic load requirement. Appropriate measures can accelerate the boost pressure build-up and reduce the delay. Especially the electric driven booster and the electrically assisted turbocharger (EATC) show satisfactory results and neutralise the turbo lag. A lightly hybridised vehicle can provide the required power and energy amount. Hydraulic-pneumatic support measures are sufficient to improve the dynamics for a short time, but they are not suitable for a permanent increase in torque.

The dynamic disadvantage of the PTS is offset by advantages in warm-up behaviour. These are demonstrated in cold start simulations in which the initially cold engine is kept at a constant operating point. Thus, the conditions

are the same for all systems. Depending on the configuration and emission type, the time to reach light-off is reduced by 75 % compared to the reference system. Additionally, advantages are found regarding active DPF regeneration with a pre-turbo DPF. The filtered soot mass is reduced more quickly than with a normally arranged DPF and less fuel is required to lift the exhaust gas temperature by means of post-injection.

In addition to the test scenarios mentioned so far, in which the engine is considered in isolation, the behaviour of the systems during real driving is simulated using a longitudinal dynamic model. The target load is set according to the power required to follow a speed profile. The conditions in the engine depend on the complex interaction between turbocharger, combustion chamber and EAT components. During transient operation with a PTS, especially the boost pressure build-up is a decisive factor. During the WLTC, increased passive DPF regeneration is observed in the pre-turbo DPF. However, without dynamic measures, the CO raw emissions are significantly higher than those of the reference system. Thus, despite a higher conversion rate, the tailpipe CO is increased.

In a cold-started low-temperature real driving emission (RDE) cycle, the potential of the PTS is demonstrated regarding the heating-up of the EAT. During the urban section, power requirements and exhaust gas temperatures are low, and long towing periods arise. Thus, no significant pollutant reduction takes place with any of the configurations, but higher catalyst temperatures are observed with the PTS. Finally, one PTS with the transient support measures of an EATC and a P2-hybrid is compared with the reference system in a high-dynamic RDE drive. The required power and energy demand for compensating the dynamic disadvantage is estimated. Furthermore, results show that the type of dynamic support influences the formation of raw emissions and the heating behaviour of the catalysts. Thus, the operating strategy of the support components plays an essential role for emission reduction.

Kurzfassung

Die meisten Schadstoffe, die bei der Dieselverbrennung entstehen, werden in den Katalysatoren der Abgasnachbehandlung in unschädliche Stoffe umgewandelt. Das Abgasnachbehandlungssystem wird durch den Dieselpartikelfilter (DPF) zur Partikelreduktion ergänzt. Um die erforderliche Aktivierungsenergie für die entsprechenden Reaktionen zu senken, muss die katalytische Oberfläche einen bestimmten Temperaturbereich erreichen. Hierfür reicht üblicherweise die Abgasenergie des Verbrennungsmotors aus. Die Herausforderung besteht darin, ein schnelles Aufheizen des Abgasnachbehandlungssystems auch unter anspruchsvollen Bedingungen zu gewährleisten. Bei den heute üblichen turboaufgeladenen Dieselmotoren wirkt die Turbine als Wärmsenke und erschwert die Aufheizung der Abgasnachbehandlungskomponenten. Durch die Gasexpansion über die Turbine verringert sich die Gastemperatur zusätzlich. Mit der Positionierung der Komponenten vor der Turbine, werden diese in ihrem Aufheizverhalten nicht durch den Temperaturabfall über der Turbine beeinträchtigt. Auf diese Weise wird ohne kraftstoffintensive Heizmaßnahmen die Aufwärmung des Abgasnachbehandlungssystems verbessert.

Bevor das heiße Abgas mit einer vorturbo Abgasnachbehandlung die Turbine erreicht, werden die Abgasnachbehandlungskomponenten aufgewärmt, die ihrerseits nun als Wärmesenken wirken. Dies schränkt den Aufbau des Ladedruckes ein und verringert das dynamische Ansprechverhalten des Motors. Daher wurde die Abgasnachbehandlung vor der Turbine bisher meist für den Einsatz in stationären Großmotoren oder Nutzfahrzeugen untersucht. Von PKW-Motoren wird erwartet, dass sie schnelle Laständerungen beispielsweise während eines Beschleunigungsvorganges erfüllen. Um dies sicherzustellen, sind Maßnahmen zur Steigerung der Dynamik erforderlich. Vor allem die zunehmende Hybridisierung von Fahrzeugen bietet hierfür gute Möglichkeiten das Turboloch zu minimieren oder das Drehmoment direkt mittels eines Elektromotors zu steigern.

In dieser Arbeit werden verschiedene Konfigurationen einer Abgasnachbehandlung vor der Turbine betrachtet. Die untersuchten Systeme unterscheiden sich

in der Art, Anzahl und Reihenfolge der Komponenten, die vor der Turbine platziert werden. Ohne weitere Anpassungen werden die Serienkatalysatoren des Referenzsystems in ihrer neuen Position vor der Turbine platziert. Das Referenz-Abgasnachbehandlungssystem besteht aus einem Dieseloxidationskatalysator (DOC), einem katalytischen Dieselpartikelfilter (cDPF) und einem selektiven katalytischen Reaktionssystem (SCR). Die Untersuchungen werden mittels 0d/1d-Simulation an einem repräsentativen Vierzylinder-Dieselmotor durchgeführt. Hierfür wird das Simulationsmodell anhand von Prüfstandsdaten für das Referenzsystem kalibriert und validiert. Die 0d/1d-Simulation bietet die Möglichkeit, in kurzer Zeit mehrere Konfigurationen unter exakt den gleichen Bedingungen zu vergleichen. Darüber hinaus können Komponenten untersucht werden, ohne dass sie in physischer Form vorliegen müssen, was die Analyse einer Vielzahl von Maßnahmen zur Steigerung des dynamischen Ansprechverhaltens erleichtert.

Für die Emissionsvorhersage wird ein neuronales Netz mit sieben Eingangsparametern auf Basis von Messergebnissen trainiert. Durch die hohe Anzahl an Eingangsparametern des empirischen Modellansatzes, werden auch transiente Einflüsse auf die Emissionsentstehung berücksichtigt, wie etwa ein verzögerter Ladedruckaufbau. Dies ist erforderlich, da die zusätzlichen Komponenten vor der Turbine den Ladedruck und die interne Abgasrückführungs-Rate beeinflussen. Für die Gesamtbewertung der Konfigurationen ist neben der Reduktion der Emissionen durch die Katalysatoren auch die Veränderung der Emissionsbildung ein Faktor. Es werden Testszenarien definiert, um die Vorturbosysteme (*preturbo System*, PTS) mit der Referenzkonfiguration zu vergleichen. Im ersten Szenario wird der Motor mit den Variationen des Abgasnachbehandlungssystems isoliert in stationären Betriebspunkten analysiert. Der Fokus liegt dabei auf der Interaktion zwischen den Vorturbo- Komponenten und der Turbine. Die Druckpulsationen aus dem Abgaskrümmer wird abgeschwächt und der Druckverlust des gesamten Abgastraktes beeinflusst, was einen Kraftstoffverbrauchsvorteil für ein PTS von bis zu 1,6 % bewirkt.

Während eines Lastaufschlages bei konstanter Drehzahl wird der Drehmomentaufbau in Korrelation mit der thermischen Masse vor der Turbine verzögert, da von der Turbine nicht genug Leistung für den benötigten Ladedruckaufbau abgegriffen werden kann. Mit der extremen Konfiguration, die die meisten Komponenten vor der Turbine hat, dauert es etwa 109 s länger das Zieldreh-

moment zu erreichen gegenüber dem Referenzsystem. Dies ist für den Einsatz in Personenfahrzeugen mit dynamischer Lastanforderung nicht akzeptabel. Geeignete Maßnahmen, um den Ladedruckaufbau zu beschleunigen und die Verzögerung zu reduzieren werden untersucht. Insbesondere der elektrisch angetriebene Booster und der elektrisch unterstützte Turbolader (*electrically assisted turbocharger*, EATC) zeigen zufriedenstellende Ergebnisse und neutralisieren das Turboloch. Ein leicht hybridisiertes Fahrzeug kann die erforderliche Leistung und Energiemenge bereitstellen. Hydraulisch-pneumatische Unterstützungsmaßnahmen reichen aus, um die Dynamik kurzzeitig zu verbessern, sind aber nicht für eine dauerhafte Erhöhung des Drehmoments geeignet.

Der dynamische Nachteil der PTS wird durch Vorteile im Warmlaufverhalten ausgeglichen. Diese werden in Kaltstart-Simulationen demonstriert, bei denen der anfangs kalte Motor in einem konstanten Betriebspunkt operiert. Somit sind die Bedingungen für alle Systeme gleich. Je nach Konfiguration und Emissionstyp reduziert sich die Zeit zum Erreichen des Light-off im Vergleich zum Referenzsystem um bis zu 75 %. Zusätzlich ergeben sich Vorteile bei der aktiven DPF-Regeneration mit einem Pre-Turbo-DPF. Die gefilterte Rußmasse wird schneller oxidiert als bei einem normal angeordneten DPF und es wird weniger Kraftstoff zur Anhebung der Abgastemperatur mit Nacheinspritzungen benötigt.

Zusätzlich zu den bisher genannten Testszenarien, bei denen der Motor isoliert betrachtet wird, wird das Verhalten der Systeme im realen Fahrbetrieb mit einem Längsdynamikmodell simuliert. Die Ziellast wird entsprechend der Leistung eingestellt, die erforderlich ist, um einem Geschwindigkeitsprofil zu folgen. Die Bedingungen im Motor hängen von der komplexen Interaktion zwischen Turbolader, Zylinder und Abgasnachbehandlungs-Komponenten ab. Im transienten Betrieb mit einem PTS ist vor allem der Ladedruckaufbau ein entscheidender Faktor, der auch zu einer Erhöhung der Rohemissionen führt. Ohne dynamische Maßnahmen liegen die CO-Rohemissionen deutlich über denen des Referenzsystems, so dass trotz höherer Konversionsrate das Auspuff-CO erhöht ist. Für die anderen Emissionsarten überwiegt der Vorteil des schnelleren Katalysatoraufheizens. Während des WLTC wird zudem eine verstärkte passive DPF-Regeneration im vorturbo-DPF beobachtet, die Potenzial zur Minimierung des Kraftstoffverbrauches aufzeigt.

In einem kalt gestarteten Niedertemperatur Real Driving Emission (RDE) Zyklus wird das Potenzial des PTS hinsichtlich der Aufheizung des EAT demonstriert. Im Stadtbereich sind der Leistungsbedarf und die Abgastemperaturen gering, und es entstehen lange Schleppzeiten. Bei keiner der Konfigurationen findet eine signifikante Schadstoffreduktion statt. Dennoch werden in den vorturbo Systemen höhere Temperaturen festgestellt, die darauf schließen lassen, dass weniger kraftstoffintensive Aufheizmaßnehmen benötigt werden. Abschließend wird das PTS mit der größten vorturbo Masse in einem hochdynamischen RDE-Zyklus mit dem Referenzsystem verglichen. Um die dynamischen Anforderungen zu erfüllen und Unterschiede zwischen den elektrischen Unterstützungsmaßnahmen auszuarbeiten, werden zwei Konfigurationen des PTS untersucht: eins mit EATC und eins mit einem P2-Hybrid. Der erforderliche Leistungs- und Energiebedarf zur Kompensation des dynamischen Nachteils wird abgeschätzt. Weiterhin zeigen die Ergebnisse, dass die Art der dynamischen Unterstützung die Bildung von Rohemissionen und das Aufheizverhalten der Katalysatoren beeinflusst. Daher spielt auch die Betriebsstrategie der Dynamikkomponenten eine wesentliche Rolle für die Emissionsminderung, deren Potenzial aufgezeigt wird.

1 Introduction

The volume of individual mobility by passenger cars is constantly increasing, and discussions about the future drivetrain-system regarding carbon dioxide have risen recently. Although electromobility is locally emission-free, the internal combustion engine will continue to represent the largest market share in the coming years, as infrastructural weaknesses still exist for all other types of drivetrain. In terms of CO_2 emissions, current diesel engines set the benchmark. Developments and enhancements such as direct fuel injection and turbocharging have further increased efficiency. However, in the engine's overall design, not everything can be optimised in the interest of fuel economy. Other factors such as drivability, comfort, noise generation and the formation of further pollutants must be taken into account. While driving comfort and driveability are considered important for customer satisfaction, noise and pollutant emissions are legally restricted. Emissions legislation is worldwide tightened up in terms of emission released, but also the boundary conditions for the tests are widened. The real driving emissions (RDE) have been introduced, which are undertaken on public roads with portable emissions measurement systems (PEMS).This means that vehicles are evaluated under realistic driving situations that require engine operation in a wider map range, including high loads. The dynamics can be significantly higher than in the WLTC and the temperature range is extended. Emissions measured while driving must be below the legal limit.

The formation of pollutants in the combustion chamber cannot be completely avoided. Instead, the application of a diesel engine often results in a conflict of objectives between fuel consumption, comfort, and emission formation. The limited pollutant types are particulates, carbon monoxide, hydrocarbons, and nitrogen oxides. They have different formation mechanisms, and the avoidance of one type often favours the formation of the other. Exhaust gas aftertreatment (EAT) systems are therefore required to reduce emissions in order to comply with the required emission legislation.

A certain temperature level is required, that pollutant reduction takes place

on the catalytic surfaces of these systems. If the temperature is too low, no conversion will occur. This is the reason why a quick and efficient warm-up of the exhaust gas aftertreatment is desirable. The exhaust gas temperature of diesel engines is decreasing in accordance with further efficiency enhancements. Additional developments minimise fuel consumption, such as a start-stop system when the vehicle is stationary and the increasing hybridisation of vehicles, reduce the time during which the combustion engine is active. This leads to the cooling heating of the exhaust gas aftertreatment components and makes their heating-up more challenging. In general, the conditions for exhaust aftertreatment systems are becoming more difficult and requirements regarding final emissions continue to rise.

One approach to improve the heat-up behaviour is to place EAT components upstream of the turbine since higher temperatures prevail in this area. While pre-turbine EAT is already in use in large engines operating under steady state conditions, it is still a subject of research and development for passenger cars. The great challenge is the drivability of an engine with parts of the EAT upstream of the turbine because these components' thermal inertia reduces the dynamic engine response. The thermal inertia inhibits the increase of the turbine inlet temperature during strong accelerations and leads to a lack of enthalpy for the turbine expansion. However, the establishment of hybrid drivetrains in recent years offers great potential to compensate this disadvantage by means of additional electrical power. An electrical motor (P2 or P3-hybrid) and measures to increase boost pressure more quickly are options for dynamic compensation, e.g. electrical booster or air injections. This ability to compensate the dynamic delay leads to many possible combinations of pre-turbine EAT components.

0d/1d simulation is ideal for analysing a wide variety of pre-turbine (PTS) systems, as it allows a large number of configurations to be investigated in a short time. The number and type of pre-turbine components are easily adjustable and the type of dynamic support. Necessary additional components do not have to be available in physical form but can usually be modelled with low effort. Many possible systems to increase the dynamics for the PTS can be modelled and analysed. Furthermore, all physical quantities are accessible at a high temporal resolution, which allows a precise analysis of the interaction between the exhaust aftertreatment system and the turbocharger or the combustion chamber. Several different configurations of pre-turbo systems with different

pre-turbo volumes are studied in several test scenarios in this work. A reference system is used for comparability. The series catalysts of this system are placed in the new environment in front of the turbine without additional adjustments. The work is based on the research project [1].

At first, an explanation of the types of pollutants emitted during diesel combustion is given, how they are formed and what options are currently being used to reduce them. Furthermore, an overview of the current state of research on pre-turbine exhaust aftertreatment is given. In the next step, the simulation model structure is described, and its validity is ensured by comparison with measured data. The prediction of raw emissions is realised by means of a neural network in order to obtain a realistic prediction under transient conditions. For the analysis and evaluation of the PTS, different test scenarios are created. The scenarios represent a steady-state operation, load steps and warm-up behaviour during a cold start. In addition, various options for increasing dynamics with PTS are investigated and evaluated. The investigations on pre-turbine exhaust gas aftertreatment are concluded with simulations of entire driving cycles using a longitudinal dynamics model. Within these cycles, the dynamic engine responses with and without PTS are compared to each other. Furthermore, the total emitted emissions and fuel consumption are compared with the reference system.

2 State of the Art

Compared to gasoline spark-ignition engines, the higher efficiency of self-igniting diesel engines has led to its widespread use in passenger vehicles, light-duty, and heavy-duty vehicles. This makes them indispensable for further reducing global carbon dioxide (CO_2) emissions. However, the advantage of lower CO_2 emissions is counteracted by the formation of other pollutants such as soot and nitrogen oxides (NO_X).

In this chapter, the essential characteristics of turbocharged diesel engines for passenger vehicle application are discussed. One fundamental challenge regarding the diesel combustion is to achieve good mixing of fuel and air in order to increase efficiency and lower emissions. The fuel injection plays a crucial role in the mixture formation. Both are explained firstly, followed by the sequences of the diesel combustion. Furthermore, the focus is set on turbocharging, with a brief overview of its value. The first part is completed by the used model of the diesel combustion for 0d/1d simulation.

The next parts deal with the pollutants formed during the combustion of directly injected diesel fuel within an internal combustion engine. The primary pollutants are carbon monoxide, hydrocarbons, particle matter, and nitrogen oxides. Several in-engine features are applied and discussed for the reduction of these pollutants. However, often a trade-off between the formations of different types of pollutants must be made. Since it is not possible to avoid emission formation, an exhaust gas aftertreatment is required. The most common components of the exhaust gas aftertreatment for diesel engines, their main features, and most relevant reactions are outlined. Additionally, the used reaction kinetics for the modelling of the components within the simulation are briefly explained.

2.1 Turbocharged Diesel Engines

Diesel engines operate on the principle of compression ignition. The diesel fuel, which consists mainly of hydrocarbons, is injected into the cylinder at the end of the compression process. Mixture formation must be completed within a few degrees crank angle since it starts with the fuel injection. To obtain a mixture that is as homogeneous as possible, several measures are taken, which are described in more detail in section 2.1.1. The heterogeneous mixture ignites without an ignition source due to the high pressure and the resulting high temperatures in the combustion chamber. The engine's torque is controlled by the amount of fuel injected, which is limited by the air respectively oxygen mass in the cylinder. After the completed combustion, the burned gas is ejected and replaced by fresh air. Higher pressure in the intake increases the amount of fresh air in the cylinder, positively affecting the combustion process. The use of a turbocharger has been established to increase the boost pressure. With an exhaust gas recirculation, the NO_X formation during the combustion process is diminished. All aspects and influences are modelled within the quasi-dimensional combustion model that is used within this work.

2.1.1 Gas Mixture Formation and Fuel Injection

The diesel combustion's energy conversion depends on the speed of mixture formation of fuel and air since the fuel requires locally enough oxygen to oxidise. Therefore, the aim of mixture formation is to achieve the best possible distribution of the injected fuel. Two factors play a role here: firstly, the gas movement within the cylinder during and after injection increases the fuel distribution in the cylinder. Secondly, the injection itself influences the mixture formation via the injection pressure and the nozzle geometry.

The gas movement in the cylinder is divided into the air swirl and the squish flow. The air swirl occurs during intake stroke due to the shape of the intake port and is a gas movement flowing around the cylinder axis [46]. A fast piston speed correlating to high engine speeds favours the swirl formation. The swirl remains even during the compression process. Shaping the intake port to increase swirl usually involves increased flow losses. Therefore, modern diesel engines are equipped with two different intake ports, one for swirl generation

and one for better filling the combustion chamber. The filling channel is closed in the low part-load range using a swirl flap to generate a particularly high swirl. A high swirl supplies enough oxygen to the diffusion flame so that high energy conversion rates are achieved, and combustion takes place quickly. In addition, long phases in which the mixture is locally rich are avoided, which reduces soot formation.

The piston geometry and piston movement cause the squeeze flow during compression. While the piston moves upwards, the air is squeezed into the piston cavity. Its shape creates vortices that align toward the centre of the cylinder. This air flow helps to reach the combustion chamber areas above and below the injection jet. Furthermore, the squeezing flow also increases the rotational speed of the swirl flow due to the pirouette effect [39]. The dominant effect in mixture formation is the kinetic energy of the injected fuel jet.

The injected fuel must be spatially evenly distributed in the combustion chamber to achieve good mixing for which purpose multi-hole nozzles are used. The jet direction is adapted to the combustion chamber to achieve the best possible distribution of the fuel. The nozzle design can also be used to influence the jet cone angle. Depending on the injection pressure and the number and size of the nozzle holes, the kinetic energy of the injection jet and its penetration depth vary. High kinetic energy strengthens the momentum exchange between fuel and air, which promotes mixing. In today's common rail injection systems, the injection pressure corresponds to the rail pressure. However, the penetration depth of the fuel jet is limited since the fuel should not reach the cylinder walls.

The heterogeneous fuel-air mixture will only be ignitable if the fuel is in vapour form. Therefore, the injected fuel should quickly break down into the smallest possible droplets. This enlarges its total surface area and allows vaporisation to proceed more quickly. Finer atomisation is also favoured by the injection pressure and jet impulse, as these increase the velocity difference between the fuel droplets and the combustion chamber gas. The larger surface enhances the heat transfer from the hot compressed gas to the droplets, further improving the evaporation rate [39].

The conditioning of the mixture, the combustion process, and the temporal position of the combustion are determined by the injection with a common rail system. The high-pressure fuel pump generates the injection pressure, which is

approximately constant. Therefore, the injected fuel mass flow is approximately proportional to the switching time of the valve. The valve timing is controlled very precisely by means of electrically actuated control elements. As a result, injection shaping, multiple pre-injections, and multiple post-injections can be realised [46].

The injection timing of the main injection controls the position of fractional mass burn (e.g. crank angle to achieve 50 % mass burn – MFB 50). To achieve the best efficiency, the MFB 50 should be between 6 and 10 degrees after the top dead centre (TDC). An early start of injection usually results in faster combustion around TDC, so that peak pressure and temperature are very high, resulting in large wall heat losses. A late timing results in slower combustion with less wall heat losses, but more energy is lost in the hot exhaust gas.

With suitable pre-conditioning in the combustion chamber, a sudden increase in the burn rate is avoided. This is desired to minimise noise generation. For this purpose, one or more pre-injections are applied before the main injection, whose mass fraction is small. In addition to slightly increased fuel consumption, pre-injections promote soot and NO_X formation due to an increased diffusion fraction and higher combustion temperatures [39].

In certain situations, an early post-injection is also applied after the main injection. Due to the short time gap between the injections, it still burns in the cylinder and increases the exhaust gas temperature. Late injected fuel of a post-injection does not burn in the cylinder but passes unburned into the exhaust tract. The oxidation of the fuel in the diesel oxidation catalyst generates a heat release to increase the gas temperature for the downstream components.

2.1.2 Diesel Engine Combustion Process

If the conditions are appropriate, the high compression temperature causes the fuel-air mixture to ignite itself. The exothermic reaction releases heat that leads to a rise in temperature and pressure. The high pressure causes the piston to move downward, which corresponds to the technical work. An earlier increase in pressure thereby favours the rate of conversion to technical work. If the expansion has already progressed further, the pressure increase of the larger volume hardly accelerates the downward moving cylinder.

The mixture of fuel and air in the cylinder is heterogeneous: there are places with pure air ($\lambda = \infty$), some with pure fuel ($\lambda = 0$), and others where fuel and air are mixed. For an ignitable mixture, the equivalence ratio should be between 0.3 and 1.5 ($0.3 < \lambda < 1.5$) [39]. Fuel injected before the start of ignition is usually well mixed and burns quickly as part of the premixed flame. Low gradients of the equivalence ratio are present in these areas due to the good mixing, which inhibits soot formation. Since injection takes longer than ignition delay at most operating points, the oxidation rate of the fuel depends on the processes of mixing and evaporation already described. This type of combustion is called diffusive combustion. The ignitable mixture is formed at the edge of the injected fuel droplets with considerable evaporation in this region. The gas movement in the cylinder enhances the process of oxygen supply to these areas. The differences in mixture quality are also visible in local temperature differences. The combustion temperature is highest in the areas with a stoichiometric mixture ($\lambda = 1$).

2.1.3 Gas Exchange

With the completion of the expansion stroke, the charge exchange begins. The burned fuel-air mixture is expelled and replaced by fresh air. Shortly before reaching the bottom dead centre (BDC), the exhaust valves are opened. Due to the higher pressure in the cylinder compared to the exhaust manifold, most of the hot exhaust gas flows out of the cylinder quickly on its own. The remaining residual gas is pushed out by the subsequent upward movement of the piston. Since the pressure in the cylinder is rapidly reduced, the amount of work required to push the gas out is small. Even before TDC is reached and before the exhaust valve is closed, the intake valve opens. During the phase in which both valves are open, the outflowing air column exerts a suction force on the gas in the cylinder and the gas in the intake port. Suppose the outlet valves are closed at TDC. In that case, the compression volume remains in the cylinder because this part of the residual gas cannot be transported out of the cylinder by the piston extension process alone. Shortly after TDC is exceeded, the exhaust valve is closed. With the piston's downward movement, fresh air is now drawn into the cylinder through the intake valves. The intake valves close after the BDC has been exceeded since the inertia of the air column soaked in lasts even

longer. This allows the filling of the cylinder to be optimised, corresponding to the maximum volumetric efficiency [44].

2.1.4 Turbocharging

Given the same gas temperature, increasing the pressure in the intake port increases the gas density and the air mass in the cylinder. Since the amount of fresh air limits the maximum fuel mass to fuel ratio, more fuel can be injected and converted. The maximum engine power is increased with the same displacement, which is equivalent to an enhancement in power density. Turbocharging enables the downsizing of diesel engines, i.e., to reduce the displacement per cylinder or the number of cylinders while maintaining maximum power. Reducing the number of cylinders brings improvements in engine friction and, therefore, positively affects fuel consumption. In addition, the exhaust gas recirculation rate (EGR) can be increased with a high boost pressure, which reduces the formation of nitrogen oxides (see section 2.2.2).

The optimum charge in terms of fuel consumption and emissions depends on the target load and engine speed. A target boost pressure is therefore specified for each operating point. Air from the environment is compressed to the target pressure. Compression also increases the gas temperature, which means that the full potential of the higher pressure is not transferred into a higher mass since density decreases with higher temperatures. An intercooler follows the compressor in the intake tract, which cools the intake air. This increases the density of the intake air and consequently the air mass in the cylinder.

Two options have gained practical importance for the compression of ambient air. One is mechanical supercharging, in which an engine-driven compressor is used. No modifications are required on the exhaust side of the engine for this purpose. This results in a positive charge exchange work [44]. The second method is exhaust gas turbocharging, which extracts energy from the exhaust gas with the aid of a turbine that drives the compressor. By equating the turbine power with the compressor power, the first turbocharger main equation (eq. 2.1), in which the compression pressure ratio π_C as a function of the overall efficiency of the turbocharger η_{TC}, the compression start temperature T_{01},the exhaust gas temperature before turbine T_{03}, as well as the pressures before

turbine p_{03} and afterwards p_4. As an assumption, compressor and turbine are assumed to be adiabatic machines [44]:

$$\pi_C = \frac{p_{02}}{p_{01}} = \left\{ 1 + \frac{\dot{m}_T}{\dot{m}_C} \cdot \frac{c_{pT}}{c_{pC}} \cdot \frac{T_{03}}{T_{01}} \cdot \eta_{TC} \cdot \left[1 - \left(\frac{p_4}{p_{03}} \right)^{\frac{\kappa_T}{\kappa_T - 1}} \right] \right\}^{\frac{\kappa_C}{\kappa_C - 1}} \quad \text{eq. 2.1}$$

With the mass flows over the turbine m_T, the compressor m_C, the gas properties of the specific heat capacity c_p and the isentropic exponent κ each for the turbine and compressor according to the indices. With constant mass flows and gas properties, the pressure ratio across the compressor depends on the efficiency, the temperatures upstream of the compressor and upstream of the turbine, and the pressures upstream and downstream of the turbine. Since the conditions upstream of the compressor and downstream of the turbine are significantly influenced by the environment, the only remaining factors for a boost pressure increase are the pressure p_{03} upstream of the turbine and the temperature T_{03} upstream of the turbine, assuming the same efficiency.

Two variants of radial turbines have become established for controlling boost pressure with exhaust gas turbochargers. In one, a wastegate is attached to the turbine, which is used to regulate its upstream pressure. A closed wastegate means that the pressure upstream of the turbine is correspondingly high, and the entire exhaust gas flows through the turbine. Thus, much energy is tapped, resulting in high boost pressure. With an open wastegate, the exhaust gas energy escapes almost unused. The alternative is a turbocharger with a variable-geometry turbocharger (VGT), which has become established in diesel engines. These regulate the boost pressure by changing the inflow cross-section to the turbine impeller by pivoting the guide vanes of the VGT turbine. Changing the guide vanes modifies the inflow direction to the runner blades and the effective flow cross-section between the guide vanes, which is illustrated schematically in Figure 2.1. A smaller cross-section causes greater flow resistance and thus

increases the pressure upstream of the turbine. At the same time, the gas in the smaller cross-section is accelerated to a higher velocity. This increases the amount of extracted exhaust energy at low exhaust gas mass flows [14].

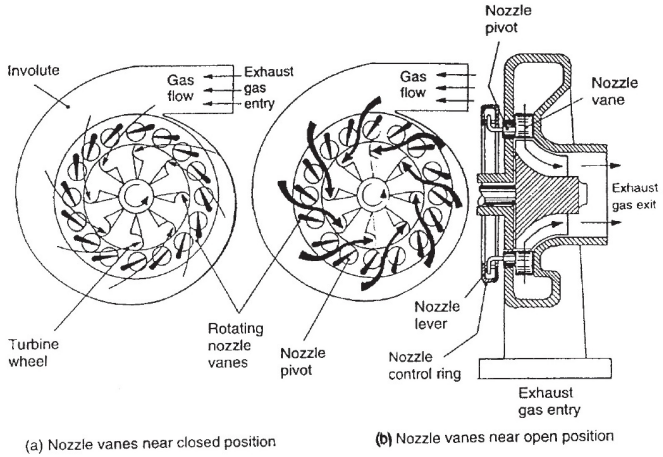

Figure 2.1: The general construction of a VGT device. (Taken from [21])

VGT turbochargers can cover a wide range of boost pressures at one engine speed by flexibly adjusting the effective flow cross-section and the flow to the rotor blades. Additionally, the variability brings advantages in boost pressure build-up and, thus, the dynamic response of the entire engine [21]. The VGT turbine can also be used to support high-pressure exhaust gas recirculation (HP-EGR). For this purpose, at high EGR rates, the guide vanes are retracted further than necessary to increase the pressure upstream of the turbine. This increases the pressure gradient towards the inlet duct, allowing higher EGR rates to be realised, especially at low loads [14].

High pressure and mass flow are created at the exhaust valve opening for a short time and leaves the cylinder into the exhaust tract. Depending on the design of the turbine, the kinetic energy of this pulse can be utilised. In this case, it is referred to as pulse charging. The cylinder exhaust lines usually lead individually to the turbine to maintain the pulses in the best possible way. Usually, the exhaust gases from the cylinders are combined into one volume,

which results in a smoothing of these fluctuations. In this case, the turbine uses the uniform pressure difference between the exhaust manifold and the surrounding area [44].

2.1.5 Exhaust Gas Recirculation

With an exhaust gas recirculation (EGR), the burnt exhaust gas is brought back to the combustion chamber. The exhaust gas recirculation rate x_{EGR} is defined as the ratio between recirculated exhaust gas mass flow and total mass flow into the cylinder:

$$x_{EGR} = \frac{\dot{m}_{EGR}}{\dot{m}_{Air} + \dot{m}_{EGR}} \qquad \text{eq. 2.2}$$

With the recirculation mass flow rate $\dot{m}_{EGR}$ and the fresh air mass flow rate $\dot{m}_{Air}$.

A distinction is made here between internal and external EGR. The internal EGR returns the exhaust gas to the cylinder using the exhaust valve timing. Usually, the exhaust valves remain open longer than necessary to expel the burnt gas. During the subsequent intake by the piston's downward movement, the hot exhaust gas is drawn back into the cylinder. Closing the exhaust valves early also results in high internal EGR rates because not all of the exhaust gas is pushed out of the cylinder. With a variable valve train, the internal EGR rate can be flexibly controlled.

In the case of external EGR, the exhaust gas is fed back into the intake tract via external pipes and returns to the combustion chamber through the intake valves. The EGR rate is controlled via a valve that regulates the flow rate of the recirculated exhaust gas, which makes control much simpler than that of an internal EGR. In addition, with external EGR, the recirculated exhaust gas is cooled, which positively affects the final compression temperature and peak temperature. A distinction is made between external high-pressure EGR and low-pressure EGR. With a high-pressure EGR, the exhaust gas is recirculated upstream of the turbine via a separate pipe and reintroduced into the air path downstream of the compressor (see Figure 2.2). At most operating points, the

pressure difference between exhaust backpressure and intake manifold pressure is large enough to control the desired EGR rate with the EGR valve. In the low load range, it may be necessary to throttle on the intake side or to increase the exhaust backpressure with the aid of the VGT. The low-pressure EGR is realised with the branch located after the turbine and usually after the exhaust gas aftertreatment. The exhaust gas is fed to the air side before the compressor.

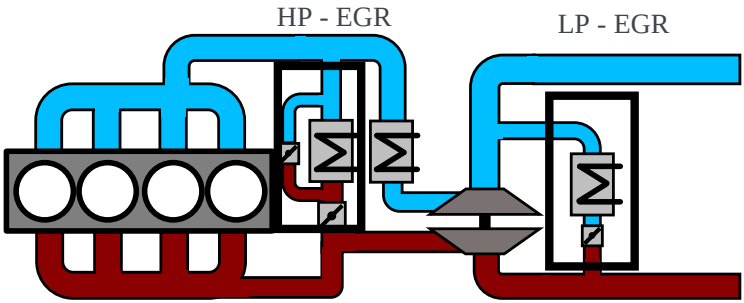

Figure 2.2: Schematic gas path of an engine with a high-pressure EGR and low-pressure EGR

A low-pressure EGR has the advantage over a high-pressure EGR that a more equal distribution between exhaust gas and fresh air is achieved due to the longer common path. This reduces the differences in gas composition between the individual cylinders. In addition, more intensive cooling of the exhaust gas and temperature control of the mixture of exhaust gas and fresh air is possible since the mixture flows through the charge air cooler after the compressor. By feeding the exhaust gas upstream of the compressor, the low-pressure EGR is decoupled from the boost pressure, in contrast to the high-pressure EGR, and the entire exhaust gas mass flow flows through the turbine [46]. As a result, the exhaust gas turbocharger has a higher speed, which is advantageous in transient operation. However, the low-pressure EGR control has disadvantages in dynamic operation since the air paths are significantly longer [46].

An EGR reduces the exhaust gas mass flow, which means fewer harmful particles are emitted while the pollutant concentration remains the same. However, the recirculated exhaust gas also has a major influence on the processes and

pollutant formation in the combustion chamber: The exhaust gas acts as an inert gas, which lowers the oxygen concentration and the oxygen partial pressure. This extends the ignition delay and reduces the combustion rate, resulting in lower combustion temperatures. The higher heat capacity of exhaust gas compared to fresh air increases this effect. The high temperatures and high oxygen partial pressure are lowered by the EGR, which is required for NO_X.

2.1.6 Model of the Simulation of the Diesel Combustion

There are several approaches for the simulation of diesel engine combustion. Among them are 0d phenomenological models for the wall heat transfer and the energy release rate of the combustion, which are often supplemented by a simplified view of the surrounding engine components. In 1d models, gas dynamic quantities in the entire air path are additionally computed in a temporally and spatially transient manner, averaged over the cross-section of a pipe or a component. The combustion chamber is additionally divided into an unburned and a burned zone. The most complex approaches are 3d simulations with CFD (computational fluid dynamics). The entire area under consideration is divided into small cells, for each of which the Navier-Stokes equations are solved. If chemical reactions are also taken into account, these are referred to as CRFD simulations (computational reactive fluid dynamics). The calculation time usually increases with increasing dimensions and level of detail.

At this point, a brief introduction into the phenomenological combustion model of Rether et al. [48] is given, which is used in this work. The model is predictive and calculates ignition delay and diesel combustion under inhomogeneous conditions.

For each injection, an ignition integral is calculated with a joint Arrhenius and Magnussen approach to determine the physical (according to Magnussen) and chemical (according to Arrhenius) ignition delay [12]. The calculation of the ignition delay of all pre-, main- and post-injections can be performed with only one equation. In both approaches, a factor is taken into account, which represents the influence of the evaporation of the fuel as a function of the injection quantity. In the Magnussen approach, the injection rate is

introduced by a parameter representing the specific turbulent energy. If the common ignition integral exceeds a certain value, ignition is assumed to occur.

During an injection, fuel discs are generated in discrete time steps and move into the combustion chamber in the injection direction (see Figure 2.3). Before the end of the ignition delay, the fuel is distributed into two pools: The premixed I pool and the diffusion pool. The entire fuel injected after the end of the ignition delay is allocated to the diffusion pool.

A certain amount of cylinder charge is added to the fuel from premixed I directly during injection as initial entrainment. After that, constant entrainment is assumed for the lean out. With the onset of ignition, this portion of the fuel burns rapidly, according to the approach of Barba [5] for calculating premixed combustion with a laminar flame velocity depending on the local air-fuel ratio. If too lean, the flame expires, and the portion of unburned fuel is assigned to the premixed II pool of the subsequent injection. The heat release of this combustion is calculated according to the premixed model of Pirker [42]. This means that the model can be used to model any number of pre- and post-injections.

If the injection duration is longer than the ignition delay, the injected fuel after ignition will be converted to the diffusion combustion. According to Figure 2.3, the injected fuel is discretised into discs, whose propagation initially proceeds at a constant speed. In a second phase, the injection jet breaks up, the disc slows down, and the addition of combustion chamber gas into the disc begins. This process is specified by an empirical distribution of the equivalence ratio and is delimited into three areas, like in Figure 2.3: Area A is very rich and cannot burn. A fuel disc is initially in this area at the time of injection. In area B, an ignitable mixture is present, and combustion is modelled as diffusion combustion I. Area C is very lean, and the combustion in this area is more slowly after diffusion combustion II.

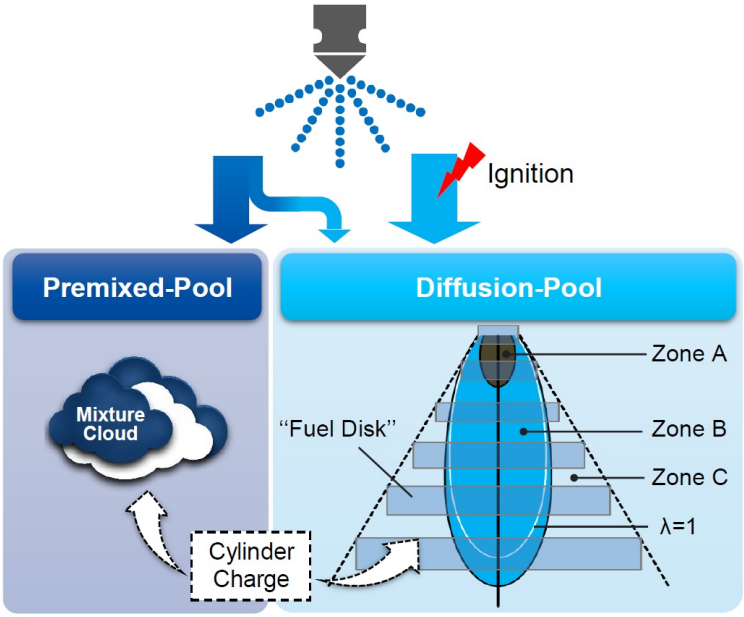

Figure 2.3: Schematical illustration of the QDM-Diesel with a single injection [66]

Diffusion combustion I and II differ only in the tuning of their parameters. Both are calculated as a function of the specific turbulence, which can be calculated from the velocity distribution in the injection jet. The total burn rate is finally the sum of the individual fractions of the two premixed and two diffusion combustions.

2.2 Pollutants of the diesel Combustion and their Formation

The idealised, complete combustion produces only the products water vapour (H_2O) and carbon dioxide (CO_2) [36]. The exhaust gas of a diesel engine also contains oxygen (O_2) due to the lean combustion process and nitrogen (N_2), an inert gas. Real combustion, which is never complete, forms by-products

that can harm humans and the environment. These are mainly nitrogen oxides (NO_X), particulate matter, carbon monoxide (CO), and hydrocarbons (HC) [47]. The formation of these pollutants is complex and depends on many factors, some of which are in opposition to fuel economy, comfort, and drivability. To minimise harm to people and the environment, exhaust emission regulations for diesel engines were introduced in the US in the 1960s. In Europe and Japan, emissions were also limited by law shortly afterwards. Figure 2.4 summarises the development of emission regulations in Europe since the introduction of EU1 legislation. This has become increasingly stringent over the years. With EU3 and following, all four of the main pollutants mentioned above are covered [9].

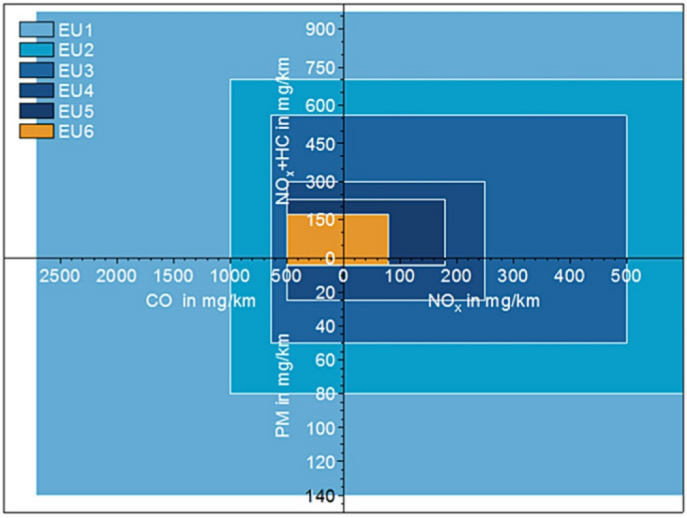

Figure 2.4: Development of emission standards EU 1 to 6 [9]

In contrast to the pollutants formed during actual combustion and affecting mainly the local surrounding, CO_2 is not considered a pollutant. However, as a greenhouse gas, it plays a part in global climate warming. The following subsections describe in more detail the in-engine formation of the four types of pollutants and their effects on humans and the environment. CO_2 formation is

not considered further, as it is directly related to fuel consumption and can be reduced by improving the engine's efficiency.

2.2.1 Carbon Monoxide

Humans cannot detect being exposed to carbon monoxide because it is odourless, colourless, and tasteless. When inhaled, it simply passes from the lungs into the bloodstream, where it combines with haemoglobin (Hb) to form carboxyhaemoglobin (COHb) [45]. Hb is necessary for oxygen transport in the bloodstream, but its affinity for combining with CO is up to 240 times higher [41]. Since COHb cannot transport oxygen, the blood's oxygen transport capacity is greatly reduced by CO, and the organs are less well supplied with oxygen. Less than 0.05 % CO in the breath can lead to a COHB concentration of 50 % in blood over a longer period [45]. In contrast to the formation of COHb, the reverse reaction that is the release of Hb for oxygen transport proceeds very slowly. This emphasises the dangers of carbon monoxide poisoning and shows why CO emissions into the environment must be minimised.

CO is always formed in larger quantities during combustion when there is not enough oxygen available, or the temperature is too low for complete oxidating hydrocarbons [35]. Since diesel engines are usually operated with an excess of air ($\lambda > 1$), there is at least globally enough oxygen available for complete combustion. However, due to direct injection, perfect mixing of fuel and air is never achieved, and locally rich areas occur. In these, the fuel cannot be completely converted to CO_2 and remains as CO. The measures described in section 2.1.1 for increasing gas mixing therefore also reduce CO emissions. A large proportion of the locally produced CO continues to oxidise to CO_2 at high temperatures if there is still enough oxygen in the combustion chamber after combustion. Since EGR lowers the oxidation rate in the combustion chamber due to a lower temperature and oxygen content, this leads to increased CO formation.

The formation of CO depends on the operating point of the engine. High engine speeds favour CO formation, as there is less time for mixture preparation. As a result, the fuel is mixed more poorly with the air in the combustion chamber [47]. Thus, larger locally rich areas are created, in which the fuel partly oxidises

to CO. Higher torque, on the other hand, reduces raw CO emissions up to a certain point, as the temperature increases during combustion. As a result, a more stable condition is reached in the combustion chamber and formed CO continues to oxidise to CO_2 in larger quantities. When the load is too high, raw CO emissions increase as the air-fuel ratio decreases. Due to the increasing lack of air ($\lambda < 1.4$), there is an increased lack of oxygen for complete combustion and partially oxidised CO is increasingly left behind [47].

2.2.2 Nitrogen Oxides

Nitrogen oxides is a collective term for gaseous oxides of nitrogen. The most common representatives are nitrogen monoxide (NO) and nitrogen dioxide (NO_2). Nitrogen monoxide is colourless and odourless but reacts in oxygen-containing environments at lower temperatures to form nitrogen dioxide, which is brownish and has a pungent chlorine-like odour. Nitrogen dioxide is very corrosive and highly toxic and reacts with water to form nitric acid, among other things. This can cause acid rain in the earth's atmosphere, damaging nature and the environment. Furthermore, nitrogen oxides promote the near the ground formation of ozone and photochemical smog.

The direct effects of nitrogen oxides on human health have been investigated in several studies. In most urban areas, where NO_2 is apparent in measurable amounts, it is not the only pollutant in the air. Thus, it has not yet been possible to determine the health impact of NO_2 in isolation [11]. Some of these studies conclude through statistical analysis that NO_2 promotes respiratory diseases. However, this has never been proven beyond doubt. Studies in which test persons were exposed to NO_2 in a controlled manner clearly show that NO_2 has an irritating effect on the respiratory tract. Additionally, NO_2 is occasionally associated with an increased risk of stroke and cardiological diseases [11].

Nitrogen oxides are divided into three types according to their formation process: thermal NO_X, prompt NO_X, and fuel NO_X. The Soviet physicist Jakov Borissovitch Zeldovich describes the steps of atmospheric nitrogen reacting with oxygen to thermal NO [70]. This mechanism was later used by Lavoie, Heywood and Keck [28] for the formation of NO in combustion engines and consists of the following three reactions:

$$O + N_2 \xleftrightarrow{k_1(t)} NO + N \qquad \text{eq. 2.3}$$

$$N + O_2 \xleftrightarrow{k_2(t)} NO + O \qquad \text{eq. 2.4}$$

$$N + OH \xleftrightarrow{k_3(t)} NO + H \qquad \text{eq. 2.5}$$

With the three equilibrium constants k_1, k_2 and k_3.

The equilibrium constants are strongly temperature-dependent, which gives the NO formed by this mechanism the name "thermal NO". When the reactions are in chemical equilibrium, forward and reverse reactions proceed at the same rate, and the respective substance concentrations no longer change. In the case of motor combustion, the forward reaction is decisive for the total formation since the instantaneous NO concentration is below the equilibrium concentration until the late phase of combustion [35].

In the initiation reaction (eq. 2.3), the triple bond of N_2 is broken, producing the atomic nitrogen for the subsequent reactions. Since the initiation reaction has the highest activation energy, it determines the reaction rate of thermal NO formation, which is negligible at temperatures below 1600 K, given the short residence times in the combustion chamber. The atomic oxygen required for this reaction is formed at temperatures above 2200 K. The concentration of atomic nitrogen remains almost constant since it immediately reacts further to NO in the second and third steps due to the significantly higher rates of the outward reactions [35].

The chemical reaction kinetics under the conditions prevailing in the combustion chamber are slow compared to the physical flow field changes, which is why chemical equilibrium is not achieved. Therefore, in the first phase of combustion, the amount of formed NO is far below that of the chemical equilibrium. In the late phase of the combustion, the temperature is significantly lower, and the NO concentration is above that of chemical equilibrium. However, since the reverse reactions occur more slowly at the lower temperature, most of the formed NO remains, and the reactions are referred to as "freezing".

At temperatures lower than 2000 K, almost no NO back-formation occurs. The other NO formation mechanisms, such as prompt NO or formation from nitrogen bound in the fuel, are of secondary importance in diesel engine combustion [62].

The amount of NO_2 in total nitrogen oxide emissions in diesel engine combustion is between 5 and 15 %, although higher shares are possible in the lower partial load range. In these ranges, total NO_X emissions are relatively low. Under ambient conditions, the chemical equilibrium is almost entirely on the side of NO_2, but it takes several hours to days to reach this equilibrium. In the combustion chamber, the formation of NO_2 occurs completely via the oxidation of NO by a peroxide radical R [49]:

$$NO + RO_2 \longleftrightarrow NO_2 + RO \qquad \text{eq. 2.6}$$

Since high HO_2 concentrations are apparent during combustion, NO oxidation by HO_2 is dominant [49] [26]:

$$NO + HO_2 \longleftrightarrow NO_2 + OH \qquad \text{eq. 2.7}$$

The formation of NO_X during diesel engine combustion is strongly temperature-dependent. In addition to the peak temperature, the oxygen concentration, the available time for the reactions, and the pressure all influence the NO_X formation rate. Reducing each of these physical parameters reduces the NO formation. The temperature reduction has the largest effect due to the exponential dependence. EGR lowers both the oxygen concentration and, in particular, the peak temperature. This is the reason for the application of high EGR rates over a wide range of the engine map in modern diesel engines, although it deteriorates the conditions for a fast combustion.

The residence time in the combustion chamber is mainly dependent on the rotational speed. There is little time for the reactions for NO formation to take place at a high engine speed. Consequently, NO emissions are generally higher at low engine speeds. With regard to torque, two effects have an opposite impact on NO emissions: A large amount of fuel is required to achieve high loads. Its conversion results in increased combustion temperatures, which

promotes NO formation. However, operating points close to maximum load are also characterised by a low air to fuel ratio. This means that much oxygen is converted during combustion and less oxygen is present for the formation of NO.

2.2.3 Hydrocarbons

Unburned or only partially burned fuel remains in the form of hydrocarbons (HC) after incomplete combustion. Hydrocarbons are generally a collective term for different molecules composed only of C and H atoms to $C_x H_y$ with different combinations of x and y. Various combinations of HC have been detected in combustion products of fossil fuels. These organic compounds contain carbon chains, rings, or combinations of both [20].

HC can penetrate deep into the lungs when inhaled because they have low surface tension and low viscosity. In doing so, they cause asthma-like symptoms and even pneumonia. The effects of HC on the environment vary and depend on the exact composition. Some HC act as greenhouse gases, such as methane (CH_4), which causes up to 25 times the greenhouse effect of CO_2. Moreover, HCs contribute to the formation of ground-level ozone [2].

Diesel engines always emit an increased proportion of HC emissions when the fuel is insufficiently conditioned or the temperatures are too low for complete combustion. In normal engine operation, a rich mixture or a low temperature is usually only present in locally small areas of the combustion chamber. Thus, the mixture formation measures mentioned in section 2.1.1 also reduce raw HC emissions. High HC emissions often occur during cold starts because the low temperatures do not ensure complete fuel evaporation. Similarly, in the lower part-load range, temperatures are often too low for good vaporisation and stable combustion of the entire injected fuel. Lowering the temperature and oxygen content through EGR consequently favour the HC formation.

Another source of HC emission is the fuel that remains in the injection nozzle's blind hole after the end of injection. This fuel evaporates during the expansion phase without oxidising. It is then pushed directly out of the cylinder into the exhaust tract. Reducing the size of the blind hole can reduce this contribution

to HC emissions. In locally rich areas, oxygen lacks the complete conversion of fuel, resulting in increased HC emissions [26].

2.2.4 Particulate Matter (Soot)

Particulate matter in the exhaust gas is defined as solids and accumulated volatile or soluble components. The legal particle content results from the mass of all substances remaining in a given filter after the exhaust gas has been diluted according to a defined procedure and cooled to below 52 °C (EN ISO 8178). Since the introduction of the Euro 5 emissions standard, in addition to the particulate mass, the number of particulates in diesel-powered passenger cars is limited by law. This is primarily intended to control the number of smaller particles, which contribute little to the total mass quantity. Most of the particulate matter is soot consisting of elemental carbon. Additionally, there are organic compounds from unburned hydrocarbons that originate from lubricating oil or fuel. Cooling during the test procedure causes many hydrocarbons to fall below the dew point, causing them to condense and adhere to solid nuclei. A relatively small proportion of particulate emissions is accounted for by sulphates, which enter the exhaust gases due to the sulphur content of the fuel and engine oil. The exact distribution of the individual fractions and the total number of particles are strongly dependent on the engine's operating point. At low load operation and under high excess air conditions, organic compounds dominate. With increasing load, the proportion of elemental carbon increases sharply [26].

Particles enter the human body at different rates depending on their size. Larger particles (PM10) reach the nasal cavities, smaller ones (PM2.5) even reach the bronchi and alveoli of the lungs [64]. The effects of ultrafine particles are not yet fully understood, but there is evidence that they even enter the bloodstream. However, small particles also have a stronger adhesiveness, which is why they mostly stick in the mucous membranes and do not penetrate into the lung tissue. Depending on their size and penetration depth, the health effects of particles in the body vary. They range from mucosal inflammation and local inflammation in the lung area to plaque formation in the blood vessels, an increased risk of thrombosis, and changes in the regulatory function of the autonomic nervous system [43].

The exact process of particle formation is still not completely understood. However, it is generally agreed that polycyclic aromatic hydrocarbons (PAHs) play a decisive role as precursors for soot particles. PAHs are ring-shaped molecules consisting of carbon and hydrogen atoms, such as benzene, and are formed at high combustion temperatures. The formation of the first hydrocarbon ring is considered the most important step in soot formation and is often the rate-determining step. McEnally et al. [34] address several approaches to the formation of the PAHs, whose percentage of carbon content increases as dehydrogenation progresses. Above a certain size of these rings, they stick together due to Van-der-Waals forces when colliding with another molecule. They then join together to form soot nuclei (nucleation), which have a size of 1 to 2 nm and are crucial for further soot formation. Further surface growth occurs on the soot nuclei due to the attachment of molecules from the gas phase (mainly ethyne C_2H_2). Besides, further PAHs or sulphates can adhere to the surface. This process produces carbon black primary particles with a size of 15 to 35 nm. A distinction is made between coagulation, in which relatively small particles fuse to form a larger spherical particle, and agglomeration, in which the particles retain their original shape. The growth rate decreases with time, as fewer and fewer particles are available with which the soot particles can continue to grow. Figure 2.5 shows the sequence of the individual steps in soot formation schematically.

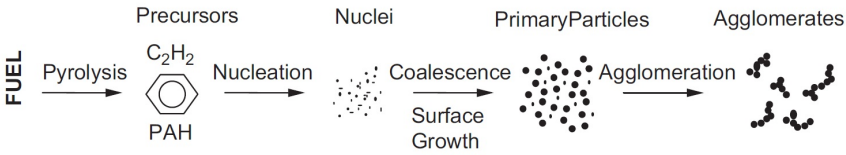

Figure 2.5: Schematic diagram of the steps in the soot formation process from the gas phase to solid agglomerated particles [61]

On a soot particle in a flame, the processes of surface growth, oxidation, condensation, coagulation, and agglomeration always occur simultaneously at different process rates. This results in soot particles of different sizes between 2 and 150 nm, whose size distribution can be described by a probability function. The centre of the distribution is at about 100 nm [26].

In diesel engines, soot formation in rich mixture regions increases with increasing temperature because this favours the formation of PAHs. In contrast to this, in lean areas, oxidation of soot particles is accelerated at elevated temperatures [61]. Since good mixture formation promotes combustion quality, most hydrocarbons burn directly and less PAHs is formed, which has a positive effect on soot formation. High EGR rates lower the combustion temperature and the oxygen content in the cylinder. This results in a significant increase in soot emissions. In terms of soot formation, there are two opposing effects concerning the injection timing: With an early injection, more time is available for mixture preparation, so soot formation is reduced due to good mixing. On the other hand, the atomisation of the fuel is poorer at a very early start of injection because the pressure and temperature in the combustion chamber are still lower at this time. Therefore, the fuel droplets formed after injection a larger, promoting soot formation [3].

Since a later injection timing reduces the temperature, the post-oxidation rate is correspondingly lower. Furthermore, there is less time for good mixture preparation, which increases soot emissions. Only at low loads, the temperature may be low enough that a late start of injection results in almost no soot formation [26]. In general, soot emissions can be reduced by a post injection attached to the main injection. A post injection shortly after the main injection brings additional turbulence into the combustion chamber through the injection jet. This accelerates mixture formation, combustion and increases the rate of soot post-oxidation. However, the interval between main and post injection must not be too long; otherwise, soot emissions will continue to rise, and fuel consumption will also deteriorate significantly.

2.3 State of the Art Diesel Exhaust Gas Aftertreatment

Current diesel exhaust gas aftertreatment targets the reduction of soot, carbon monoxide, hydrocarbons, unburned fuels, and nitrogen oxides. Due to the lean combustion, the three-way catalyst that is used for gasoline engines is not applicable. Recently an exhaust gas aftertreatment system containing a Diesel Oxidation Catalyst (DOC), a Diesel Particulate Filter (DPF), and

a Selective Catalyst Reduction (SCR) system or NO_X storage catalyst has been established in order to fulfil the strict emission limits for diesel engines. Modern DPF have a catalytic or selective coating that has the same properties as that of a DOC respectively an SCR. Combining the DPF and DOC or SCR enhances the reactive surface area without increasing the pressure drop remarkably. Regarding the SCR system, a split into two SCR catalysts is beneficial. The first SCR catalyst is positioned close to the engine where higher temperatures prevail. The second one is placed in the underfloor, to avoid too high temperatures. In this section, a brief overview of each component's most important aspects shall be given to understand the main interactions between the emission species and the components.

The catalysts for passenger vehicles usually consist of various components. Ceramics as cordierite or metal foils are used as the substrate material that is formed in a honeycomb structure with a high number of thin channels. A washcoat layer of aluminium oxide is applied to create a large surface by its throatiness on the substrate. In the washcoat, the catalytic substances are embedded. These differ depending on the type of catalyst. For ceramic cordierite, a bearing mat connects the catalytic cell structure with the metallic housing, the so-called canning. Metallic catalysts have a fixed connection to the canning [8].

The geometrical values as cell density (number of channels per cross-sectional area), length, cross-sectional area, and the thickness of the substrate and washcoat are significant parameters of a catalyst. The thermal mass and heat transfer rate of the catalyst are directly dependent on these values and determine the heat-up characteristic. Additionally, these parameters have a great impact on the pressure drop and mechanical resilience of the catalyst. Too high exhaust gas temperatures cause a sintering process in which several small particles of the precious metal melt together to one larger. This reduces the total surface area of the washcoat and thus the reaction activity [8].

2.3.1 Diesel Oxidation Catalyst (DOC)

The standard method for oxidising HC and CO into CO_2 and water is a DOC with a ceramic substrate and a precious metal coating. Its maximal conversion

rate starts at temperatures above 200 °C [8]. To achieve this temperature as fast as possible after the engine's cold start, the DOC is usually the first component of an after turbine exhaust gas aftertreatment (EAT) system because the exothermic oxidation reactions release heat into the gas stream.

The washcoat of the DOC increases, as mentioned, the active exposed surface area and has a big impact on the catalyst performance. Alumia (Al_2O_3), silica (SiO_2), or zeolites are most commonly used as washcoat materials for a DOC solely and combinations of these materials. Each of them has different properties that affect oxidation. Each washcoat material has its advantages and disadvantages, and an appropriate choice can lower the amount of required precious metal and thus the cost of the catalyst. For example, zeolite adsorbs HC at low temperatures, enhancing the cold start performance. When the catalyst is warmed up, the HCs are released from the zeolite and oxidised [50].

Platinum (Pt) and Palladium (Pd) are the most common precious metals used for the DOC, with Rhodium (Rh) sometimes added to increase the stability against sintering at high temperatures [8]. The precious metals are the active side for the oxidation reactions and show different performances regarding the oxidation activity for CO and HC. Pt exhibits better performance with higher weight HCs compared to Pd, but its activity decreases faster due to thermal degradation at high temperatures [53]. Often, a combination of precious metals is used for automotive applications to combine the properties of each material.

The fundamental reactions at a DOC above a certain temperature level under oxygen excess are the CO-, HC- and NO-oxidation. Several reaction mechanisms have been established to describe the kinetics of the CO oxidation that have no consens about the reaction rate-determining mechanisms. They have in common that CO self inhibits its oxidation at low temperatures, and oxygen promotes it. Consequently, the CO oxidation rate decreases with the amount of apparent CO since it blocks the catalytic surface for other molecules, including oxygen [63].

Similar to CO oxidation, at low temperatures, the HCs have a strong chemisorption on the Pt surface of the DOC and inhibit the oxygen adsorption on the surface. This mitigates the oxidation rate of all gas components. Generally, the surface interaction between O_2, CO, HC, and NO plays a crucial role in DOC oxidations. The surface area is limited and will be blocked for other emission

types if one species has dominating adsorption. The adsorption and chemisorption tendency of different species varies with temperature. Thus, the oxidation rate of one species depends not only on the temperature, available oxygen, the resting time, and the concentration of that species but also on the concentration and adsorption tendency of other species. Figure 2.6 depicts an experimental temperature programmed oxidation (TPO), during which the temperature was increased with a variation of the gas composition. The temperature at which CO conversion starts is remarkably increased as soon as other species are contained in the gas flow [4].

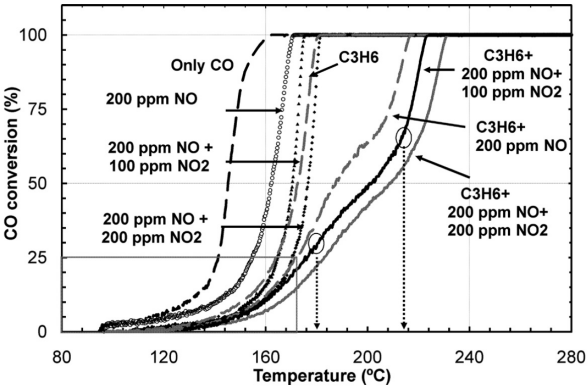

Figure 2.6: Conversion of CO during TPO. The inlet gas stream contained 3240 ppm CO, and either 1080 ppm C_3H_6 and/or 200 ppm NO, 200 ppm NO_2 and 10 % O_2, 5 % CO_2, 5 % H_2O, and balance N_2 [4]

In general, DOCs can achieve more than 90 % reduction in CO and HC emissions at exhaust temperatures higher than 300 °C [32]. However, at low operating temperatures, as in low-speed driving and warm-up conditions, the catalytic oxidation of HC and CO remains a significant challenge [55]. The DOC can also contribute to the soot reduction by oxidising the soluble organic fraction of the particulate matter [50].

Not directly demanded is the NO oxidation's side effect to NO_2 since the harmful substances are not removed. However, it positively impacts downstream

placed components like the DPF and SCR system, which is described later in more detail. NO oxidation is exothermic, and its reaction is less favoured at high temperatures [50]. Its forward reaction rate is first-order dependent with respect to the NO and O_2 concentration. The reverse reaction proceeds very slowly and is usually of less importance. NO and NO_2 are under the presence of oxygen in a temperature-dependent equilibrium that lies at low temperatures (< 250 °C) on the side of NO_2. Especially at low temperatures, a high NO_2 to NO_X ratio is desired to improve the performance of a downstream positioned SCR system [8].

The exothermic reactions in the DOC can be used as a heating measure for downstream components by increasing the CO and HC raw emissions deliberately. Late post-injections are barely burned within the cylinder and increase the HC emissions drastically. A less complete combustion is achievable by increasing the EGR rate, which increases CO emission. The heat release in the DOC is useful during warm-up phases or to trigger an active DPF regeneration. As a coarse assumption, every 1 Vol % CO that is oxidised increases the exhaust gas temperature by 90 K [8]. In some cases, the oxidation only happens in the first part of the DOC, which means that the rear part of the catalyst is heated-up before any other components benefit from higher temperatures.

Kinetic Model for the DOC Reactions

In diesel exhaust, many HC species are apparent due to the incomplete diesel combustion, which are denoted by the collective term of total hydrocarbons (THC). These are, for example, aromatics, saturated (paraffin), and unsaturated (olefin). Since most modelling applications are not able to consider each single HC species, the HC oxidation performance is tested by taking into account only propylene and propane representing unsaturated and saturated HC, respectively [50]. In this manner, the THC oxidation reaction rate is split into two reactions that have temperature and concentration dependencies. Additionally, the coinhibition of multi-component HC systems is better replicable.

One possibility to model the reactions within the DOC is the global kinetics by Sampara et al. [51], described briefly in the following. The model was established using a wide temperature and concentration range for the oxidation of diesel fuel (DF), propylene (C_3H_6), CO, H_2, and NO. The large number of different hydrocarbons species is split into a combination of propylene -

representing partially oxidised hydrocarbons - and diesel fuel representing unburned fuel. For the CO, HC, and H_2 oxidation, a first-order concentration dependency is set up and complemented by a global inhibition term implementing the effects of CO and NO. The NO oxidation rate is first-order dependent on NO and 0.5 with respect to oxygen. Its inhibition term is a function of DF and NO.

2.3.2 Diesel Particulate Filter (DPF)

The main task of the DPF is to filter particulate matter, also called soot, and ash out of the exhaust gas. For automotive applications, the standard DPF is a wall-flow filter made of cordierite, where exhaust enters channels that are blocked at the filter outlet, forcing the gas through the filter wall where the alternate ends are blocked [50]. The engine exhaust gas flows through the porous filter walls of a channel that are typically a fraction of a millimetre thick. Ceramic filters achieve a filtration efficiency of 95 % for particles over the entire relevant size range [8] [69].

The DPF pressure drop consists primarily of four components: The flow through the filtration wall, the flow friction at the filter channel walls and flow contraction and expansion losses at the filter inlet and exit. These losses are only dependent on the shape of the DPF and the current exhaust flow properties. The fourth part is the flow through the particulate layer (also: "soot cake layer"), which additionally depends on the current amount of soot and ash within the filter [33]. The pressure drop increases with the amount of particles loading. A too significant pressure drop causes high backpressure and negatively affects fuel consumption. The filtered soot is removed by oxidising into CO_2, which is called DPF regeneration. However, this is only possible for the soot; the filtered ash remains in the DPF until it is exchanged during vehicle maintenance.

DPF Regeneration

It is distinguished between active and passive DPF regeneration. The active regeneration is characterised by the soot oxidation process with oxygen apparent in the exhaust gas of lean diesel combustion. This process is described with eq. 2.8 and eq. 2.9, with the carbon atom representing soot. Usually, these reactions require temperatures above 500 °C, dependent on the catalytic filter

walls [50]. eq. 2.8 is the desired one, to avoid a large amount of CO tailpipe emission.

$$C + O_2 \longrightarrow CO_2 \qquad \text{eq. 2.8}$$

$$C + 0.5\,O_2 \longrightarrow CO \qquad \text{eq. 2.9}$$

The required high exhaust gas temperatures occur under normal conditions only at high engine loads. However, there are several possibilities to force high exhaust temperatures. Early post-injections are burned within the cylinder and do not contribute to the torque remarkably but increase the exhaust temperature directly. An additional shift of the main injection towards late intensifies this effect but reduces the engine efficiency. Both changes in the injection strategy increase the exhaust temperature on the cost of higher fuel consumption. A second method to achieve high exhaust gas temperatures within the DPF requires an upstream DOC. By means of a late post-injection, the amount of HC is increased intentionally to obtain high HC oxidation rates within the DOC that increase the exhaust gas temperature. For both variants, besides high temperatures, a large amount of oxygen is required to trigger the active DPF regeneration. Thus, the EGR rate is often reduced [27].

The oxidation of particulate matter is an exothermic reaction. Thus, high temperatures that lead to melting or cracking of the DPF may occur during the regeneration. Therefore, the maximum local temperatures during regeneration should stay below the melting temperature of the filter. Additionally, large temperature gradients might cause cracks in the support material and should be avoided . The maximum temperature gradient increases with the maximum temperature. Therefore in most cases, it is sufficient to limit the maximum temperature [69].

While the active regeneration is mainly triggered externally, when the filter loading and the pressure drop of the DPF are too high, the passive DPF regeneration is a continuous process that starts at temperatures between 200 and 300 °C [22]. The particulate matter is oxidised by NO_2, according to the following reaction formula:

$$C + NO_2 \longrightarrow CO + NO \qquad \text{eq. 2.10}$$

NO_2 has a higher oxidation activity towards the atomic carbon compared to oxygen. Therefore, the oxidation with NO_2 starts already at lower temperatures. An upstream positioned DOC can increase the amount of NO_2 in the exhaust gas by oxidising NO and therefore increase the passive DPF regeneration rate[50].

In further developments, catalytic or selective coatings are applied to particulate filters. These coatings have the same characteristics as the coating of a DOC catalyst respectively of an SCR catalyst. In this manner, the reactive surface is enlarged, and higher conversion rates are possible without adding an extra component. This reduces the thermal mass and backpressure of the EAT system compared to a single DOC/SCR and DPF.

2.3.3 Selective Catalytic Reaction (SCR)

SCR systems are used to reduce NO_X emissions in the diesel exhaust using an additional reductant. HC-SCR systems use the apparent HC for the NO_X reduction on many different types of catalysts. The problem regarding the application for lean operating diesel engines is the competition between NO_X and O_2 for the reaction with HC [50]. The most common SCR technology for reducing NO within the diesel exhaust uses ammonia (NH_3) as a reductant. Since the storage, handling and transportation of NH_3 are complicated, the NH_3 is carried within urea for automotive DeNOx emission control [68]. Urea is typically carried as an aqueous solution of 32.5 % urea content, also referred to as diesel emission fluid (DEF), to obtain the best properties regarding the freezing temperature [56]. This solution is injected into the hot exhaust gas stream, where the first step is the evaporation of water from the DEF. The remaining pure urea is decomposed into ammonia and isocyanic acid (HNCO). This reaction is called thermolysis and occurs at temperatures higher than 152 °C [52]:

$$NH_2 - CO - NH_2 \longrightarrow NH_3 + HNCO \qquad \text{eq. 2.11}$$

In the last step, HNCO reacts with water to ammonia and carbon dioxide (eq. 2.12). This reaction has a high rate of hot metal oxide surfaces, although HNCO is very stable in the gas phase [68].

$$HNCO + H_2O \longrightarrow NH_3 + CO_2 \qquad \text{eq. 2.12}$$

eq. 2.11 and eq. 2.12 show that one mole of urea produces two moles of ammonia required for the SCR reactions. Cu and Fe-exchanged zeolite materials are currently used for the NH_3-SCR because they have superior thermal durability compared to other materials [17]. While Cu-zeolite catalysts are favoured at temperatures below 450 °C, Fe-zeolite features a better NO_X reduction performance at higher temperatures [18]. A combination of both types is also possible to increase the temperature range. Independent of the catalyst material, the NH_3-SCR is based on three main reactions. The standard SCR reaction occurs in the presence of oxygen:

$$4\,NH_3 + 4\,NO + O_2 \longrightarrow 4\,N_2 + 6\,H_2O \qquad \text{eq. 2.13}$$

The fast SCR reaction (eq. 2.14) requires an equimolar amount of NO and NO_2. This reaction is the fastest SCR reaction and is of great importance at low temperatures. The NO_X reduction rate is increasing with a more equal NO_2/NO ratio. Since under normal conditions, NO predominates, an upstream DOC enhances this ratio and can improve the SCR efficiency. Above 200 °C, the fast SCR reaction becomes limited by the diffusion rate; for the standard SCR reaction, this temperature is close to 300 °C on Fe zeolite catalysts [37]. This underlines the importance of the fast SCR reaction at low temperatures.

$$2\,NH_3 + NO + NO_2 \longrightarrow 2\,N_2 + 3\,H_2O \qquad \text{eq. 2.14}$$

The third reaction is essential under conditions with more NO_2 than NO and is called the NO_2-SCR reaction (eq. 2.15). These conditions are rarely apparent in the exhaust gas of diesel passenger vehicles [49].

$$8\,NH_3 + 6\,NO_2 \longrightarrow 7\,N_2 + 12\,H_2O \qquad \text{eq. 2.15}$$

The NH_3 needs to be adsorbed by the catalyst first before it reacts with NO_X. A large amount of adsorbed NH_3 favours the reaction rates and would be desired for that reason. However, at high temperatures, the desorption rate of the NH_3 becomes too fast as that NH_3 is kept stored within the catalyst and the SCR NO_X conversion decreases drastically [56]. The desorbed NH_3 leaves the catalyst, which also happens if the urea injection rate is too high for complete adsorption of the NH_3. An ammonia oxidation catalyst can be placed after the SCR catalyst to avoid the NH_3 slip into the environment. Another adverse effect at high temperatures is the ammonia oxidation that removes the stored ammonia from the catalyst and decreases the NO_X reduction rates. At temperatures above 400 °C, NH_3 mostly oxidises to H_2O and N_2. At higher temperatures, the ammonia oxidation can even increase the NO emissions:

$$4\,NH_3 + 5\,O_2 \longrightarrow 4\,NO + 6\,H_2O \qquad \text{eq. 2.16}$$

However, it is not entirely clear at which temperatures this reaction starts. In order to maximise the SCR activity with minimum urea, a complex dosing strategy is required. The transient conditions of passenger vehicles make this task very challenging.

Kinetic Model of the SCR Reactions

The model for a commercial Cu-zeolite SCR catalyst of Pant and Schmieg [40] contains the already explained reactions of the NO_X reduction (eq. 2.13 - eq. 2.15). They are complemented by ammonia adsorption and desorption reaction to obtain the stored amount of ammonia. At higher temperatures, SCR catalysts can convert NO to NO_2. Therefore, a term for NO oxidation is added. Additionally, the model contains a reaction for the nitrous oxide (N_2O) formation:

$$2\,NH_3 + 2\,NO_2 \longrightarrow N_2 + N_2O + 3\,H_2O \qquad \text{eq. 2.17}$$

Ammonia oxidation was found to form NO above temperatures of 500 °C, and it is assumed that the NO is reduced again by NH_3. Thus their model only contains reaction eq. 2.16 for ammonia oxidation instead of the direct oxidation into N_2 and H_2O.

2.3.4 Lean NOx Trap (LNT)

Although the LNT is not considered within this work, it is described very briefly to have mentioned all common NO_X reduction possibilities. The LNT can store a certain amount of NO_X by forming solid nitrates and nitrites on a component of the LNT surface when the exhaust is lean. Before the NO_X adsorbing sites become saturated, the catalyst is regenerated. The regeneration is conducted under rich conditions, where the exhaust gas contains no oxygen but a more significant amount of H_2, CO and HCs. These substances react immediately with nitrates and nitrites to N_2 that are released by the rich purge. The low NSC light-off temperature has benefits during cold starts and low load operating points compared to an SCR system. Like the SCR system, an LNT has a better performance with a high NO_2/NO_X ratio achieved by an upstream DOC [8].

2.4 Former Studies on Pre-Turbine Exhaust Gas Aftertreatment

Most work on exhaust gas aftertreatment has focused on stationary operation and applications in heavy-duty vehicles. The additional heat sink of a catalyst upstream of the turbine increases the turbo lag significantly. It results in a slower increase of boost pressure up to the steady state value. The catalyst size directly influences the turbine speed increase during a load step at constant engine speed [23]. Apart from the reduced dynamics, higher fuel consumption during accelerations was observed [31].

During steady state operation, many promising aspects of pre-turbine EAT systems have been found: An EAT upstream of the turbine is exposed to higher temperatures and pressures. Due to the higher pressure level before the turbine, the gas density in the catalyst is higher compared to a post-turbine catalyst. This leads to lower gas velocities in the catalyst and thus longer residence time for the oxidation of the pollutants. Besides the higher temperatures and longer resting times, a higher pressure level also increases the reactivity of catalytic oxidations, resulting in higher emission conversion rates [57]. The same effect was detected on Cu-based SCR catalysts in pre-turbine applications. The higher pressure before the turbine was found to increase the SCR activity [19]. A pre-turbine DPF showed higher filtration efficiencies that might allow

the reduction of the filter size [54]. The lower gas velocity in the pre-turbine position reduces the pressure drop of a component that is strongly dependent on the local flow velocity.

A reduction of pre-turbine catalyst volume or cell density is possible because of the already described higher conversion efficiency upstream of the turbine. Smaller catalysts and filters have a lower package size, cost, and thermal inertia [57]. Additionally, a more compact EAT system reduces the engine's backpressure, which leads to an advantage in fuel consumption and lowers the soot formation. Thus, an even more significant reduction of a pre-turbine DPF of up to 40 % is possible [54]. The turbo lag is reduced if smaller pre-turbine catalyst were used, and thus the engine dynamics are improved.

Investigations of a pre-turbine DPF showed higher passive regeneration rates compared to a standard positioning, especially for low load operation [30]. Thus, the active DPF regeneration needs to be triggered less often. The pressure drop of the DPF stays at a lower level, resulting in a fuel consumption advantage for pre-turbine DPF configurations.

The pressure level in the exhaust manifold is an indicator of the scale of the pumping losses. To determine the pressure in the exhaust manifold, the pressure drops of all exhaust components have to be added. At the turbine, the apparent downstream pressure is multiplied by the turbine's pressure ratio to obtain the pressure before the turbine. Thus, a pre-turbine pressure drop acts singularly, whereas a post-turbine pressure drop is multiplied by the expansion ratio. Especially for high loads, the expansion ratio of the turbine is large. This effect reduces the pumping losses of the engine with a PTS and improves fuel consumption [30].

PTS show great potential in terms of their warm-up behaviour. During a cold New European Driving Cycle (NEDC), the tailpipe CO emissions with a pre-turbine DOC could be reduced by more than 14 % compared to a reference post-turbine DOC. This is due to an advance in the maximum conversion efficiency of 345 s. Similar observations were made in terms of HC emissions [31].

Approaches to increasing the engine response with PTS were investigated. On a heavy-duty turbocharged engine, the drivability was enhanced employing

proper management of the boost and EGR control. These measures showed no significant influence on the specific fuel consumption, but a balance between driveability and transient NO_X emissions has to be found [6]. Furthermore, the impact of the size of a pre-turbine catalyst on the turbo lag was analysed, and a VGT control was identified to increase the dynamics [59].

Recently the focus of research is set more and more on the examination of entire driving cycles. During WLTC tests on the test bench, a small pre-turbine DOC was investigated to focus on HC and CO emissions. Due to the higher pressure in the exhaust manifold, the internal EGR rate was increased, which caused up to 50 % higher CO and 53 % HC raw emissions. Despite the higher conversion rates with the pre-turbine DOC, the tailpipe emissions were still higher than the baseline. Additionally, the fuel consumption increased because the pressure drop of the exhaust gas aftertreatment system was higher than with the baseline system. One reason for this was the higher soot formation that increased the pressure drop of the filter.

Further steps include an additional external compressor in order to increase the dynamic response and provide enough boost pressure. A pre-turbine DOC-SCR system in combination with an underhood SCR was analysed. The pre-turbine SCR heats-up quickly, whereas the underhood SCR requires more time but less likely to achieve the upper temperature limit. Various combinations of these pre-turbine catalysts regarding their size were examined during low dynamic RDE drives at the test bench and with the aid of simulation.

3 Simulation Setup and Validation

In this section, the set-up of the 0d/1d-simulation model and the validation by means of data from the test bench is described. The model is set up within the engine performance simulation software GT POWER. Once the simulation model is set up, the examination using 0d/1d simulation has various advantages. For example, hardly measurable values at the test bench are accessible with the simulation. These values are calculated directly without any inertia, which enables a fine temporal resolution of the values. This offers more possibilities regarding the evaluation and interpretation of the results.

Firstly the structure of the test engine is described with the standard placing of the exhaust gas aftertreatment components. Hereafter, the required models for the combustion, the exhaust gas aftertreatment components and the emission prediction are discussed. In the last part, the longitudinal vehicle model is explained, which is necessary to simulate driving cycles.

3.1 Test Engine with Reference Exhaust Gas Aftertreatment System

The test engine is a four-cylinder diesel engine – VW's EA189 – with a VGT and a cooled high-pressure EGR. Additionally, in the simulation model, a cooled low-pressure EGR was implemented to maintain a state of the art EU6 diesel engine. The EGR rate is controlled on a target value that depends on engine speed and target torque. The main characteristics of the engine are summarised in Table 3.1.

Table 3.1: Characteristic data of the test engine

Engine displacement	1968 cm^3
Cylinder number	4
Max. effective power	125 kW at 4200 rpm
Max. effective torque	350 Nm at 1750-2500 rpm
Bore x stroke	81.0 mm x 95.5 mm
Compression ratio	16.5:1
Pressure charging	Turbocharger with variable geometry

This test engine is used for all investigations with the standard application obtained from the engine control unit (ECU) of the test bench to get comparable results for all configurations. The ECU does not have a series production applications, which is not of interest because the same test engine is used to compare the different EAT system. Solely, the application of the combined low and high-pressure EGR was adopted for the simulation compared to the test bench. The low-pressure EGR is mainly active for engine speeds below 2000 rpm. In Figure 3.1, the engine layout is shown schematically with the reference exhaust gas aftertreatment system. By adjusting the turbine VGT rack position, the boost pressure is controlled. The desired target boost pressure depends on the engine speed and target load. After the compressor, the charged air cooler is arranged to cool the compressed air and increase the air mass in the cylinders.

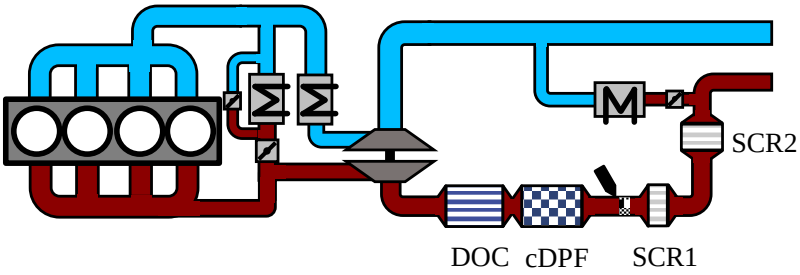

Figure 3.1: Schematic drawing of the engine with the reference exhaust gas aftertreatment system

The reference exhaust gas aftertreatment system consists of a DOC, a coated diesel particulate filter (cDPF) and a SCR system. The SCR system is split into two single underfloor catalysts. Upstream of the first catalyst, the urea injection system with a mixer is installed. The amount of injected urea is controlled to match a target value for the stored ammonia in the catalysts that depends on temperature, pressure and mass flow rate. Table 3.2 summarises the shape of the standard EAT components.

Table 3.2: Properties of the exhaust gas aftertreatment components

	DOC (ellipsoid)	cDPF (ellipsoid)	SCR1 (circle)	SCR2 (circle)
Length in mm	139.2	198.3	-	-
Width in mm	74.2	101.6	-	-
Diameter in mm	-	-	143.4	144.7
Height in mm	65.6	174.3	76.0	152.8
Volume in l	0.2	2.75	1.2	2.5
Cell density in cpsi	200	320	400	400
Cell type	triangle	square	square	square

3.2 Engine and Flow Model

The length, diameter, bending, and material of the flow pipes are modelled according to the set-up on the test bench. The material and thickness of the pipes determine their thermal inertia. The heat transfer that depends on flow characteristics (velocity, turbulence, temperature) is used to calculate the wall temperature during steady state operation and under transient conditions. The pressure drops are determined accordingly with the surface roughness. When the diameter of a pipe changes, an additional expansion or contraction pressure drop is added. Due to the small flow channels of the catalysts and the cDPF, their pressure drop is exceptionally high, which is discussed in section 3.3.

The turbocharger was measured on a hot-gas test facility to maintain the compressor map and turbine maps for various VGT rack positions. Dependent

on the operating state and temperatures, the thermodynamic changes over the turbine and compressor are overlapped by heat transfer. The measured maps contain these heat transfer rates that affect the efficiencies, especially at low mass flow rates. At these conditions, the turbine efficiencies are unrealistically high and over predict the boost pressure. This falsifies the transient response at low loads and can affect the low-end torque as well. In order to avoid this, a heat flux correction was subjected to the data before its usage.

All applications are implemented map-based, dependent on target load and engine speed. This map-based application is used for the start of injection (SOI), the target EGR rates, the amount and timing of the pre injections, the swirl flaps, and the target boost pressure. The flow model was calibrated based on the steady state operation points that are shown in Figure 3.2. At lower and higher engine speeds, a robust engine operation was not possible.

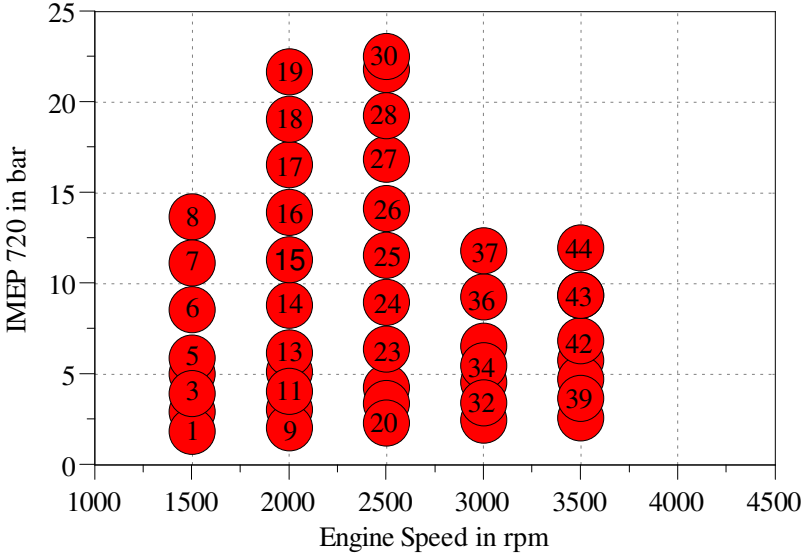

Figure 3.2: Operating points for the model calibration and validation

When calibrating the simulation model, one crucial physical quantity to match is the air mass flow rate, shown in Figure 3.3 for the operating points. It greatly

impacts thermal behaviour during transient engine operation: a higher mass flow rate accelerates the warm-up of the exhaust gas aftertreatment for a given gas temperature.

For most operating points, the difference between the measurement on the test bench and the simulation is within an acceptable tolerance. The simulation underestimates at lower mass flow rates; at higher mass flow rates, it overestimates compared to the results from the test bench. One reason for the deviation is the map-based application and the missing values from the test bench for the swirl valves. However, the aim is to create an engine simulation model that describes a modern diesel engine in order to compare various EAT configurations. This goal is achieved even with the small discrepancies. Thus, a perfect match with the results from the test is not required.

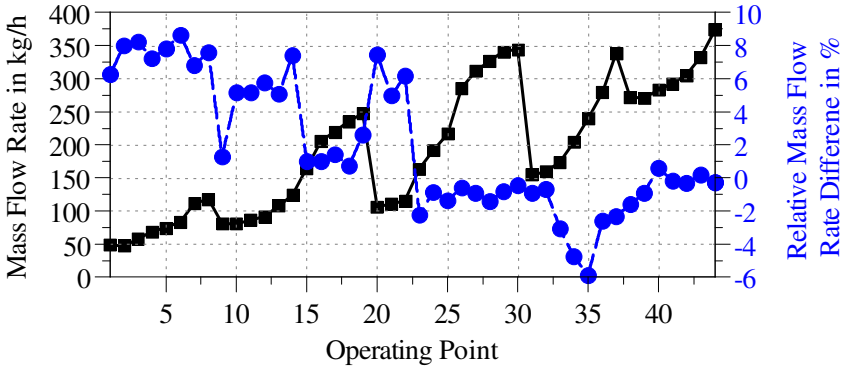

Figure 3.3: The mass flow rate of the engine model and the relative difference in the mass flow rate between measurement and simulation. A positive value means a higher mass flow rate on the test bench.

Once the air flow rates are within a reasonable tolerance, the focus is set on the combustion model. For the calibration of the combustion model, the pressure in the cylinder and the intake and exhaust manifold is measured over the crank angle. A pressure trace analysis was conducted with this data and the quasi-dimensional diesel combustion model was calibrated. Figure 3.4 visualises the

combustion process calculated by the quasi-dimensional combustion model and the comparison with the pressure trace analysis for selected operating points.

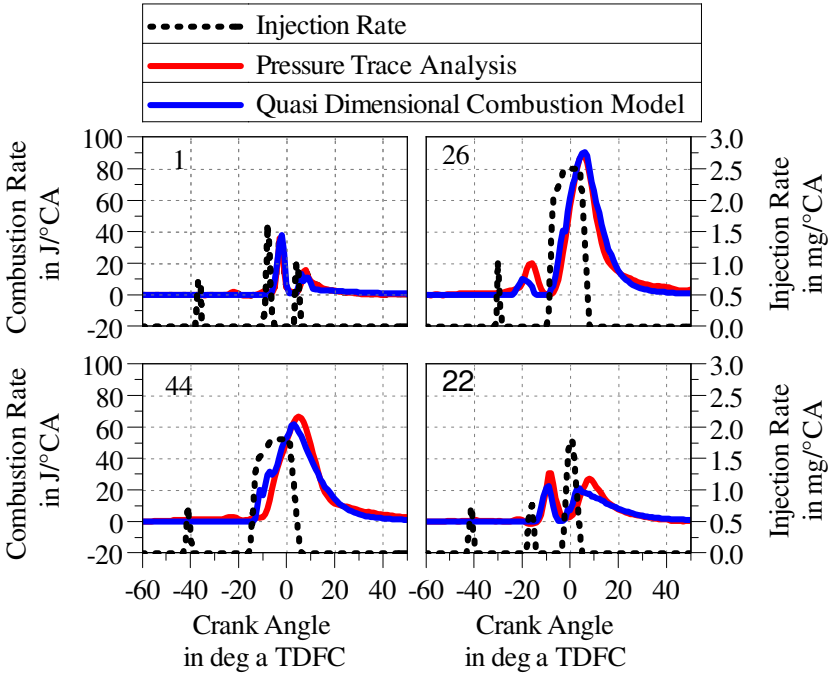

Figure 3.4: Comparison of the combustion process obtained by the pressure trace analysis and the quasi dimensional combustion model for given operating points 1, 22, 26 and 44.

The agreement of the combustion process in a wide range of the engine-operating map ensures that the model works reasonably with only one set of calibration parameters. Considering the energy balance, the relative difference in specific fuel consumption is within a tolerance of 3 % for 42 of the 44 considered operating points. Besides the mass flow rate, the exhaust gas temperature is another factor that affects the warm-up of the EAT components. It depends on the MFB 50 point and the amount of burned fuel, for which the agreement was adequate. The exhaust temperature of each operating point

is plotted in Figure 3.5, along with the absolute deviation from the measured temperatures.

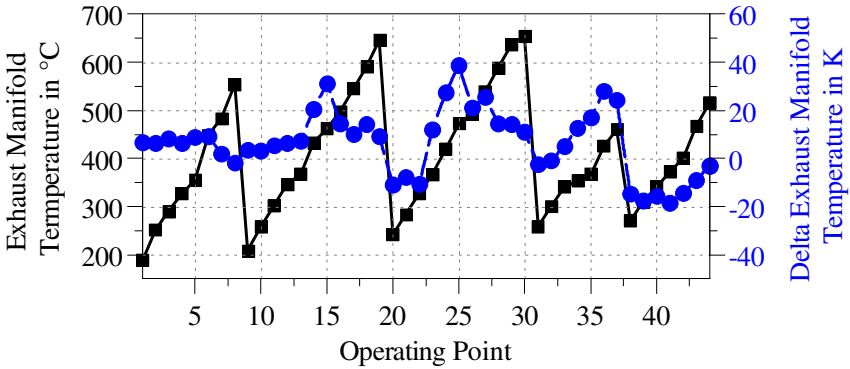

Figure 3.5: The simulated temperature in the exhaust manifold and its absolute deviation from the measured temperatures

For the deviations, no clear tendency regarding load or engine speeds are recognisable. The injection timing (SOI) determines the MFB 50 of the combustion that influences the exhaust temperature remarkably. A late MFB 50 usually implies higher exhaust gas temperatures. Therefore, the map-based application of the SOI might be a root for the differences.

3.3 Exhaust Gas Aftertreatment Components

Two properties are essential in modelling exhaust gas aftertreatment components: firstly, the pressure drop over the component significantly influences the charge exchange work. Secondly, the chemical reactions in the catalysts are of great importance to accurately predict the tailpipe emissions and the heat release of oxidation reactions.

The pressure drop was determined for various flow velocities and temperatures on the test bench and adjusted by means of friction coefficients in the simulation

model; one coefficient for the linear dependence on the velocity and one for the quadratic. A specific test sequence was carried out to adapt the catalytic reactions: the engine was initially towed at a constant speed until all components had cooled down completely. Subsequently, the load was adjusted, which increased the exhaust temperature. The emissions were measured before and after the EAT components. With this procedure, the conversion rate depending on the temperature is determined for an approximately constant mass flow rate. Additionally, this procedure delivers data for the calibration of the thermal inertia of the components. Each EAT component was calibrated first in a standalone model to minimize the simulation time. The calibration was conducted by optimizing parameters for pressure drop and the reaction rates.

The chemical modelling of the DOC and the cDPF is based on the model of Sampara et al. [51]. They propose the split of total measured hydrocarbons into partially oxidized hydrocarbons and unburnt diesel fuel as not oxidised representative of the HC. Polypropylene (C_3H_6) is implemented as a representative of the partially oxidized HC. Besides the HC, reactions for the oxidation of NO, H_2, and CO are implemented. The reaction rate is calculated using the standard Arrhenius equation, for which the activation temperature is calibrated using the test bench measurements.

The SCR reactions are based on the kinetic model of Pant and Schmieg [40], in which ammonia oxidation is implemented in addition to the standard SCR, NO_2-SCR, and fast SCR reactions. As only the total concentration of nitrogen oxides is measured on the test bench, and no individual measurement of NO and NO_2 is carried out, a constant NO_2 to NO_X ratio of 5 % is assumed. Urea decomposition is required to obtain ammonia from urea. Two reactions are applied to the gas site as described in section 2.3.3: the urea thermolysis (eq. 2.11) and the isocyanic acid hydrolysis (eq. 2.12). Since in a pre-turbine surrounding pressure and temperature change much quicker than in the standard post-turbine position, the urea dosing strategy becomes a challenging part for the EAT system. At low gas flow rates, a lower urea injection rate causes a high ammonia concentration. The urea injection rate is limited by the mass flow rate through the SCR catalyst to avoid ammonia slip.

While the explicit solver is used for the simulation of the overall engine and flow model, the simulation of the chemical reactions is ideally calculated

with the quasi-steady solver (QS solver). The chemical reaction calculation usually needs many iteration steps, and with an explicit solver, the required time steps are very small. The QS solver is a faster converging method for the chemical reactions and assumes a steady state problem for each time step. To optimize simulation duration, the exhaust gas aftertreatment components and their inlet and outlet sections are duplicated. In the duplicated components, the chemical reactions are calculated with the QS solver. For each time step of the explicit solver, the QS calculates a stationary solution, including the chemical equilibrium for the chosen reactions in the component. The boundary conditions of pressure, temperature, and mass flow rate are transferred to the duplicated parts from the engine model. The heat released from the chemical reaction is transferred back to the explicit model in the other direction. This is particularly necessary for the heat release of the oxidation reactions.

Validation of the EAT Components

The EAT components are validated using a single catalyst model, for which the inlet mass flow rate, temperature and pressure are given. In Figure 3.6, the calibrated pressure drops of the DOC, cDPF and SCR1 are compared with the measured ones. For all considered mass flow rates, temperatures and pressures, a close agreement was found.

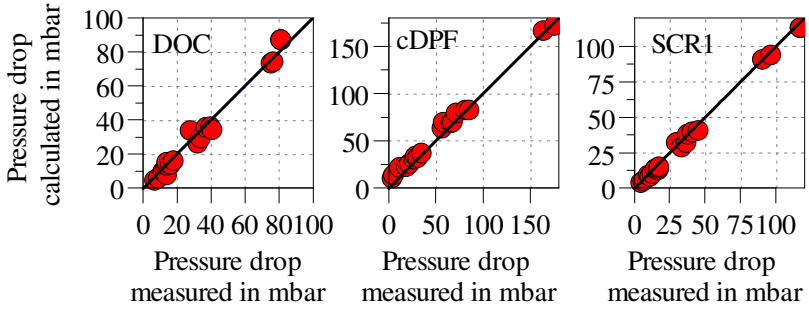

Figure 3.6: The pressure drop of the DOC, cDPF and SCR catalyst for different mass flow rates at various temperatures

The results of the previously described test procedure for the calibration of the catalyst reactions is shown in Figure 3.7 for the DOC and the cDPF at two

different engine speeds. For the DOC, the load was increased from towing to a BMEP of 6 bar at an engine speed of 1750 rpm, and for the cDPF the target BMEP is 3 bar at 1500 rpm. In the upper plots, the temperature development after the components is illustrated. The thermal inertia of the components, their cell density and the heat transfer rate determine this temperature.

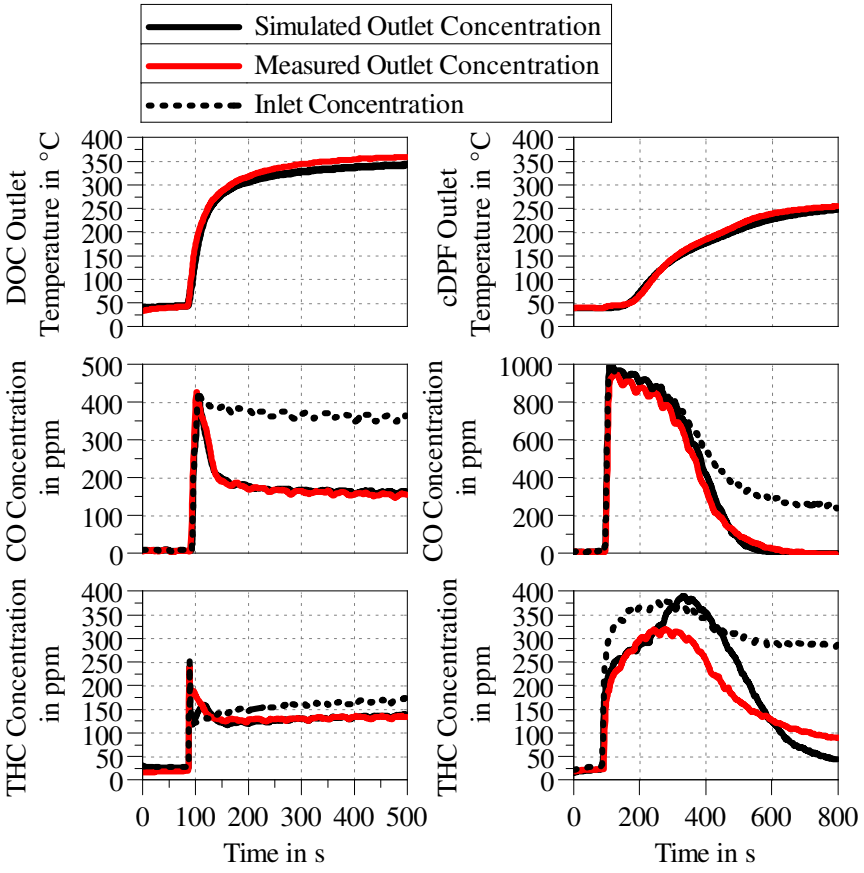

Figure 3.7: Outlet temperature, CO concentration and THC concentration after the DOC (left) and cDPF (right)

The temperatures do not match perfectly, but the first temperature gradient

does. The small deviation becomes apparent after some time. The reason for this might be a different mass flow rate that could not be measured precisely. During the temperature rise, the output CO concentration of simulation and measurement are identical for the DOC (left plots). This implies that the temperature-driven CO oxidation is calibrated well. For HC, the output concentrations are similar, but there is a small difference in the first peak. This is the result of a different amount of adsorbed HC at the start. The HC oxidation rate is lower than the CO oxidation rate, and despite a hot temperature, they are not high enough to convert the entire CO respectively HC due to the small size of the DOC. For the cDPF, the output temperatures are almost identical between the simulation and the measurement. For this case, the temperature rise is lower, which extends the warm-up time. In the simulation, the CO concentration after the cDPF is again very similar to the measurement. The largest difference occurs for the HC output concentrations. Here no optimal calibration parameters could be found to match the measurement. The difficulty is that all types of HC are measured as total hydrocarbons (THC). For their modelling, they are split into partly oxidised HC in the form of propylene (C_3H_6), unburned absorbable HC and unburned non-absorbable HC. Assumptions for the split of the THC into single species have to be made, which are explained in section 3.4. Each of these species has a different set of calibration parameters for the oxidation that determines the temperature-dependency and the overall reaction rate. Additionally, the adsorption and desorption rates have to be considered. Too many uncertainties make it difficult to find the correct calibration parameters. However, the coarse tendencies of the HC oxidation are represented in the model. For the calibration of the SCR reactions, no data was available. Therefore the default calibration values are chosen.

3.4 Emission Models

For the prediction of raw emissions, a data-based empirical model approach is used in the form of an artificial neural network (ANN). This approach has already been successfully applied for the emission prediction of diesel internal combustion engines in several other projects [60][67][38][16]. Artificial neural networks act as "black box" models that teach themselves non-linear relation-

ships between input variables and output target values. For this purpose, datasets of the input and the output are analysed and set into relation. The data required for this procedure (input and output variables) were generated in a design of experiment (DoE) on the test bench. In order to be able to predict emissions as accurately as possible, even under transient conditions, the characteristic values rail pressure, boost pressure, and the EGR rate were varied in the DoE in addition to engine speed and torque. Complementarily, the injection timing was modified to obtain a variation in the combustion process. About 220 data sets were generated in this way, with each of the points being analysed three times to compensate for measurement inaccuracies.

An ANN generally consists of three different types of layers: An input layer, at least one hidden layer, and an output layer. Each layer consists of a certain number of nodes. The number of input variables determines the input layer's size, and accordingly the number of output variables determines the size of the output layer. However, the size and number of hidden layers are flexible.

With the choice of the input variables, all notable effects of the emission formation should be taken into account. The engine speed is generally a measure of the residence time of the gas in the cylinder. Additionally, the indicated mean effective pressure (IMEP) and the injected fuel mass are set as input parameters. Especially for the NO_X formation process, the peak temperature is an essential factor and chosen as an input. The air to fuel ratio is a parameter of the apparent oxygen amount required for complete combustion and the NO formation. A high rail pressure increases the fuel atomisation and turbulence in the cylinder, which results in a higher homogenisation and fewer locally rich zones, in which the HC and CO formation takes place. Furthermore, with the mass fraction burned 50 % and the burn duration, the characterisation of the combustion process is completed.

The ideal number of layers and nodes per layer depends on the examined problem. Anyway, there exists no theory or method for the perfect net architecture for a given problem. Thereby, the ideal net architecture must be determined by trial and error [7]. In each node, the inputs are multiplied by a weight and then summed up or multiplied before the signal is passed forward to the activation function. Examples of activation functions are the logistic-sigmoid and the saturating-linear function. These functions make the

model behave nonlinearly. Besides the activation functions and the structural design of the network, the training function is crucial for the performance of the model. In this work, the training of the network was carried out with the Levenberg-Marquardt backpropagation. The data sets were split into 75 % training data, 12.5 % test data, and 12.5 % validation data to train the network.

Training with the training data sets only would lead to overfitting, which reduces the predictive power for unknown points. The independent test and validation data sets prevent the training algorithm from overfitting because the net is constantly checked with the independent validation data sets. It is determined how well the network handles data that it does not yet know. The test data is a second independent data set that is required at the end of the training to evaluate the quality of the neural network.

To select the best possible structure for the ANN, a variation of its architecture was performed. The number of hidden layers, their size, the activation function, and the input functions were varied and evaluated based on the test results. The input and output variables are normalized to the same range. This avoids numerical inaccuracies that are possible when the value ratios of the variables are high. For each emission type (THC, NO_X, and CO), a single neural network is set up. Their structures are summarized in Table 3.3.

Table 3.3: Structure of the neural networks for emission prediction

	NO	NO_X	THC
Number of hidden layers	2	2	2
Number of perceptrons per layer	40/17	38/37	32/40
Activation function	tansig/tansig	logsig/tansig	logsig/purelin
Input function	netsum	netsum	netsum

For the prediction of all types of emissions, a net with two hidden layers shows the best performance. The number of perceptrons per layer varies between 32 and 40. The neural network for CO prediction uses a hyperbolic tangent sigmoid transfer function (tansig) for both hidden layers. The net for the NO_X emission has the log-sigmoid transfer function (logsig) in the first hidden layer and the tansig in the second. For the THC, the logsig in the first and a linear

transfer function (purelin) showed the best results. For all emissions, the sum net input function was chosen. Although the structure of the three nets seems similar, the performance could be enhanced by generating a separate net for each single emission type.

The soot emissions are modelled with a two-zoned model [25]. Soot is formed in locally rich zones due to the lack of oxygen for complete combustion. Since the direct injection of diesel engines engenders a high mixing in the largest part of the cylinder, enough oxygen for complete combustion is apparent, and only a small portion is contributing to the soot formation. The soot formation is inversely proportional to the turbulence speed. In the burned zone, the formed soot is partially oxidised. This oxidation process depends on the total soot mass and the oxygen concentration in the burned zone. This model was later extended for the transient soot emission prediction considering the influence of the wall temperature on soot creation [24].

In this work, the focus is set to the different behaviours of various exhaust gas aftertreatment systems. For this purpose, the emission models do not have to predict the absolute amount of emission exactly, but emissions formation tendencies. The pre-turbine EAT affects the boost pressure development and backpressure in the exhaust manifold. Therefore the PTS influence the combustion conditions and, thus, on the emission formation process. Compared with a map-based emission model, the chosen approach with a multi-input ANN can predict emissions also during transient operations. Additionally, the temperature influence is considered, and more accurate predictions during the warm-up are expected.

Validation of the EAT Components

Figure 3.8 visualises the predicted emissions by the neural networks compared to the measured emissions representing the target values. The complete data set is plotted, which means that training data, validation data, and test data are shown. Since test data was never used during the training process, they indicate how the neural network acts with unknown operating points. The concordance between prediction and measurement is satisfactory for all emission types, and no large deviations are visible, even for the training data set.

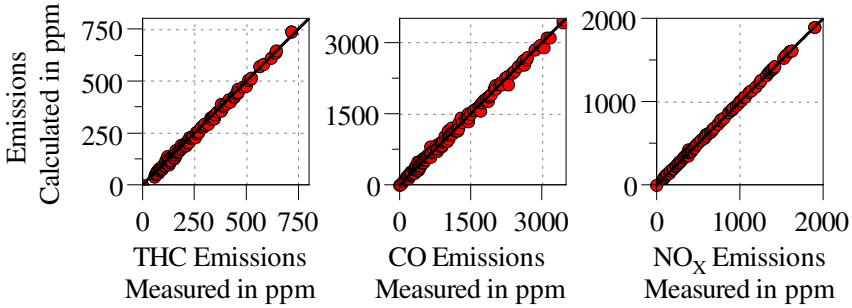

Figure 3.8: Predicted emissions vs measured emissions for all 220 data sets (training data, test data and validation data)

The NO_X prediction shows the highest agreement for most points. As summarised in Table 3.4, the maximal deviation is slightly higher than for THC, though. The THC prediction has no outlier, but the mean absolute deviation is larger despite a lower maximum concentration. The CO prediction is the less precise one, but the range in which the CO emission varies is the largest. No clear outlier is visible for any types, which demonstrates that the models provide reliable results for the entire test space.

Table 3.4: Deviations of the neural networks for the emission prediction

	NO	NO_X	THC
Mean absolute deviation	24.5	4.7	10.6
Standard deviation	38.6	7.1	12.1
Maximal deviation	167.2	49.3	29.5

3.5 Longitudinal Vehicle Model

For the simulation of driving cycles, a target vehicle speed is defined. A driver template controls the accelerator pedal position to match the demanded target speed. The pedal position is converted into a target torque dependent on the

engine speed, and the fuel injection rate is determined by the target torque. The engine's torque is transferred by a 9-gear transmission and a clutch to the driveshaft. The shifting strategy of the gearbox is kept simple as a function of the vehicle speed. When a particular value is exceeded, the gearshift is carried out. Additionally, a start-stop-system was implemented to switch off the engine when the vehicle is standing still. The vehicle model was set up based on a Mercedes-Benz E-Class regarding its mass, drag and drivetrain inertia [29]. The driving resistance is composed of the slope, air resistance and friction. Depending on the torque, the vehicle slows down or accelerates.

In a real passenger car, various effects occur that increase the heat transfer at high vehicle velocities. However, some measures are undertaken to keep the heat transfer low. In the simulation model, no relation between the heat transfer and the vehicle speed was made, and no additional isolation was modelled to maintain the simplicity of the model.

4 Simulation Scenarios

This chapter provides detailed explanation of the set-up of the simulations. The examined pre-turbine configurations, transient measures for compensating the dynamic loss and the test-scenarios are described.

4.1 Investigated Pre-Turbine Configurations

The PTS Stages only differ in the pre-turbine components and the order of the components. The common points of all PTS are:

- The size and chemical characteristics of the components stay the same, except for PTS Stage D, for which an sDPF and a larger DOC are examined
- The position of the high-pressure EGR branch is upstream of the first pre-turbine component
- The position of the low-pressure EGR branch is after the second SCR catalyst (SCR2)
- The underfloor SCR catalyst (SCR2) stays in its position
- Upstream of each SCR catalysts, an injector and mixer are placed. The target value for the amount of stored ammonia is different from that of the reference system
- The engine application is kept unchanged (target boost pressure, EGR rates)
- Pipes before the compressor and after SCR2 are kept unchanged
- The turbocharger maps are the same for all variants
- No restrictions in terms of available space or the arrangement relative to the engine are made

PTS Stage A represents the borderline case, for which all components except the SCR2 are arranged in a pre-turbine position. This increases the volume and thermal inertia before the turbine to a maximum. Figure 4.1 is a schematic illustration of this PTS with the EGR branches.

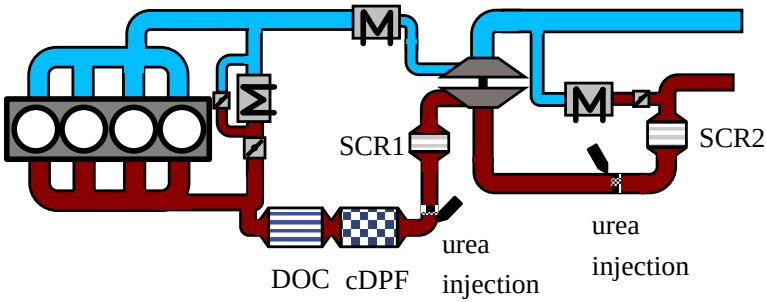

Figure 4.1: Schematic drawing of the engine with the pre-turbo exhaust gas aftertreatment system Stage A (PTS Stage A)

The pipe geometries between the compressor and the intake manifold are adopted to match the set-up of the test bench. A certain distance between the urea injector and the SCR1 is required to ensure sufficient mixing of the urea with the exhaust gas. This is necessary to achieve a high amount of ammonia out of the urea. However, the mixing process is not modelled within the 0d/1d simulation. Instead, a homogeneous mixing over the cross-section is assumed, and only the urea decomposition is modelled. The order and types of the pre-turbine components of each PTS are summarized in Table 4.1. Additionally, the pre-turbine volume of each variant is declared.

Table 4.1: Summary of the examined pre-turbine exhaust gas aftertreatment systems

Name	Pre-turbine components with the respective order	Pre-turbine volume in l
PTS Stage A	DOF-cDPF-SCR1	7.55
PTS Stage B	DOC-SCR1	4.00
PTS Stage C	SCR1	2.91
PTS Stage D	DOC-sDPF	6.03

In contrast to PTS Stage A, the entire intake path is the same as for the reference system for the other PTS. PTS Stage D is built up with different exhaust gas aftertreatment components: The size and cell density of the DOC have risen,

but the catalytic coating of the DPF was replaced by a selective one and SCR1 drops out. The geometrical data of the new components are summarised in Table 4.2. The amount of the stored ammonia within the selective catalytic surface does not influence the pressure drop.

Table 4.2: Summary of the geometrical characteristics of the components of PTS Stage D

	DOC (circle)	sDPF (circle)
Length in mm	100	152
Diameter in mm	140	143
Volume in l	0.822	2.084
Cell density in cpsi	400	300
Cell type	triangle	square

4.2 Transient Measures for Compensation of the Dynamic Lag

The larger volume and thermal inertia before the turbine result in transient shortcomings: the time until the turbocharger provides enough power to achieve the target boost pressure is increased remarkably. The growing grade of electrification increases the possibilities of countermeasures for the compensation of this dynamic lag. A broad range of countermeasures is considered; some of these are electrical, others mechanical-pneumatic.

4.2.1 Electrically Assisted Turbocharger

The electrically assisted turbocharger (EATC) operates like a standard turbocharger, but an electrical motor is connected to the turbocharger shaft. It supports the turbocharger in accelerating the shaft when required. Implementing an EATC in the engine model does not require any changes in the gas flow path, but the turbocharger shaft inertia is assumed to be 10 % higher than that of the standard turbocharger [58]. Its maximum power is restricted to 7 kW, and the maximum rotational speed is 150.000 rpm. Even a light hybrid passenger

car can provide enough electrical power to satisfy this power demand. Since the motor is able to act as a generator as well, a recuperation operation is possible to slow the turbocharger down. To make the results more comparable with the reference system and the standard VGT turbocharger, the EATC of this investigations has a VGT. The efficiency maps for compressor and turbine are the same as that of the reference turbocharger.

During the examinations of PTS in driving cycles, the described measure is only activated during strong accelerations to keep the required extra power and energy as low as possible. Hence, the acceleration pedal position must be greater than a value of 50 % to initiate a boost event. Additionally, the difference between target and actual boost pressure must exceed a value of 70 mbar.

4.2.2 Electric Driven Booster

Another possibility to improve the transient response is an electric supercharger. It is an electrically driven compressor that can work in parallel or series with the standard turbocharger. In this work, it is placed in series after the charge air cooler and before the high-pressure EGR inlet junction. When not in use, the intake air flows through a bypass valve to reduce the flow resistance. In contrast to the EATC, changes in the intake path are required, but the turbocharger remains the same. Its maximum power is 7 kW, and the top rotational speed is limited to 70.000 rpm. Since the compressor wheel diameter is 65 mm, it is larger than that of the turbocharger, and the compression power at the maximum speed is similar.

4.2.3 Mechanical-Pneumatic Countermeasures

For the improvement of the dynamic response, mechanical-pneumatic systems use air injections at different engine spots: on the intake side, directly in the cylinder, and on the exhaust side before the turbine. It was shown that an air injection on the intake side inhibits the pressure increase by the turbocharger because the high-pressure peak in the intake manifold counteracts the acceleration of the turbocharger [15].

The air injection into the cylinder is the most complex option because an additional valve is required on the cylinder head. Furthermore, the timing of the valve opening is more challenging than for a simple air injection in the exhaust manifold. In Figure 4.2, the timing of this boost valve is shown for two different maximum lifts. The additional air is injected when the intake valve is closing, at the beginning of the compression. In this manner, the air mass in the cylinder is increased, allowing a larger fuel mass to be injected. Due to the late opening of the valve, no air is flowing backwards into the intake manifold.

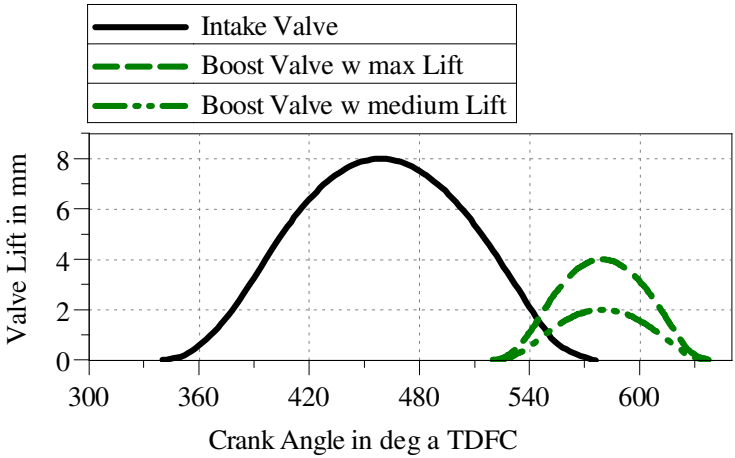

Figure 4.2: Lift timing of the air injection system directly into the cylinder

The pressure tank for the compressed air has a volume of 6 l, and the maximum pressure of it is 15 bar, according to previous investigations [13]. The boost valve lift is variable to control the amount of additional injected air. Once the tank's pressure level is too low, the system needs to be recharged before it is usable again. This is done during towing phases when no fuel is injected. The boost valve is opened at the end of the compression. Thus, the compressed air is flowing into the tank.

The second considered air injection to enhance the transient response is placed upstream of the turbine – and after possible pre-turbine EAT components. The higher pressure before the turbine accelerates the turbocharger, and the boost

pressure is increased more rapidly. For this system, the boost valve is opened independently from the crank angle position. The high-pressure tank has a volume of 4 l, and the maximum pressure is 18 bar, corresponding to [15]. It is charged externally with an electric compressor. Due to the higher pressure in the exhaust tract, higher pumping losses are expected.

4.2.4 Post Injections

In order to increase the exhaust temperature and thus the enthalpy before the turbine, post injections (POI) are examined. Early POI burn in the cylinder before the exhaust valve opens. The burn rate of an application with two POI is shown in Figure 4.3.

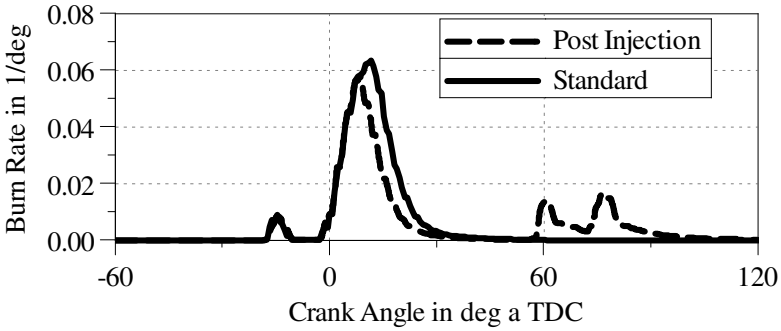

Figure 4.3: The burn rate of a standard injection strategy compared to applied post injections

Due to the late energy release, the torque is barely increased by a POI. Close to the full load, the total injected fuel mass is limited by the apparent fresh air. Thus, the main injection needs to be reduced in order to apply a POI. This results in a lower torque on the cost of a higher exhaust gas temperature.

A late post-injection is not burnt within the cylinder, but the fuel is ejected into the exhaust manifold. In a pre-turbine DOC, the fuel is then oxidised, releasing energy and increasing the enthalpy for the turbine. In this work, instead of a

late post-injection, an additional fuel injector at the exhaust manifold is used, which has the same effect.

4.2.5 P2-Hybrid

An electrical motor supports the engine torque on the driveshaft with a P2-hybrid configuration. Its maximum power is 70 kW. To apply this measure in driving cycles, a controlling strategy is necessary that is similar to that of the EATC: The difference between target and actual BMEP must exceed 0.7 bar, and the accelerator pedal position must be greater than 50 %. This ensures that the combustion engine delivers the main propulsion. The electrical motor is only activated when the power of the diesel engine is not sufficient. In this manner, an estimation of the minimal required energy amount for the compensation of the dynamic lag is made. The recuperation mode is activated during deceleration events. For the activation, the VGT turbine's rack position must exceed a value of 0.6, and the acceleration pedal value has to be 0 %.

4.3 Steady State Operating Points

The different EAT systems are examined and assessed in steady state operating points in order to detect one-dimensional effects. Fluctuations of the mass flow rate, pressure and temperature are resolved highly over the crank angle. The impact of the pre-turbine EAT components on the turbocharger is part of the investigation. Additionally, the influence of the conditions in the harsher pre-turbine environment on the chemical activity of the EAT is part of the examinations. Seven steady state operating points are chosen for the comparison of the PTS. In Table 4.3, the characteristics of these points are summarized.

Table 4.3: Characteristics of the chosen operating points for the steady state operation

Operating Point	Characteristic	Engine Speed in rpm	BMEP in bar
1	20 kW with the highest efficiency	1500	9.5
2	low load	1500	1
3	low-end torque	2000	21
4	max.load and high efficiency	2500	22
5	max. power	4000	19
6	highest efficiency	2500	20
7	medium load	3000	10

The operating points are selected to cover a wide range of the engine map. At these operating points, the interaction between pre-turbine components and the turbocharger is expected to be highest. For convenience, the points are visualised in Figure 4.4 with the isolines of the engine efficiency.

The engine usually operates frequently at points 1 and 2 during everyday driving without strong accelerations, covering most driving events. The low-end torque (point 3) is one of the most challenging operating points for the turbocharger since the mass flow rate is relatively low, but a high boost pressure is demanded. Points 4 and 6 show the effects on fuel consumption. The impact on the maximum power is delivered with point 5. Operating point 7 represents a smooth acceleration that is also achievable with a naturally aspirated engine.

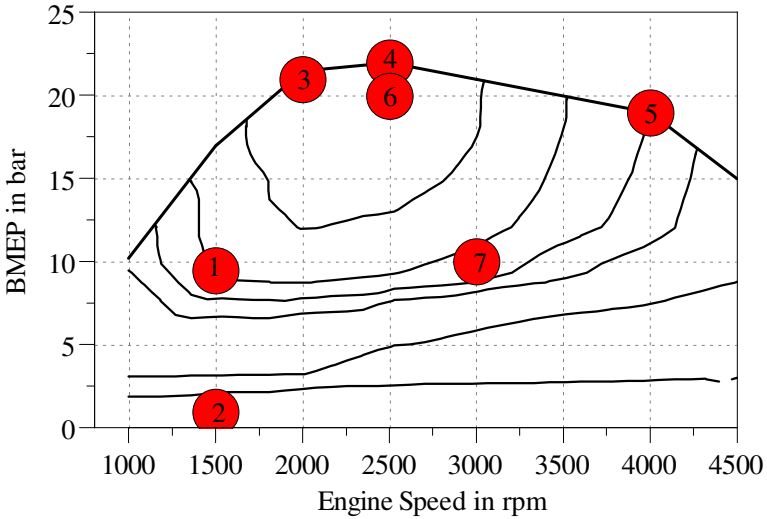

Figure 4.4: Steady state operating points in the engine map

4.4 Load Steps

The pre-turbine EAT components deteriorate the transient response. To make this delay quantitatively measurable and comparable, load steps are performed at two different engine speeds. Starting from a stationary point with a brake mean effective pressure of 0.5 bar, the target load is increased immediately to its maximum. At the same time, the engine speed is kept constant at 1500 rpm respectively 2500 rpm. In Figure 4.5, the conducted load steps are mapped. The dotted lines mark the evaluation point, which is 90 % of the target load. The time until this evaluation load is reached serves as the characteristic value for the comparison of the EAT systems. This point is set lower than the actual target load to prevent impacts of PID controllers that start changing their outputs shortly before the target is reached due to their differential part.

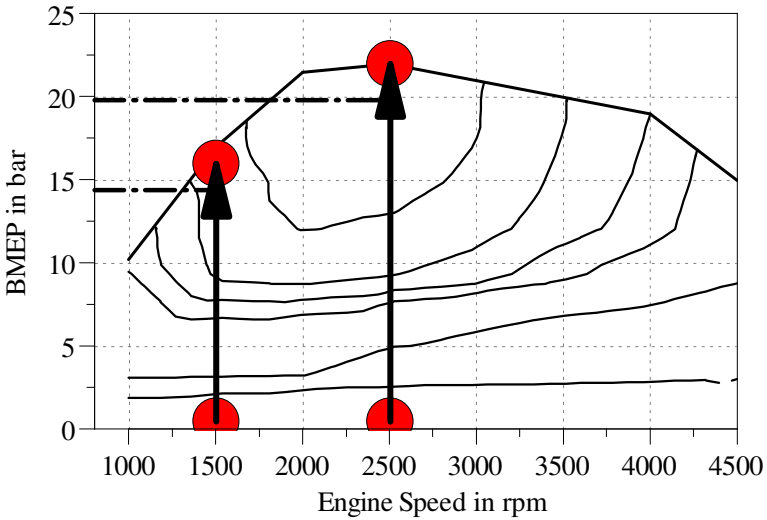

Figure 4.5: Engine map with the examined load steps and evaluation load

For the load steps, the controller for the target load, EGR rates and boost pressure are active. Their target value depends on the engine speed and the target load. In further investigations, the transient measures from section 4.2 are used to counterbalance the dynamic lag. The aim is to complete the load step within the same time as the reference system. That means that the support power is controlled to match the load curve of the reference system, respectively its boost pressure, although a faster load rise might be possible.

4.5 DPF Regeneration

The active DPF regeneration is triggered at operating point 7 from Figure 4.4 (10 bar BMEP at 3000 rpm). The exhaust gas temperature is increased by post injections and a shift of the main injection towards late. The injection rate and burn duration during the active regeneration are displayed in Figure 4.6 The pre-injection and main injection are shifted five degrees crank angle towards

late, and the mass of the two post injections is controlled to keep the DPF average filter temperature at 630 °C.

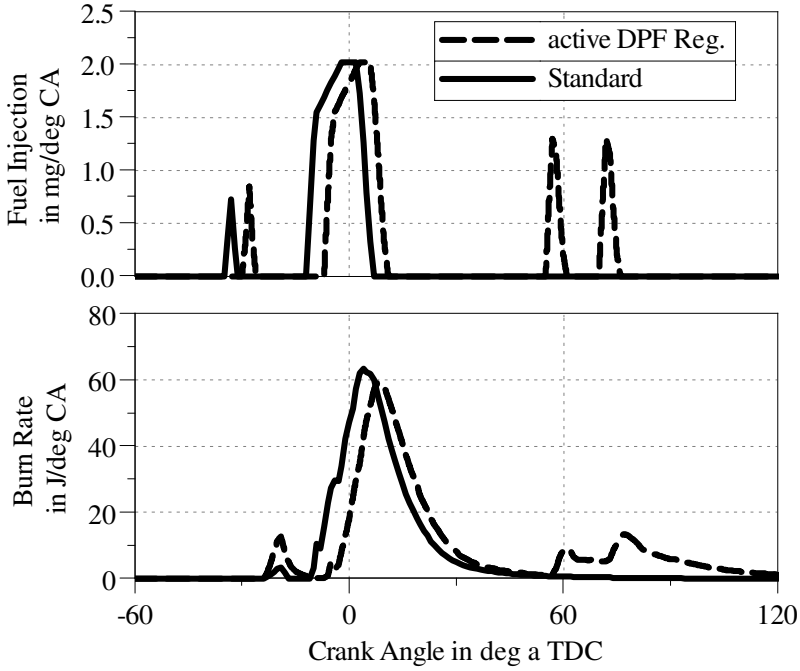

Figure 4.6: Injection pattern and burn rate of the active DPF regeneration mode compared to the standard

The aim of this scenario is not to accomplish the active DPF regeneration as fast as possible but to compare a pre-turbine DPF with a normal aligned DPF. Thus, the only PTS examined is PTS Stage A with a pre-turbine DOC, cDPF, and SCR1. Both systems are operated with the same regeneration strategy. The focus is on fuel consumption and the duration that is required to clean the DPF thoroughly. Besides the active, passive DPF regeneration is part of the investigation. Since it occurs continuously over a more extended period, it is not examined in a separate scenario but in the context of the driving cycles.

4.6 Cold Start

A cold start scenario is set up, in which the different EAT systems are studied regarding their warm-up performance. For the assessment, the time to reach a particular temperature and conversion rate is compared. At the beginning of this test scenario, the entire structure of the engine and the coolants have an ambient temperature of 25 °C. Starting from this state, a steady operating point with a constant BMEP of 3 bar is held at an engine speed of 1500 rpm. For the coolant temperature, a linear increase of 50 K/10 min is assumed, derived from [10]. The oil and coolant temperature determine the engine friction according to the Schwarzmeier-Reulein model. It is decreasing according to the temperature rise of the engine. Since the purpose is not to achieve a specific temperature in the shortest possible time, no particular warm-up strategies are applied to compare the systems.

4.7 Driving Cycles

For assessing the PTS and its support systems, WLTC and RDE drive cycles are simulated with the longitudinal model. In contrast to the described synthetic scenarios, the driving cycle simulations represent more realistic driving cases with real, time-dependent load requirements. For a better comparison, no warm-up strategies are applied.

4.7.1 Worldwide Harmonised Driving Cycle (WLTC)

The WLTC is mainly used to determine the fuel consumption of a powertrain system. Its velocity profile for light passenger cars is displayed in Figure 4.7. The cycle is split into low, medium, high and extra high velocity part. The drive is conducted in the flat, without any slopes.

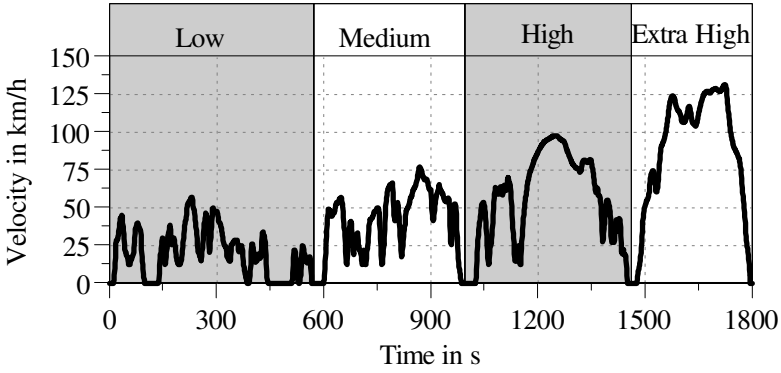

Figure 4.7: Velocity profile of the WLTC, split into single sections

The reference system is compared to PTS Stage A regarding engine efficiency, passive DPF regeneration, and the end emissions during the WLTC. The PTS is examined without any transient measure. At the start of the cycle, the engine is completely cold, similar to the cold start examinations with an ambient temperature of 25 °C.

4.7.2 Low-Temperature RDE Cycle

The aim of the investigation of the PTS during a low-temperature RDE is to make the boundary conditions as hard as possible regarding the EAT systems' warm-up. Therefore, an RDE profile was generated out of short measured driving sections that is characterised by:

- A long city part, mainly downhill
- Long standing times
- Moderate accelerations
- A low ambient temperature of 0 °C

The result is the velocity and altitude profile of Figure 4.8 that complies with the RDE dynamic limits. During the stop phases, the engine is switched off. The EATC was implemented for the considered PTS to make the conditions for the raw emission formation more equal. Additionally, the ability to follow the target

speed has higher accordance with the reference system, consequently. In this manner, the tailpipe emissions are mainly influenced by the EAT configuration.

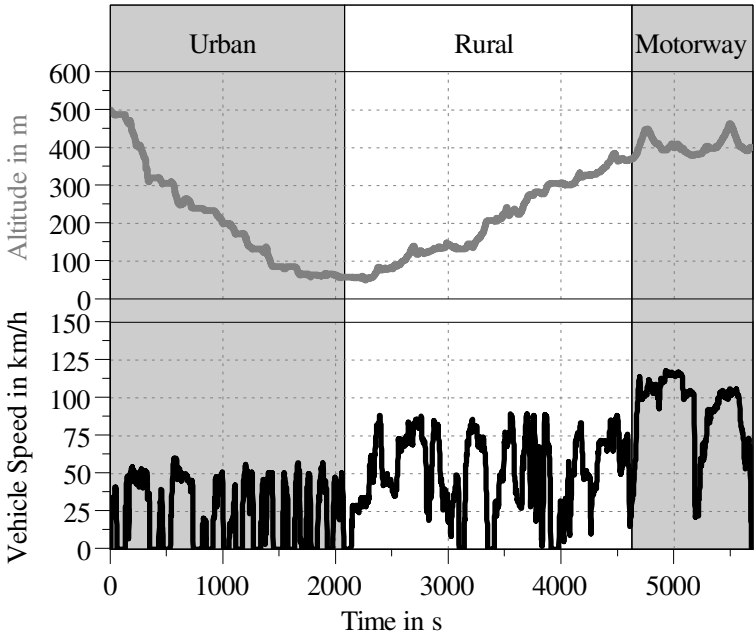

Figure 4.8: Velocity and altitude profile of the low-temperature RDE cycle

4.7.3 High Dynamic RDE Cycle

The high dynamic RDE cycle aims to estimate the required extra power and energy required for compensating the dynamic lag of the PTS. Hence, the borderline case of all components upstream of the turbine (PTS Stage A) is used in these studies. Representing the transient measures, the P2-hybrid and the EATC are assessed. They differ entirely in their characteristics: With the P2-hybrid, the torque is connected directly with the driveshaft. Therefore, the internal combustion engine and the electrical engine operate independently from each other. In contrast to this, the EATC does not increase the torque by itself but supports the charging system of the diesel engine. This affects the entire

air flow through the engine. Consequently, the combustion process, emission formation and conditions for the exhaust gas aftertreatment are changed.

In order to make the cycle as demanding as possible in terms of dynamic response, the cycle contains many strong accelerations. These are partly uphill, which increase the required power while complying with the dynamic limit. The profile of this cycle is presented in Figure 4.9. The focus is set on quick changes of load and boost pressure requirements during accelerations.

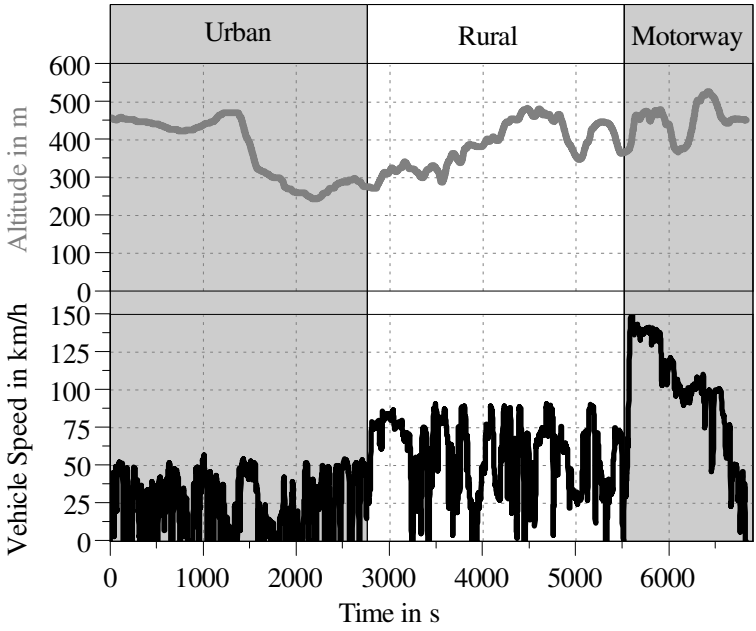

Figure 4.9: Velocity and altitude profile of the high dynamic RDE cycle

5 Results and Discussion

The in section 4.1 described PTS are first examined only changing the position of the EAT components. In the first part of this section, they are analysed under firmly defined boundary conditions. The isolated engine with different EAT systems is examined under steady state operation, during load steps at a given engine speed and during the warm-up at a given operating point. Additionally, a comparison of the active DPF regeneration is made between the reference system and the pre-turbine DPF of PTS Stage A.

The second part of this section deals with further modifications of the PTS to enhance the dynamic response and the warm-up of the EAT. For this purpose, a configuration with shortened pre-turbine catalysts is examined and the in section 4.2 described measures for the compensation of the dynamic lag are assessed.

In the final part, the systems are inserted in the virtual vehicle and subjected to test cycles like the WLTC and real driving emissions cycles. These tests show the applicability of PTS in passenger cars, as the drivability, fuel consumption, and tailpipe emissions are part of the investigation.

5.1 Standard Pre-Turbine Exhaust Gas Aftertreatment Systems

5.1.1 Steady State Examinations

The investigations on the PTS at steady state operating points are split into two parts: At first, the fluidic influence of the pre-turbine components and the interaction with the turbocharger is analysed. The second part focuses on the conversion behaviour under the changed pre-turbine environment.

Fluidic Influence and Interaction of pre-turbine EAT and Turbocharger

Since the SCR1 appears in a different position for each PTS, it is appropriate to illustrate the effects of a component's position. In the reference system, the SCR1 is placed after the turbine; in PTS Stage A, it is the third pre-turbine component, in PTS Stage B the second one, and in PTS Stage C the only pre-turbine component.

The operating points vary in engine speed and load, resulting in different mass flow rates, temperatures, and pressure levels. In Figure 5.1, some characteristic fluidic values of SCR1 are plotted. Operating points 1 and 2 have relatively low mass flow rates, and the differences before and after the turbine are small compared to the other operating points. The larger mass flow rate implies a higher boost pressure level achieved by increasing the turbine's pressure ratio. Thus, the SCR1 inlet pressure is remarkably higher in a pre-turbine position for all PTS at these operating points. Despite greater temperatures, the effect of lowering the exhaust gas density by the increased pressure is dominant. Operating point 5 (maximum power point) has the highest mass flow rate and SCR1 inlet pressure that causes for PTS Stage C a 1.5 times higher gas density compared to the reference system. This results in 1.5 times lower gas velocity. The pressure drop over a component is strongly dependent on the gas velocity. Thus, the pre-turbine EAT components benefit from their pressure drop at high mass flow rates compared to a standard positioned component. The temperature of SCR1 is lower, the more parts are placed before it because each element causes thermal losses. At operating point 5, the temperature of PTS Stage C is 19 K higher than that of PTS Stage B and 40 K compared to PTS Stage A.

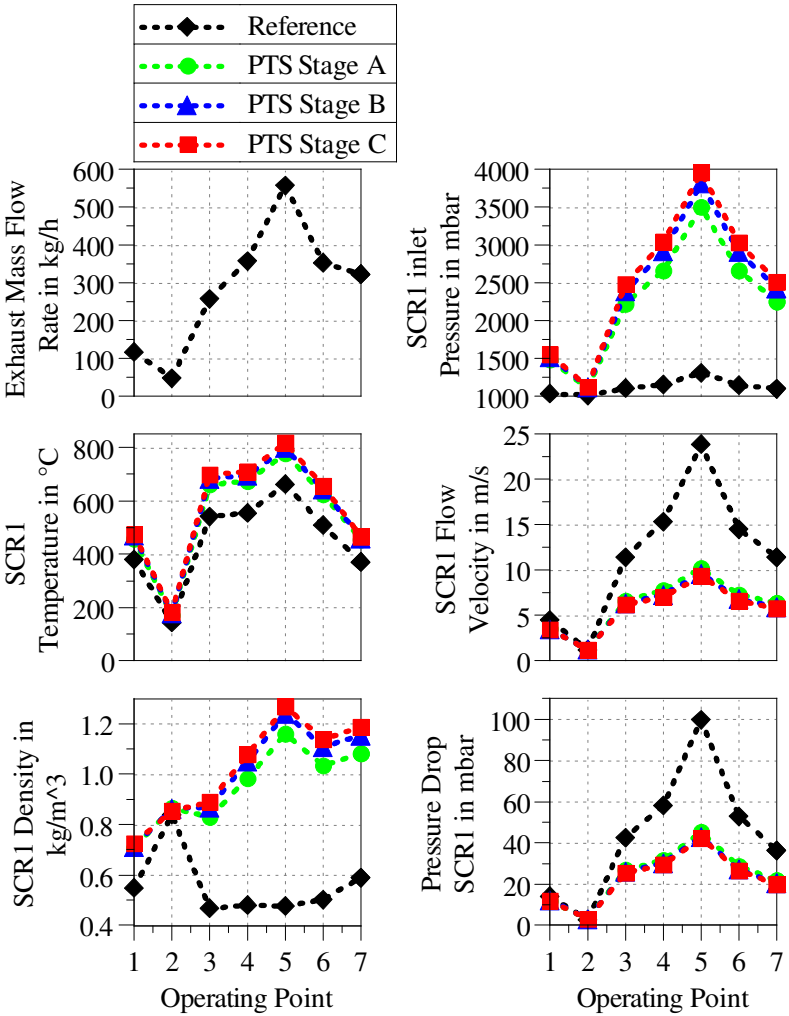

Figure 5.1: Flow values of the SCR1 during steady state operation

The pre-turbine components influence the pressure in the exhaust manifold. One reason for this was already described: Each pre-turbine catalyst has a lower pressure drop. The more components are placed before the turbine, the lower is

the total pressure drop and consequently the pressure in the exhaust manifold. Additionally, the switch of the location of the pressure drop from behind the turbine to the position before it reduces the pressure in the exhaust manifold even further: Considering the mean pressure in the exhaust tract at operating point 4 in Figure 5.2 coming from the tailpipe, the pressure is the same for all systems (ambient pressure). Moving further upwards to the turbine, the pressure after the turbine is lower for all PTS compared to the reference system because there are less EAT components. The more components are placed upstream of the turbine, the lower is the pressure at this position. To obtain the pressure before the turbine, the turbine outlet pressure is multiplied by its expansion ratio. Thus, the pressure difference after the turbine is multiplied by the pressure ratio to obtain the difference before the turbine.

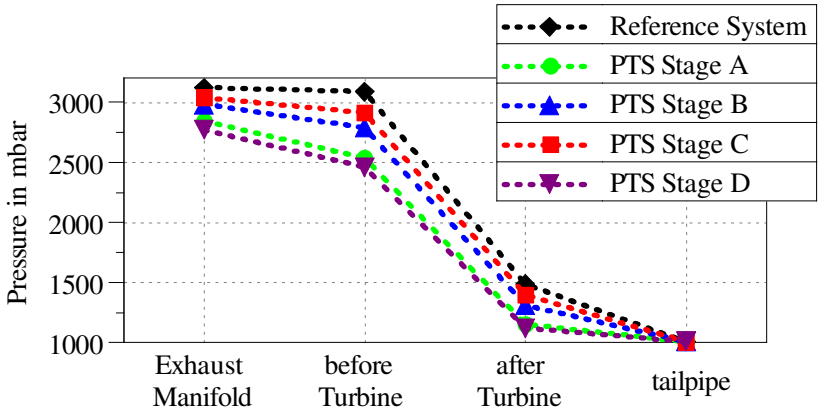

Figure 5.2: Pressure in the exhaust system at operating point 4

Moving further to the exhaust manifold, the pressure drop of the pre-turbine components is added for the PTS. This reduces the difference to the reference system. Anyway, the mean absolute pressure in the exhaust manifold is decreased the more pre-turbine components are applied. This effect is strongly dependent on the operating point and particularly dominant at high engine speeds and loads. At these points, a larger turbine's pressure ratio is required.

Low pressure in the exhaust manifold corresponds with reduced pumping losses. Figure 5.3 illustrates the difference between the reference system and the PTS regarding exhaust manifold pressure, pumping mean effective pressure (PMEP) and brake specific fuel consumption (BSFC).

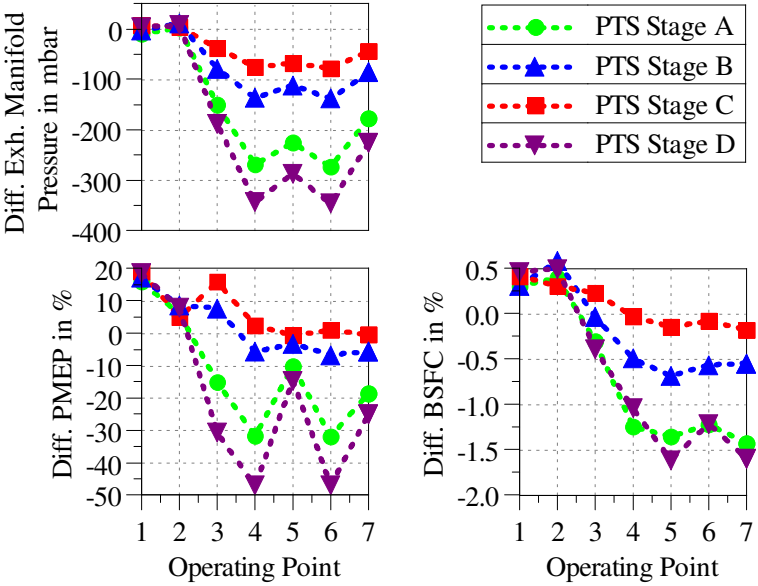

Figure 5.3: BSFC, mean pressure in the exhaust manifold and pumping losses for the steady state operating points. A positive value means that the reference value is higher.

The lower pumping losses of PTS Stages A and D at operating points 3 to 7 are the main reason for fuel consumption benefits. PTS Stage B shows this benefit only at higher mass flow rates, starting at operating point 4 that is smaller compared to PTS Stage A.

PTS Stage A and D show a peculiarity at operating point 5, where the boost pressure is higher than the target value despite a fully opened VGT rack position of the turbine, which is shown in Figure 5.4, along with the difference of the

pressure ratio over the turbine compared to the reference and the pressure after the turbine.

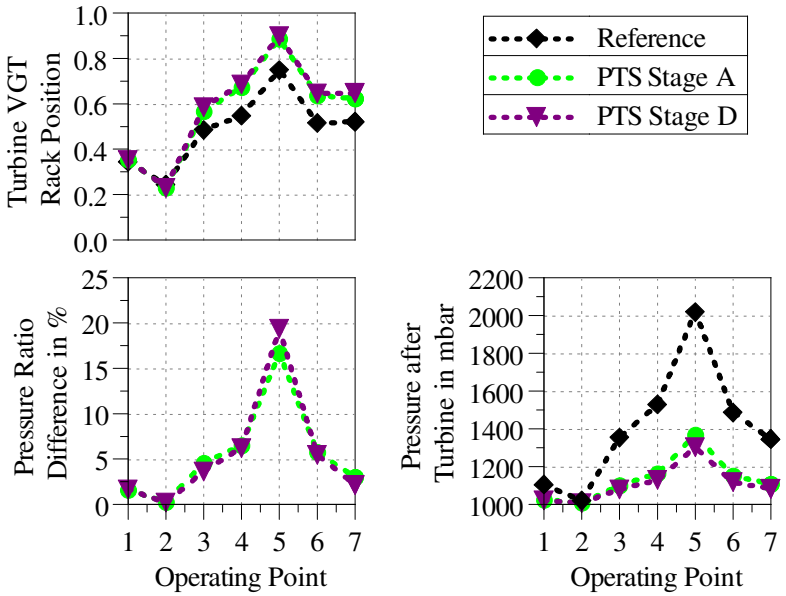

Figure 5.4: Pressure over the turbine with PTS Stage A and PTS Stage D compared to the reference system

Due to relocating the EAT components and their pressure drops, the pressure after the turbine is remarkably lower with the PTS. This pressure is determined by the pressure losses of the EAT components and the exhaust pipes up to the tailpipe and mainly depends on the gas velocity and is not controllable directly. By varying the rack position, the conditions upstream of the turbine are adjusted in order to obtain the target boost pressure. Opening the VGT rack position decreases the pressure upstream of the turbine and changes the turbine efficiency with its maximum at a rack position of approximately 0.5. At the considered operating point 5, the rack position is at the most opened position (0.9) such that the turbine pressure ratio cannot be decreased further. However, the boost pressure is above its target value. Consequently, the engine's

maximum power might be increased because the higher boost pressure increases the air mass in the cylinder. At the considered operating point, this leads to higher pumping losses and lower turbine efficiency. Alternatively, a larger VGT turbine could be employed to achieve a better turbine efficiency at maximum power. Additionally, the pumping losses are reduced due to a lower pressure ratio via the turbine, and a higher maximum power seems possible. However, a steady state operation at the maximum power is barely reached for PTS Stage A. A long drive at the full load is necessary to heat-up the entire exhaust tract and obtain the presented conditions, which does not occur in most real driving situations. A larger turbine increases the dynamic lag even further, such that the trade-off between dynamic response and fuel consumption gets greater, especially for the application in passenger vehicles.

Figure 5.3 further reveals that for PTS Stage C, the pumping losses are on the same level as that of the reference system or even higher at low engine speeds. In the first place, this does not meet the expectations since the average pressure in the manifold is lower. The reason for the larger pumping losses is the averaging of the pressure; for the pumping losses, the pressure level during the exhaust stroke is crucial. Figure 5.5 illustrates the development of the pressure fluctuations in the exhaust tract from the exhaust valve of the cylinder over the exhaust manifold to the pipe section before the turbine. The top plot also shows the valve lift of the corresponding exhaust valve. During the first phase of the open valve, the pressure of the reference system is higher. This changes at 235 ° after TDFC, where the pressure curves of PTS Stage A intersect with the reference system. In the following second phase of the open exhaust valve, the cylinder has to exert more work to expel the residual gas.

The central plot demonstrates that the smoothening of fluctuations happens already in the exhaust manifold by larger volumes for all PTS and all considered operating points. This has a retroactive effect on the pressure at the exhaust valve. For the PTS, the high-pressure peak only appears when the corresponding cylinder's exhaust valve is opened. This lets the mean pressure be smaller compared to the reference but has no benefits regarding the pumping losses.

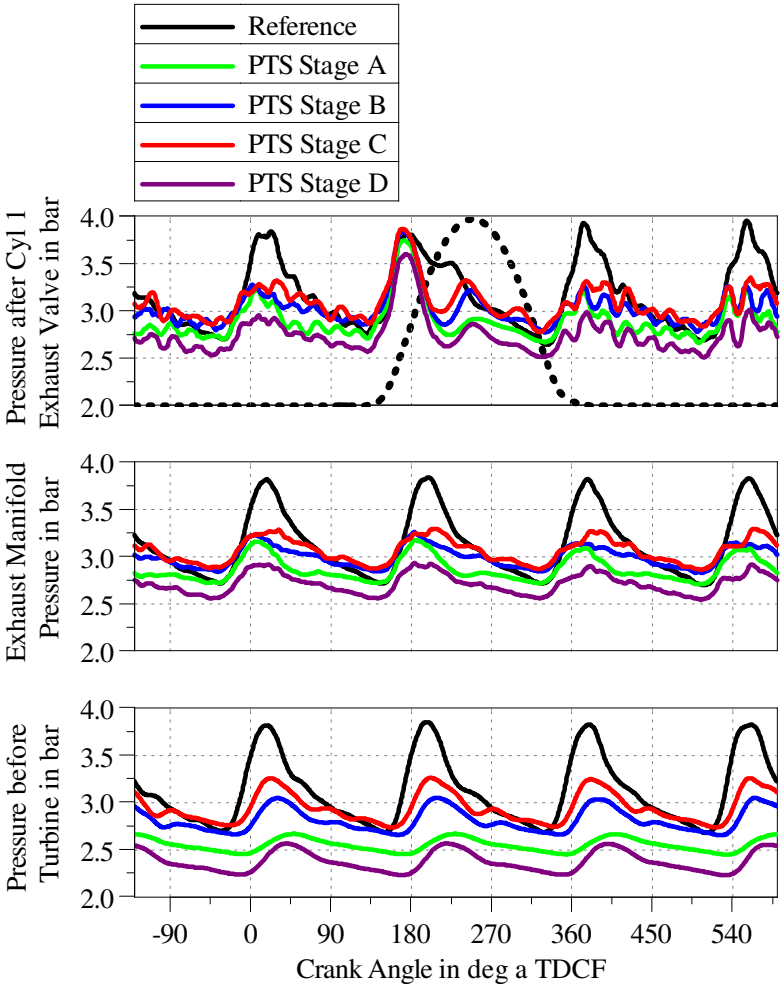

Figure 5.5: Pressure fluctuations at operating point 4 after the cylinder, in the exhaust manifold and before the turbine for all systems

The pressure fluctuations before the turbine in the bottom plot have the smallest amplitude for PTS Stage A. This displays that more components and a larger volume upstream of the turbine smoothen the pressure fluctuations. Furthermore,

the smoothening reduces the pulse charging proportion, especially for the low load operating point where the pulse charging effect is highest. For the reference system, the turbine's efficiency with pulse charging is 7 % higher than that of a steady state flow with mean values. At the same operating point, the pulse charging effect is for the PTS Stage A only 0.2 %. However, the smoothening of the pressure pulses influences the turbine only at low load and low engine speeds. At operating point 1, the pulse charging part is 1.1 % and for the others below 0.1 %.

Emission Reduction Performance of the EAT Systems

The primary motivation of placing the exhaust gas aftertreatment upstream of the turbine is to increase the conversion rates of the catalysts. Higher temperature and pressure levels favour the reaction rates of the catalysts. Furthermore, the longer resting time of the gas in the catalysts due to the higher gas density and lower flow velocities increases reaction rates.

Figure 5.6 visualises the conversion rates of CO, THC and NO_X and the comparison between the different systems. For CO and THC, there is no remarkable difference visible. The temperatures are too low to achieve remarkable conversion rates for all systems at operating point 2. The other operating points reveal a sufficient temperature for full conversion. This demonstrates that the operating points have a more significant influence on the conversion rate than the arrangement of the EAT components. The largest temperature differences occur at high loads and high engine speeds, as visible in Figure 5.1 for the SCR1 caused by the higher expansion ratio of the turbine. At these operating points, the temperatures are already high enough to achieve a full conversion, and a further temperature increase does not influence the conversion rates. In contrast to this, at lower loads, the temperature gap between a pre-turbine catalyst and the reference becomes smaller due to the lower expansion ration of the turbine.

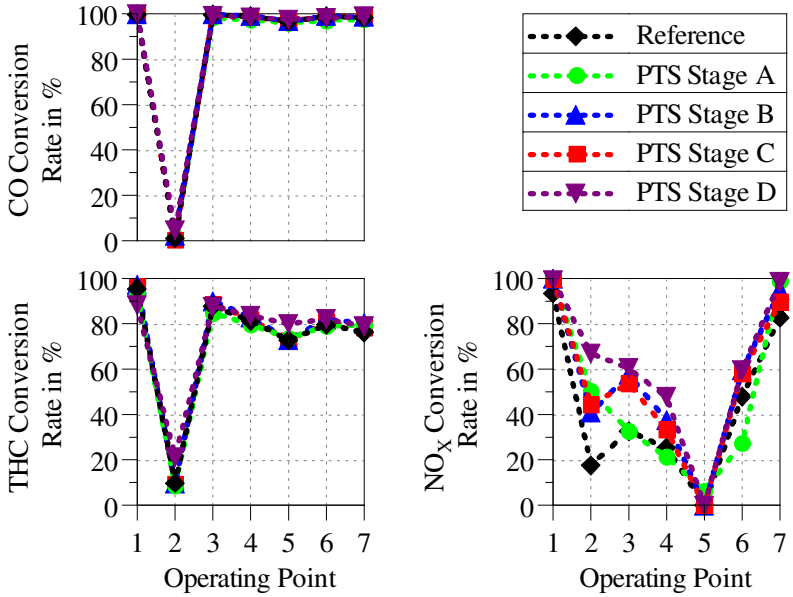

Figure 5.6: Conversion rates of CO, THC and NO_X for the different systems at steady state operation

The NO_X conversion differs between the systems: It is very sensitive to the temperature and the amount of stored ammonia in the SCR catalysts. To obtain steady state results, even with very long simulation durations, the amount of stored ammonia still varies. This causes small deviations between the systems. For operating point 2, it is visible that a pre-turbine SCR benefits from higher temperatures and has a higher conversion rate. At this operating point, the DOC before the SCR creates a further advantage because the NO_2/NO_X ratio is increased. An equal amount of NO and NO_2 is necessary for the fast SCR reaction dominating low temperatures.

Besides the temperature and the pressure, the resting time of a gas volume in the catalyst is a significant factor for the reaction rates. The longer a gas molecule remains in the catalyst, the higher is the probability that it gets in touch with the catalytic surface, where the reactions take place. The volume flow rate is an

indicator of the resting time of a gas volume in a catalyst. A low volumetric flow rate means that the part remains in the catalyst for a longer period. To figure out the different behaviour of the positioning of single components, the flow rate of SCR1 is plotted in Figure 5.7 for one work cycle.

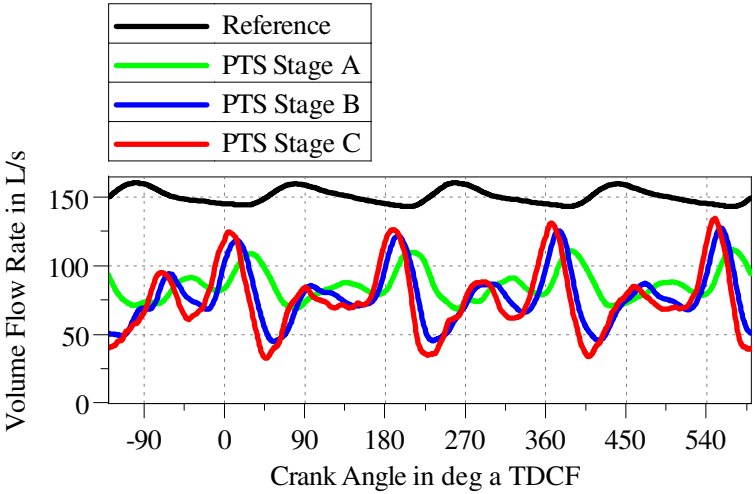

Figure 5.7: Volumetric Flow Rate of the SCR1 at operating point 7

The comparison between PTS Stage B and PTS Stage C reveals only small differences because the DOC is relatively short and has a low cell density. However, a slight timely shift and weakening of the peaks are visible for PTS Stage B. This effect becomes more significant when the DPF is placed before the SCR1, represented by PTS Stage A. The peaks are smoothened considerably, which indicates a more even flow through the catalyst. For the SCR system, a smooth gas flow is desired to avoid high velocity peaks that favour ammonia slip. A longer resting time in the catalyst reduces the risk of ammonia slip, as its adsorption has more time. The most significant contrast is visible for the reference system, where the volumetric flow rate of the SCR1 is the smoothest but on a higher total level. A lower gas density due to the lower pressure after the turbine is the reason for this.

The turbine benefits from the pulses, especially at low mass flow rates, where the pulses increase the effective turbine power by up to 7 % for the reference system. For the PTS regarding conversion rates, a smooth flow is desired so that the temperature, pressure and resting time in the pre-turbine catalyst are higher compared to a standard placed one. In the first pre-turbine component, the fluctuations are most severe. For the downstream placed components, the amplitudes of the oscillations are getting smaller, enhancing the catalyst performance.

Summary of the Steady State Investigations

Due to the higher gas density, the flow velocity in pre-turbine components is decreased, which causes a lower pressure drop over the component compared to the reference position after the turbine. Furthermore, to obtain the pressure in the exhaust manifold, the pressure drop of a component after the turbine is multiplied by the turbine's pressure ratio. In contrast to that, the pressure drop of the pre-turbine components acts singularly. Both effects reduce especially for large mass flow rates the pressure in the exhaust manifold that usually determines the pumping losses. However, it is shown that not only the averaged pressure level is important, but also the shape of the pressure fluctuations; in particular during the entire period when the exhaust valves are opened a low pressure level is desirable. This is optimised for the reference system, but not for the PTS, which is why the lower averaged pressure level does not necessarily lead to an advantage in pumping losses.

The EAT configurations with most pre-turbine components reached the most opened rack position of the VGT at the full load operating point. The low pressure after the turbine causes a high pressure ratio over the turbine that allows opening the rack. At this point, the boost pressure is higher than the target value, but the rack cannot be opened further.

Regarding the emission reduction, for CO and HC no significant difference is detected. At the low load operating points, the temperature differences between the pre-turbine components and the reference system are small. For high load operating points, the exhaust temperature is hot anyway and high conversion rates are achieved for all configurations. The second urea injector before SCR2 leads to a better controlling of the stored ammonia amount in the catalysts,

which increases the efficiency of the entire SCR system. Thus,NO_X reduction is slightly better for the PTS.

5.1.2 Load Steps

The previously shown steady state operating points require a long time to be reached with the PTS, particularly the high load operating points. This becomes clear when examining the results of the load steps. Figure 5.8 shows the development of the brake mean effective pressure (BMEP) during the load step at an engine speed of 1500 rpm. The delay is caused by the thermal inertia of the additional components before the turbine. PTS Stage A requires more than 40 times longer than the reference system to achieve the evaluation load of 90 % of the target.

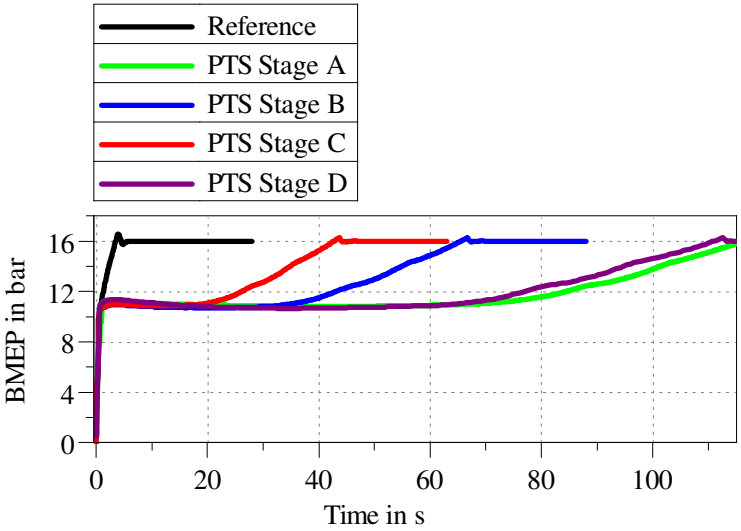

Figure 5.8: Development of the torque during the load step at 1500 rpm

The torque of a naturally aspirated engine is achieved instantly for all systems, that is approximately 11 bar BMEP. For a higher load, the turbine must deliver a higher boost pressure. The turbo lag is longer, the more components are

placed before the turbine. The pre-turbine SCR only, which is represented by PTS Stage C, shows a delay of more than 36 s, almost 13 times longer than the reference system. With an additional DOC (PTS Stage B), the required time is 21 times longer compared to the reference system. The cDPF, which is the difference between PTS Stage A and PTS Stage B, inhibits the boost pressure and the torque significantly. The required time is almost doubled between PTS Stage B and Stage A. This illustrates that the thermal inertia of the DPF is nearly equal to the DOC and SCR1 together. The thermal inertia of the pre-turbine components is the determining factor for the duration of the load step. The surface area that gets in touch with the exhaust gas is vast in the catalysts and the particulate filter, which leads to a high heat transfer from gas to structure. Therefore, with a PTS, it requires time until the hot exhaust gas reaches the turbine. This is demonstrated in Figure 5.9 by the turbine inlet temperature. The figure also shows that PTS Stage D is more compact compared to PTS Stage A, although in both systems, the DPF is arranged in a pre-turbine position.

The pressure ratio over the turbine and the turbine inlet temperature are the main factors to determine the boost pressure corresponding to the first turbocharger main equation (eq. 2.1). The correlation between increasing turbine inlet temperature and boost pressure is shown in Figure 5.9. When the turbine inlet temperature reaches a specific value, the turbine delivers enough power for the compressor. According to the inlet temperature, the pressure before the turbine is increasing.

During the load step, the VGT rack controller, EGR controller and fuel mass controller are kept actively. The VGT rack is set to the closest position at the start of the load step. Once the target boost pressure is achieved, it is opened slowly. During the period of the closed rack position, the pumping losses are heavier because the close position increases the pressure before the turbine. This increases the specific fuel consumption until the target boost pressure is achieved. The amount of injected fuel is adopted to the apparent mass of fresh air to keep the mixture in the cylinder lean but at the lowest air to fuel ratio possible. The air-fuel ratio is not increased before the target load is achieved. This leads to lower indicated efficiencies and is another reason for the higher fuel consumption due to the richer combustion.

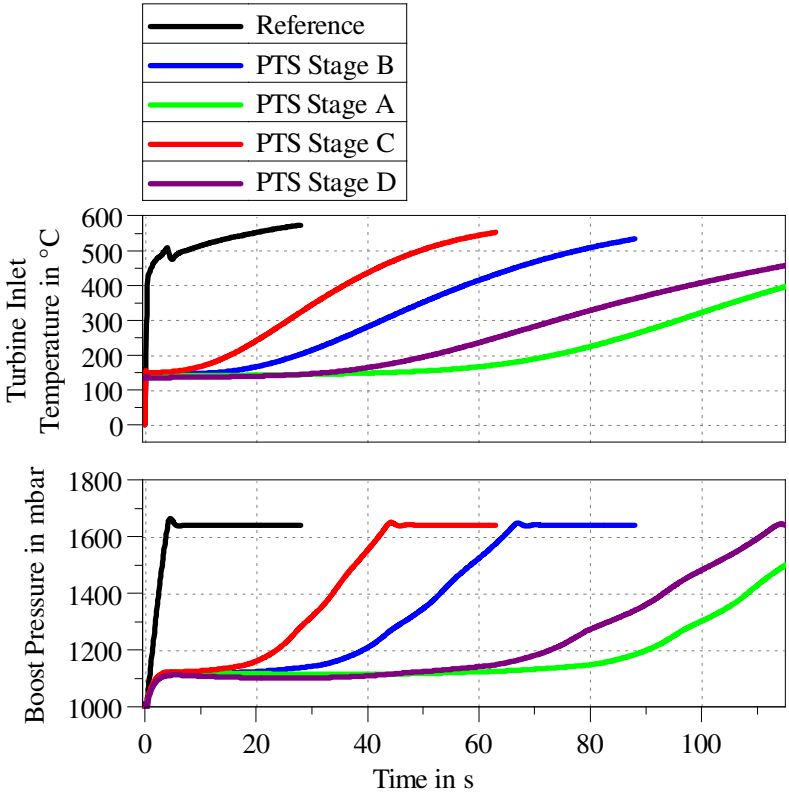

Figure 5.9: Development of the turbine inlet temperature and the boost pressure during the load steps at 1500 rpm

At higher engine speeds, the components' warm-up is accelerated due to a higher exhaust mass flow rate. Furthermore, the air mass flow rate is higher, increasing the fuel injection rates that correspond to the heat release. This reduces the time that is needed to reach the target load. The required times for all systems at both 1500 rpm and 2500 rpm are summarised in Table 5.1. The relative time reduction for the reference system is remarkably smaller than for the PTS, i.e. the reference system reaches evaluation load 2.6 times faster than at 1500 rpm. For the PTS, this factor is between 4 and 6.

Table 5.1: Required time to reach 90 % of the target load during the load steps at 1500 rpm and 2500 rpm, respectively

	Time @ 1500 rpm in s	Time @ 2500 rpm in s
Reference	2.6	1.0
PTS Stage A	111.5	27.7
PTS Stage B	56.8	10.0
PTS Stage C	36.2	6.8
PTS Stage D	103.2	21.9

The only considered PTS with only one EAT component upstream of the turbine is PTS Stage C. This is also the only PTS with the SCR1 placed as the first component after the exhaust manifold. Therefore, a closer look is taken on this PTS and some peculiarities are discussed. SCR1 has a higher cell density and larger cross-sectional area than the DOC that is the first component of all other PTS. Both aspects lead to a higher thermal mass and larger surface per length of the catalyst. The larger surface implies an enhanced heat transfer from the exhaust gas to the catalyst's substrate. These properties change the temperature distribution in the longitudinal direction of the catalyst. Compared to the DOC of the other PTS, the temperature gradient is remarkably steeper. Figure 5.10 exhibits the locally averaged temperature gradients over the catalysts that are calculated by the wall temperature difference from the inlet to the outlet divided by the length of the catalyst during the load step at 1500 rpm with an EATC for dynamic compensation. With the EATC, the results are more comparable with each other since the load step is completed simultaneously for all configurations.

For the DOC, the influence of the pre-turbine position can be derived by comparing the curves of the reference system with that of PTS Stages A or B. The maximal temperature gradient is more than 60 % higher in the pre-turbine position, causing more tremendous temperature-related stress on the DOC.

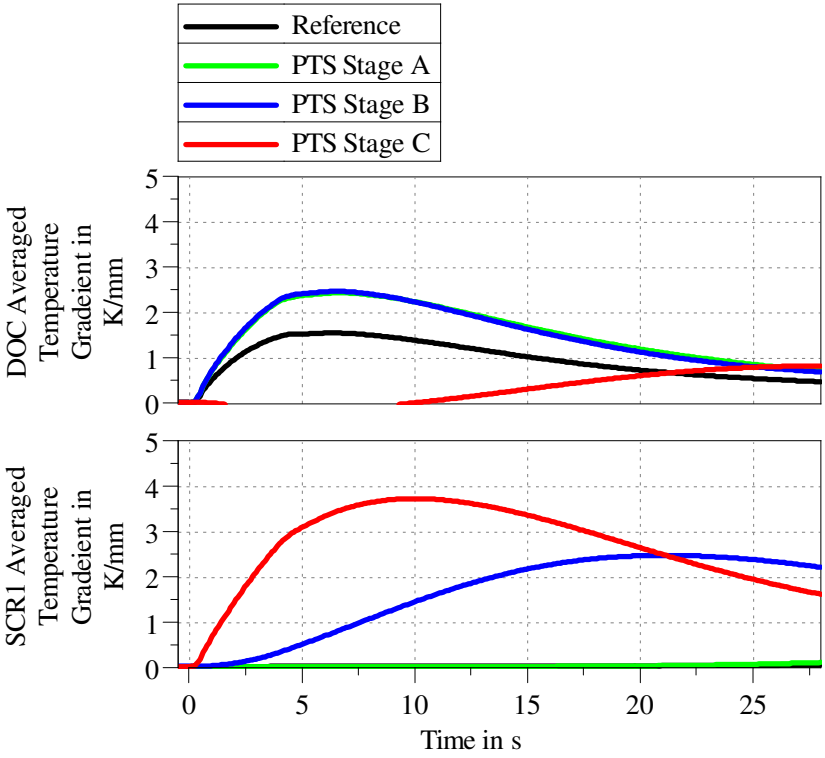

Figure 5.10: Longitudinal temperature gradients of the DOC and SCR1 during the load step at 1500 rpm

The different shape of the SCR1 with the previously described features causes an even higher maximum temperature gradient that is 1.5 times higher than that of DOC in the reference system. The SCR1 of the reference system has a very homogeneous temperature distribution because the upstream positioned large DPF reduces the temperature increase drastically. Under normal circumstances, SCR1 will never see such a temperature difference between inlet and outlet. Even when placed in the second position (PTS Stage B), the temperature gradient is still steeper than that of the DOC.

This example outlines the harsher conditions upstream of the turbine due to

higher temporal temperature fluctuations of several 100 K within a short period. This increases the risk of fracture due to thermal stress for the first pre-turbine component. SCR1 of PTS Stage C must be designed for constantly changing conditions, and its thermal durability must be guaranteed. One possibility to decrease the longitudinal temperature gradient is a lower cell density or a smaller cross-sectional area. The DOC combines both and shows a better temperature gradient during the load step.

The fast-rising temperature during the load step revealed another challenging aspect of PTS Stage C with SCR1 in the first position. In contrast to the DOC, an SCR system's temperature should not exceed 500 °C to avoid ammonia oxidation. Figure 5.11 presents the inlet temperatures of SCR1 and SCR2 during the load step with PTS Stage C. The exhaust temperature at the full load is too high, such that the SCR1 inlet temperature exceeds the upper temperature limit for the urea injection immediately. This makes the urea dosing strategy even more demanding. With the quick possible temperature changes, the target amount of stored ammonia changes in the same order. Above 450 °C, ammonia oxidation becomes an essential factor that reduces NO_X reduction performance. While the temperature of SCR1 is too hot to achieve high conversion rates, SCR2 experiences no remarkable temperature rise within the considered 40 s and stays below the lower temperature limit for urea injection. Thus, both SCR systems are not within the working window until SCR2 is heated-up or the load is reduced.

There are possibilities to keep the exhaust temperature lower and avoid ammonia oxidation. It has been proven that by increasing the boost pressure by 20 %, the exhaust gas temperature is lowered by at least 55 K during the entire load step. The higher amount of fresh air reduces the combustion temperature and the exhaust temperature. An EATC is able to provide enough power to increase the boost pressure to that level. Alternatively, a P2-hybrid could support more power than necessary to keep the combustion engine's load and the exhaust temperature low. This shows that the countermeasures are necessary to reduce the dynamic lag and have the ability to control the exhaust gas temperature. In the cold start examinations of section 5.1.4, the NO inhibition effect on the DOC and cDPF is exhibited. An efficiently working SCR before the DOC also has a positive impact on the CO and HC conversion rates. Thus, it is more critical to keep SCR1 within the temperature window than to speed up the

warm-up of SCR2. Overall, to operate PTS Stage C with the highest conversion rates, optimisation of several factors is required.

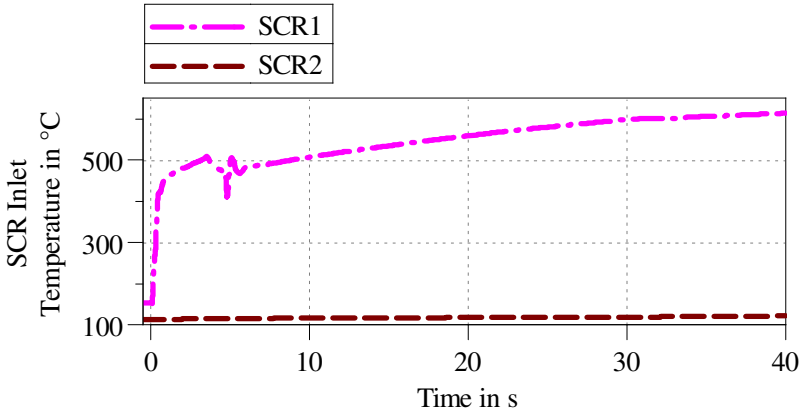

Figure 5.11: SCR1 and SCR2 inlet temperatures during the load step with PTS Stage C and an EATC

It shall be mentioned that with the SCR at the first position, the ratio of NO_2 to NO_X is lower compared to a system with an upstream DOC. Therefore, the fast SCR reaction is only occurring to a small extent. However, the warmer temperatures counteract this. Especially at low loads, the advantage of the quicker warm-up overcompensates the lack of NO_2, which was demonstrated with the cold start simulations. The NO_2 is also desired for passive DPF regeneration. If the upstream SCR reduces the NO_X, almost no passive regeneration will occur.

The examined load step simulations demonstrate that even for the smallest pre-turbine exhaust gas aftertreatment, the time to achieve a higher load than the limit for the naturally aspirated operation is too long. These long turbo lags are not applicable in a passenger car, even when the delay might be smaller for a warm engine and higher engine speeds. Thus, in section 5.2.1, various transient measures for compensating this dynamic lag are examined and assessed.

5.1.3 DPF Regeneration

PTS Stage A is the only considered PTS with the DPF upstream of the turbine, making it the only interesting PTS in terms of active DPF regeneration. It is compared with the reference system during a triggered active DPF regeneration by means of post-injections. Section 4.5 describes the applied injection pattern. The amount of fuel mass of the post injections is controlled to keep the average filter temperature between 600 and 650 °C at the steady state operating point of 3 bar BMEP at 3000 rpm. The DPF filter temperature and the BSFC during the first 320 s of the regeneration are plotted in Figure 5.12. At the beginning of the regeneration, the post injections are limited by the DPF inlet gas temperature that shall not exceed 630 °C. Despite the same DPF inlet temperature, the gas temperature in the exhaust manifold is 100 K higher for the reference system compared to PTS Stag A. The higher temperature is realised by larger post injections that cause a higher BSFC. The DPF filter temperature rises gradually until 600 °C is exceeded. In the following, the DPF temperature is kept within the range of 600 to 650 °C. The BSFC is alternating once the target filter temperature is set in. When the temperature is decreasing, it is increased by the post injections. The intervals are shorter for the PTS, during which the post-injection was applied because the jump of the exhaust gas temperature reaches the DPF more quickly and with fewer heat losses.

Almost the entire time, the BSFC is lower with PTS Stage A than compared to the reference system. The fuel consumption of PTS Stage A during the first 300 s is 1061 g, and with the reference 1168 g are injected. This corresponds to a fuel consumption benefit of 9.1 % for PTS Stage A to keep the DPF filter temperature above 600 °C. The oxidation of the soot by means of oxygen is an exothermic reaction that can increase the temperature clearly above the target temperature of this examination, especially when the target temperature for the regeneration is higher. The uncontrollable temperature rise is a possible risk of the pre-turbine DPF because it increases the turbine inlet temperature. If it gets too high, the VGT turbine might be damaged. However, a high temperature speeds up the regeneration process. Thus, a good compromise must be found, such that the turbine is not damaged, and the regeneration is conducted fast.

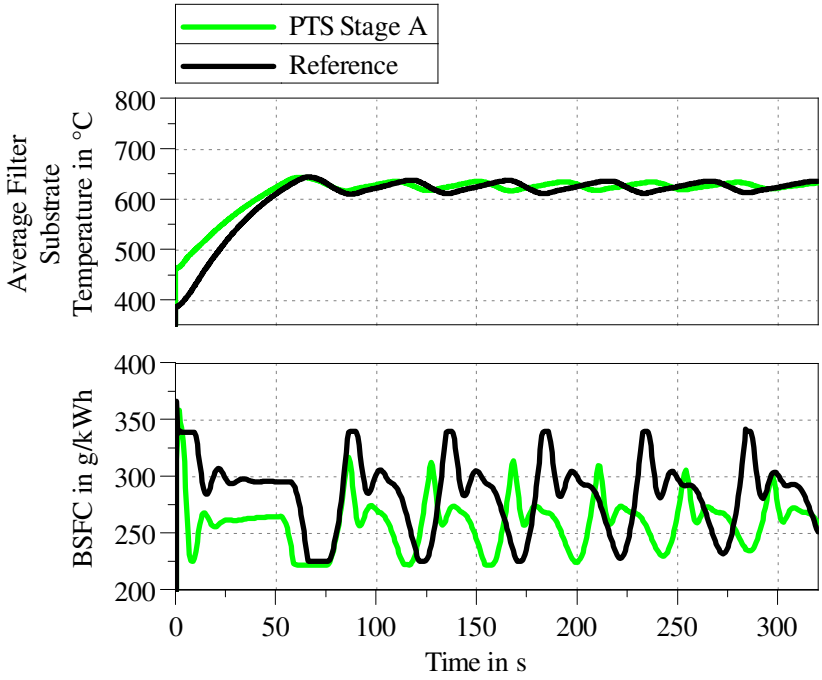

Figure 5.12: DPF filter temperature and brake specific fuel consumption during the active DPF regeneration for the reference system and PTS Stage A

The total soot amount in the filter during the regeneration process is visualised in Figure 5.13, starting with a filter loading of 51 g. The regeneration rate is higher with the DPF in the pre-turbine position, although the inlet and averaged filter temperature are the same. The pressure in the pre-turbine DPF is 0.9 bar higher compared to the reference positioned DPF. This is one reason for the higher soot oxidation rate. Additionally, the shorter intervals between the post-injections cause a more even temperature contribution within the DPF. This enlarges the area within the DPF, in which temperatures are high enough for soot oxidation.

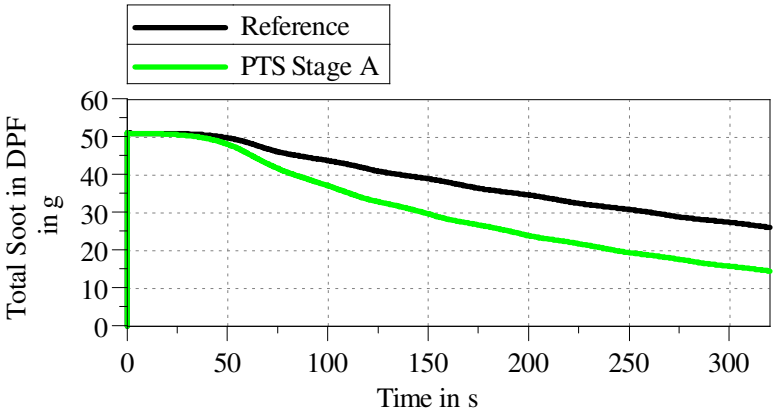

Figure 5.13: Development of the total soot amount in the DPF during the active regeneration

To assess the regeneration quantitatively, the required time and fuel for the oxidation of 20 g of soot is compared. With PTS Stage A, this point is reached after 140.5 s, which is 106.5 s faster than with the reference system. Assumed that the engine with PTS Stage A is operated in a normal mode afterwards, the fuel consumption after 247 s is evaluated, when the reference system has regenerated the DPF by 20 g. The reference system requires a fuel amount of 963 g during this period, and PTS Stage A shows an advantage of 15 % less fuel consumption with 818 g. This benefit is caused by the two effects of the pre-turbine DPF: The active regeneration proceeds faster and to obtain the same DPF filter temperature, smaller post-injections are required. The impact of the passive DPF regeneration that occurs already at lower temperatures in combination with high NO_2 concentrations is examined during the driving cycles in section 5.3.

5.1.4 Cold Start

The starting temperature for the cold start simulations is 25 °C, and a low load steady state operating point is chosen as described in section 4.6. At a BMEP of 3 bar, the temperature-dependent effects are demonstrated with large time scales

and small temperature gradients. This reflects the temperature-dependency of the EAT components. The emission formation rates are relatively low for all types and almost identical for all considered configurations at the operating point. Therefore, low reaction rates impact the tailpipe emissions and the conversion rates, and minor differences between the systems are reflected more clearly in the conversion rates. Besides, the lower exhaust mass flow rates enhance the emission reduction rates.

The temperature development of the DOC and the DPF is displayed in Figure 5.14. The DOC inlet temperature is highest for PTS Stage A, B and D. For the reference system, it is mitigated by the turbine that is placed upstream of the DOC. In the beginning, the thermal mass of the turbine delays the rise of the temperature. Once it is heated-up after approximately 100 s, the temperature difference of 25 K results from the temperature drop by the gas expansion over the turbine. This correlates to the temperature difference during steady state operation. PTS Stage C is the only system with the SCR1 as the first component. The DOC is the first post-turbine component, so its inlet temperature is remarkably lower during the entire cold start compared to the other configurations.

Considering the DPF inlet temperature, the difference between the positions of the DPF becomes visible in the comparison of the reference system with PTS Stage A. The temperature difference starts to increase after 40 s, and shortly later, the temperature gap is 25 K that stays persistent and is the consequence of the pre-turbine arrangement. With progressing time, the temporal temperature gradient becomes smaller. The pre-turbine DPF of PTS Stage D experiences the temperature rise later than the previously described systems. The longer DOC of PTS Stage D, that also has a higher cell density, has a larger thermal inertia that is heated-up first. This requires more energy than the heat-up of the smaller DOC. However, once the DOC is heated-up, the DPF inlet temperature rises and exceeds that of the reference system. After 450 s, the temperature is approximately 25 K above that of the post-turbine DPF.

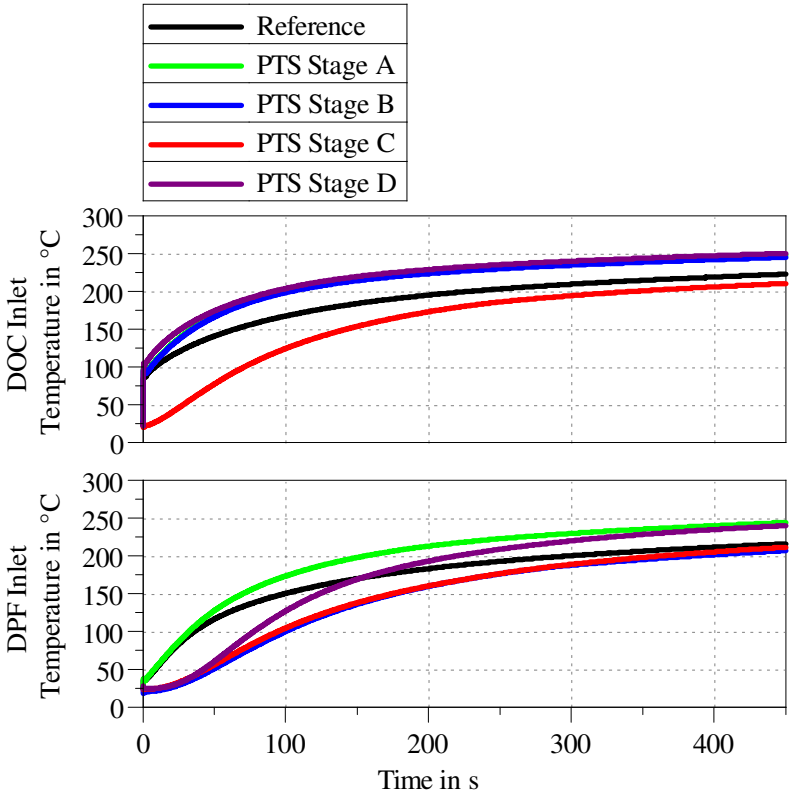

Figure 5.14: DOC and DPF inlet temperatures during the cold start phase

The DPF inlet temperature of PTS Stage B and Stage C are almost identical. In both systems the DPF is the third EAT component, after the DOC, SCR1 and the turbine. This indicates that the order of the components is less important for the following components. Only the number of upstream components and the placement regarding the turbine has a significant impact on the temperature. The temperature of PTS Stage B is slightly lower because the DOC has larger heat losses in the pre-turbine position than after the turbine of PTS Stage C. Additionally, the pressure ratio of the turbine is higher, which leads to a larger temperature decrease of the gas expansion. The temperature is one determining factor for the reaction rates of the catalyst. In Figure 5.15, the CO and THC

conversion rates of the EAT systems are displayed for the first 450 s of the cold start.

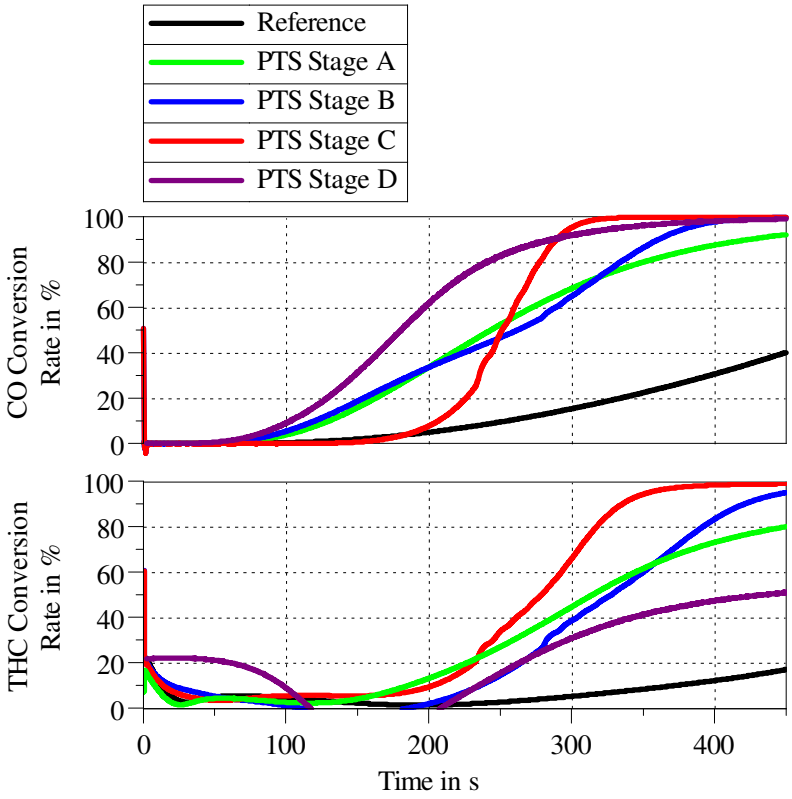

Figure 5.15: CO and HC conversion rate during the cold start

The CO conversion rate starts at this operating point when the DOC inlet temperature is higher than 200 °C after approximately 100 s for PTS Stages A, B and D. PTS Stage D shows the most elevated CO conversion rate due to its longer and denser pre-turbine DOC. The different shape of the catalyst increases the heat transfer from the exhaust gas to the catalyst. Therefore, the catalyst heats-up faster and its reactivity is enhanced. The second-fastest increase is monitored for the systems with the pre-turbine DOC (PTS Stage A and PTS

Stage B). During the first 200 s, only small discrepancies between both systems are observed. In the following, the increase of the CO conversion rate of PTS Stage B slows down before speeding up and exceeding that of PTS Stage A. The reason for this is best explained by the CO conversion rate of PTS Stage C. Although its DOC perceives the lowest temperatures, the CO conversion rate suddenly increases after 200 s due to the avoidance of NO inhibition on the catalytic surface. On the catalysts oxidation site the adsorption between CO, NO, and HC is competitive. Thus, a reduction of NO reduces the light-off temperatures for the CO and HC reduction remarkably. Precisely this effect dominates with the upstream positioned SCR1 of PTS Stage C that starts to reduce NO and thus reduces the demanded temperature for the CO oxidation. The same effect occurs on the catalytic site of the cDPF of PTS Stage B, which is visible by the second rise of the CO conversion rate after 280 s. The single DOC is only capable of achieving a CO conversion rate of 70 % at the given operating point. The remaining CO is then oxidised within the cDPF.

The lower temperature of the DOC in the reference system has an impact on its CO and HC conversion rates, which require more time to increase compared to all PTS. The exothermic reaction's heat release has only a small impact on the warm-up because the raw emissions are relatively low for this operating point.

The THC conversion is corresponding to the CO conversion, but a higher temperature is necessary. Solely the DOC of PTS Stage D has a significantly lower HC conversion compared to CO in the second part of the cold start. During the first period, it shows a high HC adsorption rate because its DOC is larger compared to that of the other configurations. The DOC reactions of PTS Stage D are calibrated according to the DOC of the reference system that is characterised by a high CO conversion rate, but the HC oxidation starts at warmer temperatures, especially that of unburned fuel. In the reference system, the HC emissions are mainly oxidised within the cDPF, providing a better HC oxidation performance. The NO inhibition of PTS Stage B and Stage C is also apparent for the HC conversion rates.

The already mentioned higher NO_X reduction of PTS Stage C has its root in the faster warm-up of the SCR1. Figure 5.16 illustrates the inlet temperatures of SCR1 and SCR2. The largest temperature difference is noted after 50 s between PTS Stage C and the reference system, that is 150 K. Compared to the DOC

and DPF, the SCR1 temperature difference between the reference system and PTS Stage A is highest with up to 50 K. In the reference system, SCR1 is set up as an underfloor catalyst, which increases the exhaust pipe length between the DPF and SCR1. This means a higher thermal inertia and a larger surface for heat losses for the reference system for the pipe section between the DPF and SCR1. PTS Stage D does not include SCR1 since it has the selective DPF and is consequently not shown in the plot.

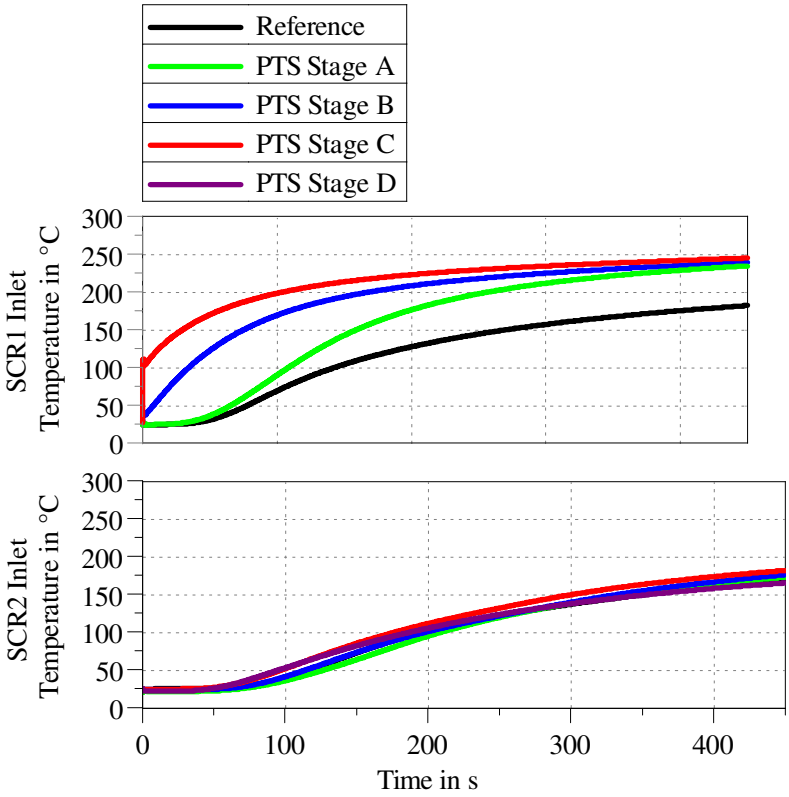

Figure 5.16: The inlet temperature of SCR1 and SCR2 during the cold start

The inlet temperature of SCR2 is almost identical for all systems, and the time needed to achieve 200 °C is longer than the considered 450 s. PTS Stage C

shows the slightly highest temperature because of the largest heat release of the oxidation reactions of the DOC and cDPF. Additionally, fewer components before the turbine allow a more opened VGT rack position of the turbine. This reduces the expansion ratio over the turbine causing higher turbine outlet temperatures. The temperature of the SCR system is one determining factor of the NO reduction rate. The other one is the amount of apparent ammonia for selective reduction. To obtain ammonia from urea, a specific temperature is required, but the temperature should not get too high to avoid ammonia oxidation.

Figure 5.17 demonstrates the NO_X and NO_2 conversion rates. It is conspicuous that the NO_2 conversion rate achieves high values very quickly. This is due to the fast SCR reaction, for which the same amount of NO and NO_2 is required. Furthermore, the amount of raw emissions of NO_2 is small and only 5 % of the total NO_X emissions. This reaction is dominant at low temperatures and shows the importance of a high NO_2 to NO_X ratio. Only at higher temperatures, the reduction reaction of NO takes place, which is why the NO_X conversion rate is increasing more slowly than that of NO_2. Since the initial amount of adsorbed ammonia is small, a jump in the NO_2 conversion rate is detectable for all systems as soon as the urea injection starts. This is for the reference system after 220 s and for PTS Stage A after 155 s. The NO_X conversion rate has a small jump for all systems, which is at a later point (PTS Stage C after 230 s, PTS Stage A after 350 s). This happens when the target amount of ammonia in the zeolite is reached, and the urea injection stops for the first time because the urea decomposition is an endothermic reaction. Thus, energy is required to obtain ammonia from urea, which reduces the exhaust gas temperature at this spot. When the urea injection stops, the reaction rates of the NO_X reduction rise suddenly in coherence with the temperature.

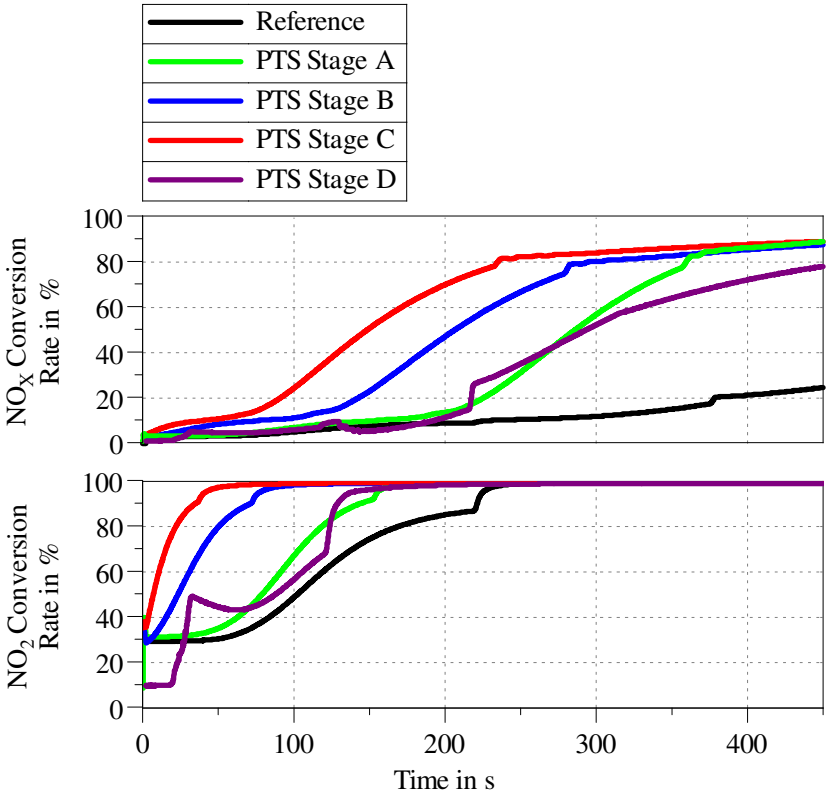

Figure 5.17: NO_2 and NO_X conversion rates for the SCR1 during the cold start

With the reference system that has two underfloor catalysts, the NO_X conversion rate after 450 s is less than 30 %. In comparison to that, all PTS achieve a conversion rate of 80 % or more. However, the fuel consumption of the reference system is 0.7 % less compared to PTS Stage A. The VGT rack position stays at a more closed position time with PTS Stage A, which results in a worse turbine efficiency to obtain the same boost pressure. Additionally, this increases the turbine's pressure ratio, which causes higher backpressure and increased pumping losses.

The significant advantage of all PTS becomes visible in the required time to

reach the light off, visualised in Figure 5.18 for each emission species. With the reference system, the time to reach the 50 % conversion point is almost doubled compared to all PTS. The largest advantage of the PTS is observed for the NO_X conversion with a pre-turbine SCR system positioned close to the exhaust manifold. For PTS Stage C, the time reduction is more than 75 % compared to the reference system.

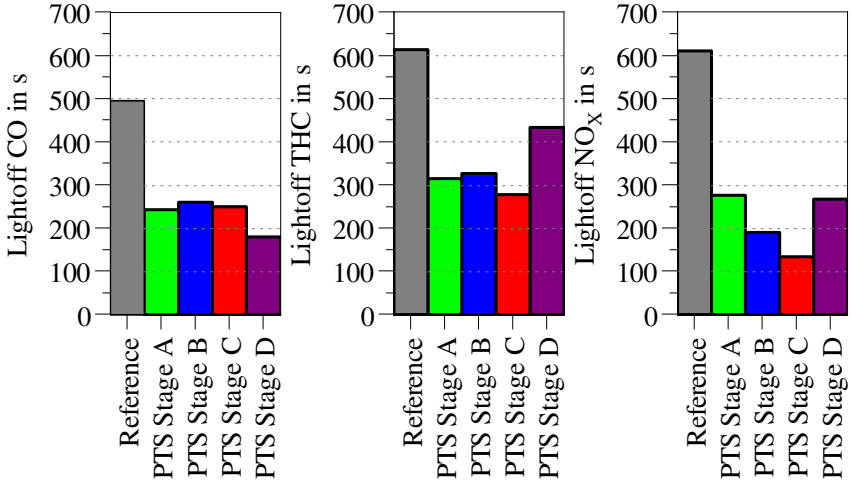

Figure 5.18: Light-off time separated into the emission species CO, HC and NO_X during the cold start

Besides the temporal development of the conversion rates, the tailpipe emissions are eventually the deceiving factor for the assessment of the EAT systems. Figure 5.19 shows the cumulative tailpipe emissions after the first 200 s and 450 s. The crosshatched bars represent the accumulated emissions after 200 s. Due to the slow onset of the reactions, those show only small differences. The major distinction becomes visible in the emission increment between 200 and 450 s. In this interval, the tailpipe emissions double for all species with the reference system. In contrast to this, for all PTS the cumulative tailpipe emissions between 200 and 450 s are distinctively lower than during the first 200 s.

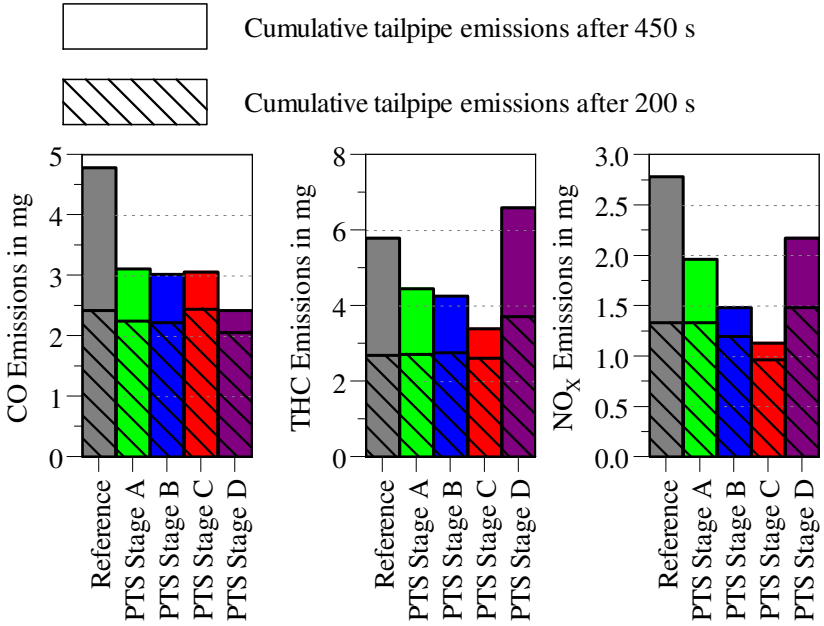

Figure 5.19: Cumulative tailpipe emissions during the cold start

PTS Stage D has the highest cumulative HC emission mass during the cold start, and the NO_X tailpipe mass is greater. The conversion rates in Figure 5.15 are calculated using the molecular concentration, which includes propylene, absorbable diesel fuel, and non-absorbable diesel fuel as representants of THC. The plotted conversion rate of PTS Stage D is higher than that of the reference system because most propylene is oxidised, but only a small amount of the unburned fuel. Since the molecular mass of unburned fuel is 3.4 times higher, the cumulative mass of the tailpipe HC emissions is higher with PTS Stage D anyway. Another reason for the high HC tailpipe emissions within the first 200 s is that a part of the unburned fuel is absorbed by the DOC when it is still cold. With a rising temperature, it is desorbed but not oxidised due to the inferior HC oxidation affinity. This is happening between 110 s and 200 s after the engine start and is the reason for the large amount of the THC mass at the tailpipe during the first 200 s. Similarly, the sDPF was calibrated conservatively

in terms of the activation temperature of the selective reactions. Thus, the NO_X emissions are relatively high compared to the other PTS, despite a high temperature of the sDPF.

In order to obtain a variation in the exhaust gas temperature at the same operating point, two modifications to the engine are made: The wall heat losses of the cylinder are decreased, which causes higher exhaust gas temperatures, and the engine friction is reduced, which enhances the efficiency and reduces the exhaust gas temperature. With both modifications, it is intended to take into account possible future technologies and advancements.

The wall heat losses are reduced by 80 % in order to increase the gas temperature in the exhaust manifold by 16 K at the same operating point. The mass flow rate, boost pressure and EGR rate are kept unchanged. Figure 5.20 shows the time required to reach the light-off for the three considered emission species. Since the temperature is higher, the EAT components of all systems are heated up more quickly, and the conversion rates increase more rapidly. Thus, the light-off is reached within a shorter time compared to the standard combustion process.

The components located closest to the cylinder experience the higher temperature first and have the most considerable reduction of the light-off time. The reference system has with the 16 K warmer exhaust gas a light-off time that is approximately 200 s shorter for CO and THC compared to the standard combustion process. However, the NO_X conversion rate of 50 % is reached only approximately 100 s earlier because the SCR catalysts are the last components within the exhaust tract. The same effect is also apparent for PTS Stage A, where the light-off time for NO_X reacts less sensitively compared to CO and THC. Similarly, the light-off time reduction for PTS Stage C with pre-turbine SCR1 is highest regarding NO_X conversion. Since the NO inhibition plays a great role for this system, the faster NO_X conversion influences the CO and THC conversion rates as well, and the lastly described effect is less dominant but still visible.

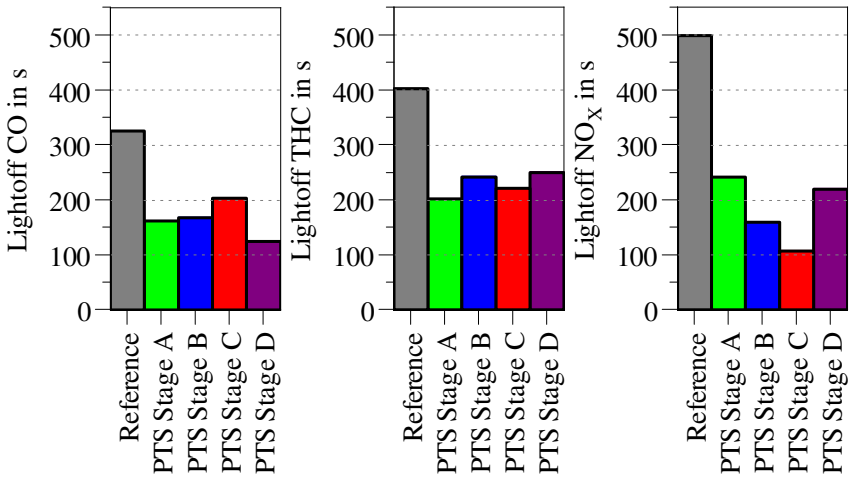

Figure 5.20: Light-off time for the emission species with less wall heat losses in the cylinder

The temperature difference between the reduction of the wall heat losses compared to the standard cylinder gets smaller after each EAT component, that is heated up. Thus, temperature variation affects the first components most. Although the reference system has the largest discrepancies of the absolute light-off time between the two different cylinder coatings, the relative enhancement of the cold start behaviour is the same for the PTS.

In order to investigate the impact of a lower exhaust gas temperature, the engine's efficiency is increased by reducing its friction. Based on the work of Wong and Tung [65], the friction is improvable by 20 % with a sophisticated crankshaft design and another 20 % by enhanced lubrication. This increases efficiency, and less fuel is required to obtain the torque of the chosen operating point. Along with the increased efficiency, the gas temperature in the exhaust manifold is reduced by approximately 17 K, which impedes the heating-up of the EAT components. The light-off times of the considered systems with the modified engine friction are illustrated in Figure 5.21 for the considered emission species.

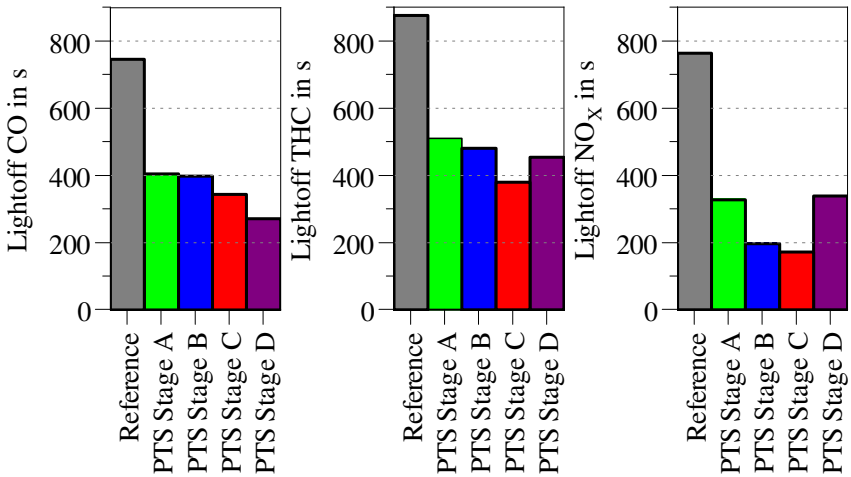

Figure 5.21: Light-off time for the emission species with an enhanced engine friction

Generally, the light off time is extended due to the lower exhaust temperature. The lower temperature affects mainly the first EAT components, like the examinations with less wall heat losses in the cylinder. When comparing the configurations, it is noticeable that PTS Stage C shows an advantage for the CO conversion. This indicates that the avoidance of NO inhibition has a more significant effect on lower temperatures. For the other species, no peculiarities are observed.

The reference system reacts most sensitively to the changes of the exhaust gas temperatures regarding the absolute time that is required to achieve the 50 % conversion rate. Even with the lower exhaust gas temperature, all PTS achieve a faster light-off compared to the reference system with the standard combustion process of Figure 5.18. This underlines the great potential of PTS regarding the warm-up, regardless of the chosen order of pre-turbine EAT components.

5.2 Modification of the Configurations

5.2.1 Transient Measures

The load step examination in section 5.1.2 shows the severity of the increased turbo lag by the pre-turbine EAT components. A wide variety of measures for compensating the dynamic disadvantages is examined in this section. Besides three electrical support systems, compressed air injections at two different spots and two post injection strategies are part of the investigation. The focus is set on the ability to compensate the dynamics with PTS. Additionally, further peculiarities that affect the engine and EAT components of the systems are discussed. The operating principles of these transient countermeasures are described in section 4.2.

Electrification of the Supercharging System

The increasing grade of electrification and the development of new components open a wide range of possibilities to enhance the dynamic response of a powertrain system. Some of them deliver additional torque directly to the powertrain shaft as a parallel hybrid engine. As a representative of these, a P2-hybrid is analysed in this work. Other systems enhance the dynamic response by supporting the bosting system. By increasing the boost pressure, the exhaust mass flow rate, temperature, and pressure are affected as well, that have an influence on the efficiency of the EAT. As representants of these systems, an electrically driven booster and an electrically assisted turbocharger (EATC) are examined and compared.

The additional power of the supporting systems is controlled to match the reference system's boost pressure during the load step to determine the required power and energy for the compensation of the additional turbo lag caused by the pre-turbine EAT. An even faster dynamic response would be possible for the considered load steps by increasing the additional power. The required mechanical power over the time of the EATC for the load step at 2500 rpm is displayed in Figure 5.22. The load step at 1500 rpm shows the same tendencies but requires a longer supporting time to hold the target load. For the assessment of the dynamic measures, only the mechanical power necessary is considered.

For a holistic view, the efficiencies of the battery, the electrical motors and possibly the power electronics must be included.

The boost pressure for the reference system constantly increases from the start of the load step, which corresponds to the increasing turbocharger speed. The external power is raised to close this gap between the reference systems and the PTS until the target boost pressure is reached. Since during the first second without support, none of the PTS increased the boost pressure (cf. Figure 5.8 for 1500 rpm), the required power during this period is identical for all PTS. Henceforth the speed of the turbocharger is kept constant, for which less power is required than for the acceleration of its rotational inertia. In the following, the differences between the PTS become visible: PTS Stage C has the lowest pre-turbine thermal inertia for what reason the required power is lowest after the first peak and reaches zero first. According to the required time without transient measures, PTS Stage A requires the external power longest. This is caused by the high thermal inertia of the cDPF that must heat-up before the temperature reaches the turbine inlet.

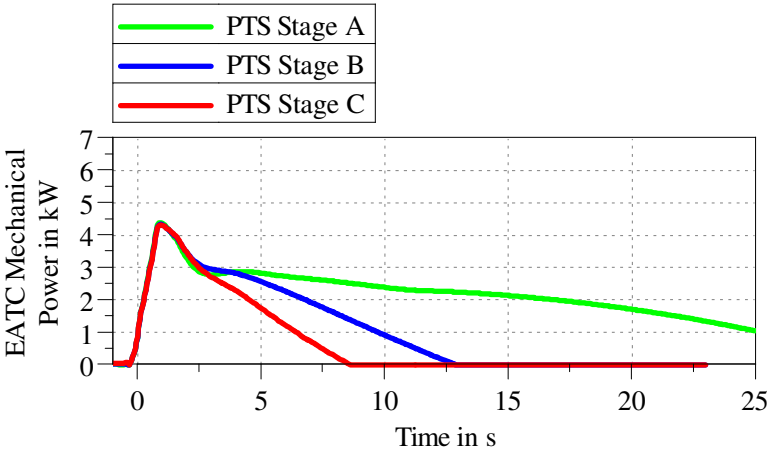

Figure 5.22: The required power for compensating the dynamic lag for the load step at 2500 rpm

The electrically driven booster (EDB) shows a very similar behaviour regarding

the shape of the curve: After a first peak, the required support power decreases to a certain level until the differences between the PTS become visible. However, the maximum power peak with an EDB is approximately 10 % higher. The EDB has a larger wheel diameter (65 mm) compared to the turbocharger (turbine wheel diameter: 41 mm) and EATC. This results in a higher moment of inertia (28 kg/mm^2) compared to the EATC (14.3 kg/mm^2). Thus, more power is required to accelerate the EDB to its target rotational speed for a short period. Once it has reached this speed, the power demand drops. A comparison between the EATC and the EDB regarding the mechanical power demand for PTS Stage C is shown in Figure 5.23.

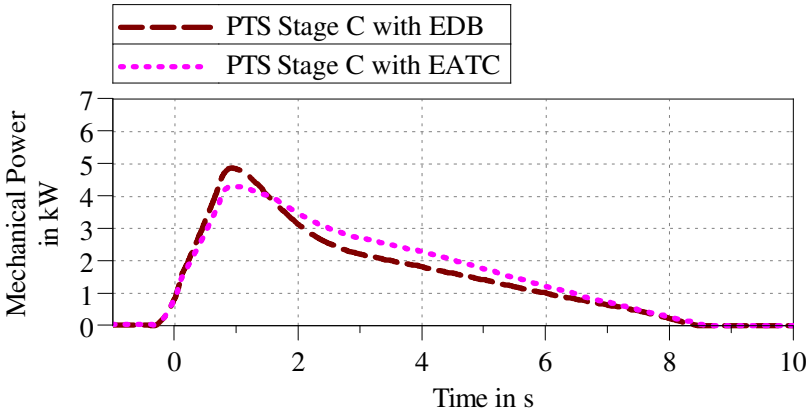

Figure 5.23: Comparison of the required power between the EATC and the EDB for PTS Stage C at the load step at 2500 rpm

At this engine speed, after the first peak, the power demand with the EDB is lower compared to the EATC. This is the same for all considered PTS. Due to the lower power demand after the first peak, the required energy amount with the EDB is lower compared to the EATC. A comparison of the required support energy to achieve and hold the target load for 25 s is shown in Table 5.2 for two different engine speeds. For reasons of capacity, only the first 25 s are used for the evaluation.

Table 5.2: The required energy for the dynamic compensation during the load steps for all PTS with electrical boosting systems

	1500 rpm with EATC	1500 rpm with EDB	2500 rpm with EATC	2500 rpm with EDB
PTS Stage A	33.7 kJ	34.3 kJ	60.0 kJ	54.7 kJ
PTS Stage B	28.6 kJ	32.0 kJ	25.6 kJ	24.8 kJ
PTS Stage C	20.5 kJ	24.1 kJ	17.5 kJ	16.0 kJ

Comparing the required amount of energy, the EATC has advantages at 1500 rpm, whereas the EDB requires less energy at 2500 rpm. At the lower engine speed, the fast acceleration of the EATC to a higher rotational speed increases the pressure ratio over the turbine and related to this the turbine power. This reduces the required external mechanical power that the electrical motor must provide compared to the EDB.

At the engine speed of 2500 rpm, the shaft rotational speed of the turbocharger with the EATC is 181,000 rpm and with the EDB 156,000 rpm one second after the start of the load step. This results in 23 % higher friction losses. Additionally, the efficiency of the EDB is approximately 10 % higher than the turbocharger efficiency at this operating point. Both effects lead to an advantage of the EDB regarding the required energy. None of the two boosting systems has benefits in all operating points because several effects come together. However, both boosting measures show similar performance, and in the following examination cases only the EATC is taken into account, assumed that with an EDB similar results would be obtained.

The higher energy requirement for PTS Stage A at 2500 rpm comes from the evaluation interval of 25 s. Suppose the total amount of energy is taken into account that is required until the turbocharger delivers enough boost pressure by itself. In that case, the energy amount with PTS Stage A is also higher at 1500 rpm. The reason for this is the faster warm-up of the pre-turbine EAT components and the turbine at the higher engine speed, which is caused by higher exhaust temperatures and mass flow rates. The difference in the energy requirement between the two engine speeds increases with a larger thermal mass in a pre-turbine position, i.e. the EATC for PTS Stage A needs more than

50 % more energy at 1500 than at 2500 rpm. For PTS Stage C, this increase is only 20 %, and for PTS Stage B it is 36 %.

Besides the energetic consideration, the emission reduction for the load steps with a supported PTS by an EATC is compared to the reference system. The electrical support ensures almost the same boundary conditions for all configurations regarding the load increase, boost pressure and mass flow rate. Thus, the effect of the pre-turbine placement can be examined more isolated. Without the EATC, boost pressure, exhaust temperature, raw emissions, and mass flow rates differ between the reference system and the PTS.

The CO conversion rate and the DOC outlet temperature for the reference system and the PTS are plotted in Figure 5.24 at the load step with an engine speed of 1500 rpm. The outlet temperature of the catalyst gives a rough estimation of how fast it heats up. For the PTS with the DOC in the first position after the exhaust manifold, the temperature rises the quickest. The longer DOC with a higher cell density of PTS Stage D has a higher thermal inertia than the other EAT systems. That is why the outlet temperature rises more slowly. However, the CO conversion rate for this system increases fastest and reaches a full conversion after approximately 25 s. PTS Stage B shows a different feature: A quick DOC outlet temperature rise indicates a fast warm-up of the catalyst. This favours the CO conversion rate, which quickly reaches the light off point, but stagnates at a conversion rate of 50 %. At this point, a further temperature increase does not improve the conversion rate because it has achieved its maximum. The single DOC is too small to complete a full conversion under these operating conditions. Only in combination with the cDPF, the full conversion rate is possible. However, the cDPF is placed after the SCR1 and the turbine at PTS Stage B and requires more time to warm-up and until the conversion of CO into CO_2 starts.

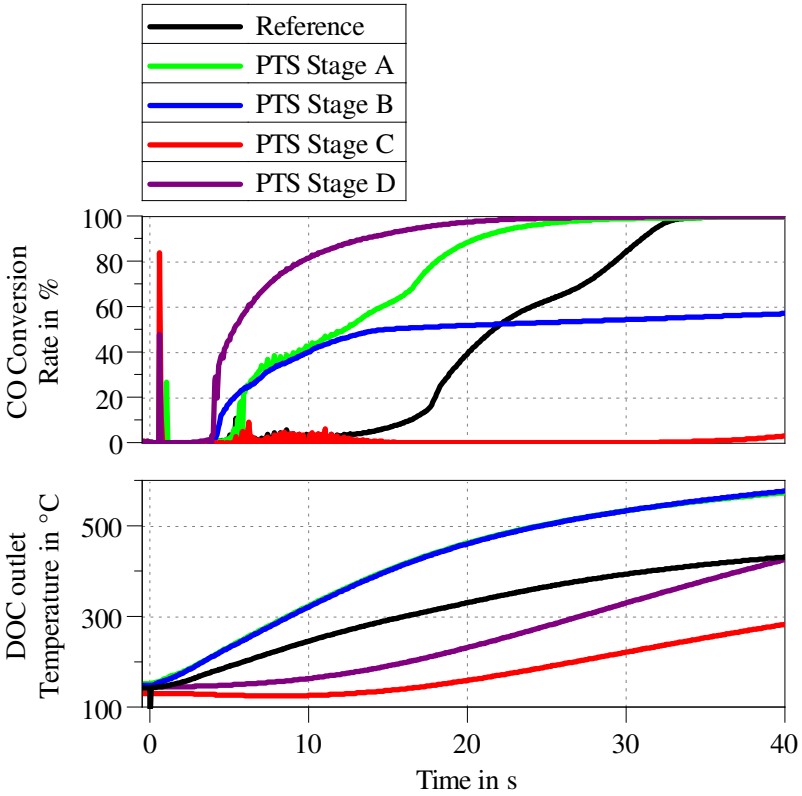

Figure 5.24: CO conversion rate and DOC outlet temperature over time during the load step at 1500 rpm

The DOC outlet temperature of PTS Stage A is identical to the one of PTS Stage B and their curves are overlapping. The DOC conversion rate of PTS Stage A is during the first phase also similar, until the cDPF reaches its working temperature after approximately 12 s. From this point onwards, the conversion rate increases again due to the increased conversion rate of the large cDPF.

The benefit of the pre-turbine EAT becomes visible in comparing the DOC outlet temperature with the reference system. From the start of the load step, the temperature rises significantly faster with the pre-turbine DOC of PTS

Stage A and PTS Stage B, which favours early high conversion rates. Since the arrangement of the reference system is the same as that of PTS Stage A – except the turbine – the shape of the curves of the conversion rate is similar but time-shifted. Since the presence of CO itself inhibits CO oxidation, the steep slope of the conversion rate is caused by high CO raw emissions. CO molecules cover the catalytic surface and inhibit other CO molecules from reaching it. This effect is implemented in the used DOC reaction mechanism described by Sampara et al. [51].

PTS Stage C does not achieve a remarkable CO conversion rate because the pre-turbine SCR1 and the turbine are heated up first. It takes longer than 40 s until the DOC temperature is rising and until the CO conversion starts. The DOC position further back causes a more equal temperature gradient over the catalyst length; at the same DOC outlet temperature, the inlet temperature is consequently lower compared to that of the other PTS. This is the reason for the lower conversion rates despite the same output temperatures.

The temperature-dependent conversion of HC reveals the same behaviour as that of CO. Thus, it is not displayed in detail. Compared to the reference system, warm-up potential becomes apparent for PTS Stage A and PTS Stage D: By the faster temperature rise and the CO and HC conversion rates are higher and the light off is reached faster. PTS Stage A achieves the 50 % conversion point 9.5 s earlier for CO and 10 s for HC. With PTS Stage D, the CO light off is reached 16.5 s faster than with the reference system. For the HC emissions, the benefit is smaller and only one second. PTS Stage B has only advantages during the start of the load step, but the full conversion is reached slower than with the reference system. PTS Stage C has no advantages regarding the CO and HC conversion because the pre-turbine SCR1 is heated-up first. The faster warm-up of the SCR1 is reflected in lower NO_X tailpipe emissions.

In Figure 5.25, the SCR1 inlet temperature and the NO_X conversion rate over time are compared between the PTS and the reference system. The inlet temperature leap of PTS Stage C results in high conversion rates shortly after the load step starts. However, the NO_X conversion achieves its maximum after 7 s, before it is decreasing again. The temperatures become too high, and the urea dosing is stopped to avoid ammonia oxidation that becomes notable above temperatures of 450 °C, as described in section 5.1.2. With the stored ammonia

in the SCR catalyst, a NO conversion is still possible, but it is lower than that within the optimal temperature window.

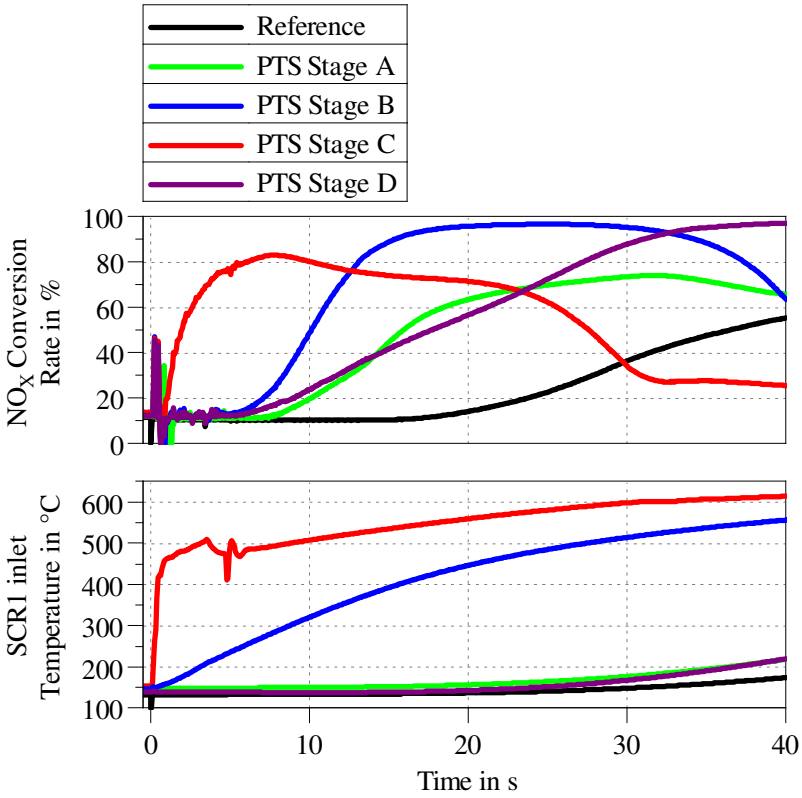

Figure 5.25: SCR1 inlet temperature and NO_X conversion rate during the load step at 1500 rpm

Placing the SCR1 in the second position, its inlet temperature rises more decently within PTS Stage B. The NO_X conversion rate increases with the temperature, and the light off is reached 10 seconds after the start of the load step. It needs to be considered that the SCR1 inlet temperature is not equal to the substrate temperature over the entire catalyst. Only with time, the higher temperature reaches the back part of the catalyst. Thus, the reaction rates vary

over the length of the catalyst with such high temporal temperature gradients. 30 s after the start of the load step, NO_X conversion rate is decreasing because ammonia injection was stopped due to the high temperatures.

Since PTS Stage D does not contain the SCR1 catalyst, the inlet temperature of the sDPF is plotted instead. It represents the pre-turbine component for NO_X reduction. The inlet temperature of PTS Stage A and PTS Stage D rise more slowly due to the larger thermal inertia between the considered component and the exhaust manifold. Compared to PTS Stage B and Stage C, the NO_X reduction rate increases faster than the inlet temperature. This has two reasons: On the one hand, the temperature rise is more even over the length of the catalyst. On the other side, the upstream positioned DOC and cDPF oxidise a larger amount of NO into NO_2. This favours the fast SCR reaction, which is the dominant NO reduction reaction at low temperatures.

Compared to the reference system, all PTS demonstrate an advantage regarding the heat-up of the SCR1 and the NO_X conversion rates. The time from the start of the load step until the NO_X conversion light-off was reached for the first time is reduced by at least 50 % for PTS Stage A and Stage D and even more for PTS Stages B and C. However, the problem during the load step with an SCR catalyst positioned close to the engine is the too high temperature. Ammonia oxidation prevents high conversion rates.

Electrification with a P2-Hybrid

In contrast to the transient measures of an EATC or EDB, a P2-hybrid does not interact directly with the gas flow through the engine. The support power is added directly to the engine shaft to increase the total torque. The required extra torque corresponds to the difference of the engine torque between the reference system and the PTS from Figure 5.8 for the load step at 1500 rpm. Figure 5.26 illustrates this required mechanical power of a P2-hybrid for the compensation of the dynamic disadvantage compared to the reference configuration.

After reaching the target load, the extra power is controlled to hold the total target load. In the beginning, the required additional power is the same for all PTS because the turbocharger does not provide boost pressure. Thus, all PTS are operating under naturally aspirated conditions, and the electric engine

must provide the missing torque. According to the results without transient countermeasures, the support time and the required energy increases with the amount of pre-turbine EAT components. However, the maximum power is the same for all PTS.

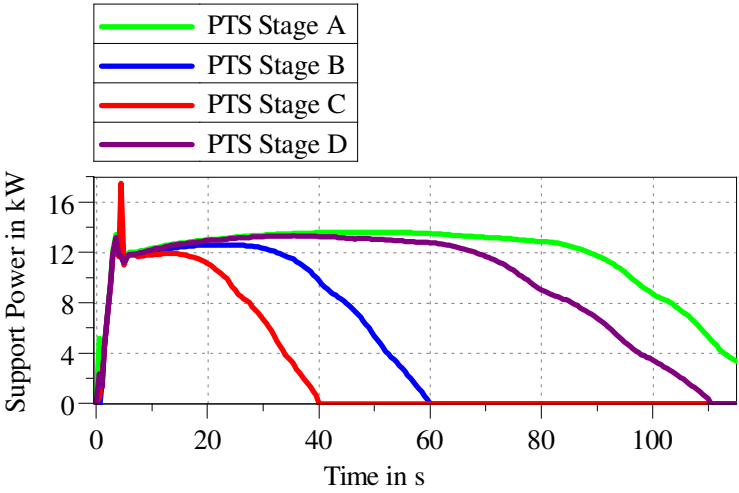

Figure 5.26: Required extra power with a P2-hybrid for the dynamic compensation during the load step at 1500 rpm for all PTS

In order to compare the P2-hybrid with the EATC, the power and energy demand during the load step a 1500 rpm are summarised in Table 5.3 for PTS Stage A and PTS Stage B. Only two PTS are taken into account because the outcome is the same for all. Furthermore, the EDB is not considered here because of its similarity to the EATC, and the same consequences as for the EATC can be made for the EDB. The total amount of external energy during the first 25 s of the load step is nine times higher with the P2-hybrid compared to the EATC for PTS Stage B and almost eight times higher with PTS Stage A. Moreover, the maximum mechanical power of the P2 is more than seven times higher. With the EATC and EDB, at the beginning of the load step, a peak in the required power was detected because the turbocharger, respectively the compressor has to be accelerated. The P2-hybrid needs only the electric motor to be accelerated, which is not considered in these examinations for all countermeasures.

Since with the P2-hybrid the boost pressure remains unchanged, the fuel injection rate is limited by the fresh air and the smoking limit. This leads to a 20 % lower injected fuel compared to the load step with an EATC. This is equivalent to an energy content of approximately 600 kJ, of which a part contributes to the engine torque. Since not the total fuel energy can be transformed into mechanical work, a part of it is wall heat losses or goes into the exhaust gas energy. The higher exhaust gas energy combined with an increased mass flow rate expedites the heat-up of the pre-turbine EAT components.

Table 5.3: Energetic comparison of the EATC with the P2-hybrid for PTS Stage A and PTS Stage B for the load step at 1500 rpm

	PTS A EATC	PTS A P2	PTS B EATC	PTS B P2
Support energy (25 s)	33.7 kJ	298.7 kJ	28.6 kJ	287.1 kJ
Fuel consumption (25 s)	58.4 g	43.9 g	59.2 g	44.1 g
Max. electrical support power	1.6 kW	13.6 kW	1.6 kW	13.1 kW
Support time	100.0 s	127.0 s	44.5 s	59.0 s
Support energy (total)	100.4 kJ	1337 kJ	35.0 kJ	565 kJ

On account of the faster heat-up of the pre-turbine components, the turbocharger is able to provide the boost pressure earlier with an EATC support compared to the P2-hybrid. The P2-hybrid must support more than 25 % longer for PTS Stage A and 30 % longer for PTS Stage B to hold the target load. This also determines the total amount of required support energy that is more than 12-times higher with the P2-hybrid for all PTS.

The faster warm-up is also reflected in the conversion rates of the catalysts. Figure 5.27 illustrates the difference between the P2-hybrid and the EATC of the DOC outlet temperature development and CO conversion rate of PTS Stage B. Due to the already described faster temperature rise of the exhaust tract in general, the CO conversion rate is also increasing earlier and faster within the first 10 s. Once the DOC reaches a specific temperature and starts

to convert the CO, it exceeds the conversion rate of that with an EATC. The reason for this is the lower mass flow rate with a P2-hybrid compared to the EATC that determines the reaction rate when the DOC is heated-up.

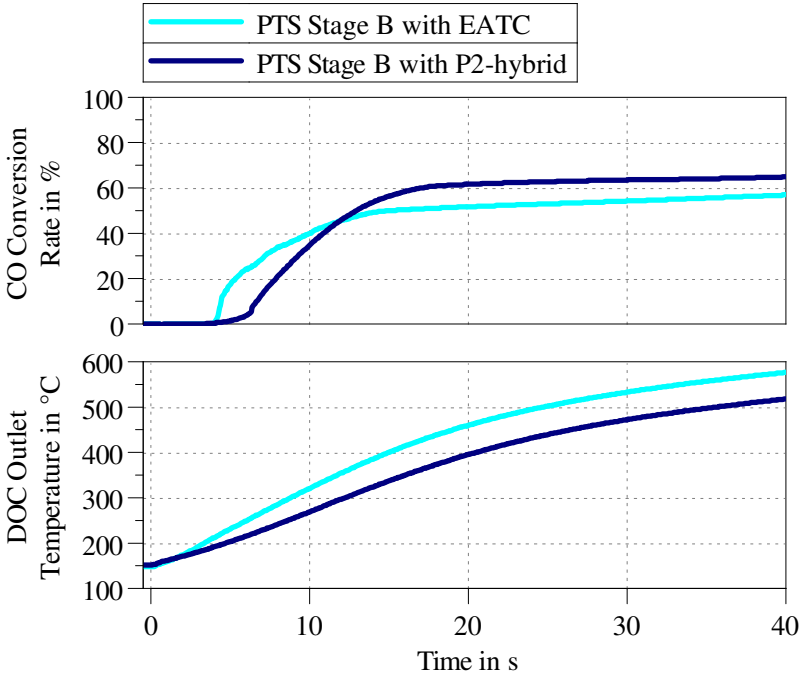

Figure 5.27: Comparison of the temperature development and CO conversion rate for PTS B with an EATC and P2-hybrid during the load step at 1500 rpm

The different boosting systems also affect the raw emission formation: The lower boost pressure with the P2-hybrid correlates with a lower air-fuel-ratio and lower combustion temperatures. Both features mitigate the NO_X formation but also the combustion efficiency. Thus, the HC raw emissions increase, whereas the effect on the CO raw emissions is small.

Mechanical-Pneumatical Countermeasures

The air injection systems described in section 4.2.3 are another possibility of increasing the amount of fresh air and the fuel injection mass. Firstly, the air injection directly into the cylinder is examined for PTS Stage A and PTS Stage C. These are considered as the borderline cases with the highest and the lowest thermal inertia upstream of the turbine. The load step results at 1500 rpm are mapped in Figure 5.28 during the first 15 s. For both PTS, the target torque is achievable with this transient support system. However, after 7 s, the load is decreasing because the boosting system is too small. This point is slightly earlier with the larger pre-turbine EAT system of PTS Stage A. Furthermore, the load drops to a lower level with PTS Stage A, where the impact of the additional components becomes visible.

The tank pressure is an indicator of the remaining support energy. Once it drops to a value below the boost pressure, no additional air is injected into the cylinder. When the tank is relatively full, it is difficult to control the valve opening to match the load development of the reference system. This causes the oscillations at the beginning of the load step in the BMEP curves of the PTS that are larger for PTS Stage A. The larger fluctuations might be one reason why the tank pressure is decreasing marginally faster for PTS Stage A. Despite achieving the target load, the boost pressure with the PTS never reaches the reference system's level. Since the amount of fresh air is directly increased by the support system, the target boost pressure is not required to obtain the target load without exceeding the smoking limit. After the first peak, the boost pressure is decreasing similar to the engine load. The lower pre-turbine mass of PTS Stage C makes it possible to hold the boost pressure longer and decrease slowly.

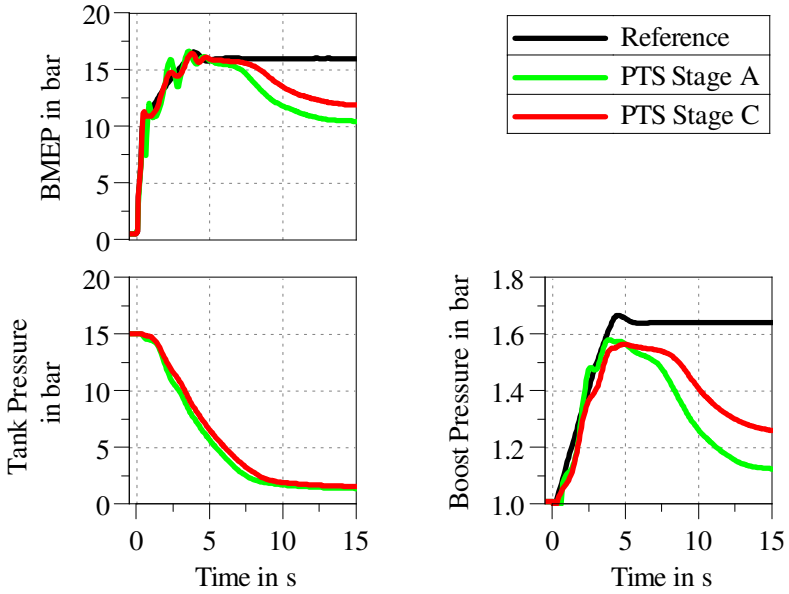

Figure 5.28: Tank pressure, BMEP and boost pressure development with an air injection directly into the cylinders

Once the pressure tank is empty, it must be recharged before another boosting phase is possible. Since the tank is charged during towing, it depends on the driving situation, when the next support period is possible. Although the energy is not applied directly, it is suitable for the comparison with the electrical support systems: The required energy for the compression of the air in the tank is approximately 36 kJ, which is more than the EATC needs during the first 25 s. This underlines that this system is not applicable in combination with a pre-turbine EAT system. For a longer boosting ability, the tank volume and pressure might be increased, which raises the structural weight. However, even with a larger pressure tank, several boosting events in a row are not able. This makes the application of this system in combination with PTS for passenger cars unattractive.

The second mechanical-pneumatic support system injects compressed air upstream of the turbine to increase the turbine's pressure ratio and thus the turbine power. Generally spoken, the principle is like that of the EATC: increasing the boost pressure by accelerating the turbocharger. This system has the advantage that its implementation is much simpler because no additional valve on the cylinder head is required, and the boosting valve opening is independent of the crank angle. Figure 5.29 visualises the engine torque development with the air injection system, the tank pressure, and the boost pressure. Like the air injection into the cylinder, this system can provide enough fresh air for a short time and reach the target load as quickly as the reference system. Nevertheless, the target boost pressure is not reached. After five seconds, the pressure tank is empty and the turbocharger speed drops. This decreases the boost pressure and BMEP further than with the air injection into the cylinder.

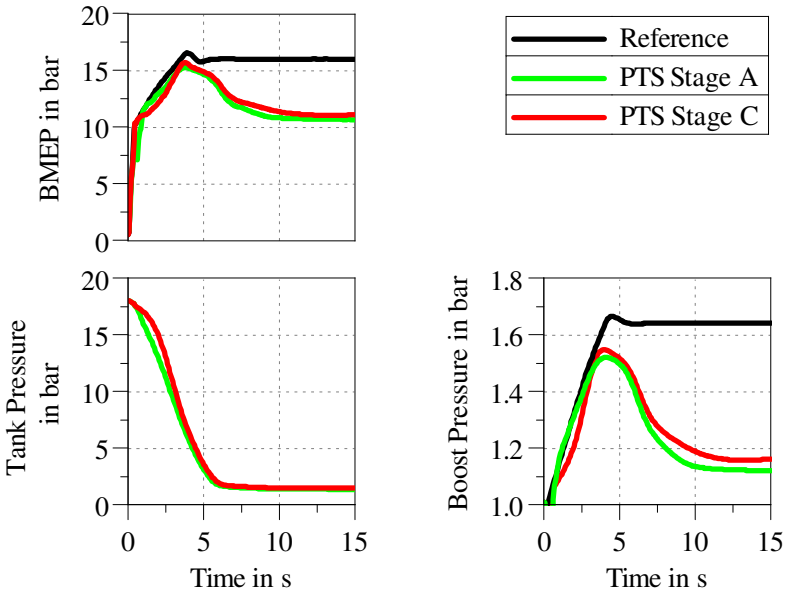

Figure 5.29: Tank pressure, BMEP and boost pressure development with an air injection before the turbine

To compress fresh air into the 4 l tank on a pressure of 18 bar, the external energy amount of 32.15 kJ is required without considering the compressor efficiency. This energy amount is in the same dimension as that with an EATC or EDB, but the engine load is not retained for a long duration. All in all, the conclusion for this boosting system is the same as for the air injection into the cylinder: the system is not suitable to compensate the dynamic disadvantage of a PTS compared to the reference system because the boosting time is too short.

Early Post Injection in the Cylinder

In contrast to the electrical or mechanical-pneumatic compensation measures, a post-injection application does not need additional components. The injection pattern and the controlling of the mass of the post-injections are described in section 4.2.4. Its effects on the engine torque, boost pressure, gas temperature in the exhaust manifold and gas temperature before the turbine are plotted in Figure 5.30. The reference system is compared to PTS Stage A and PTS Stage C with and without post injections for each PTS.

With the post-injection, the exhaust gas temperature is immediately 200 K higher compared to the regular injection pattern. However, the higher temperature does not reach the turbine immediately. Instead, it takes 10 s with PTS Stage C and 60 s with PTS Stage A until a considerable difference in the turbine inlet temperature is detectable. Only after the heat reaches the turbine, the turbocharger is able to provide more boost pressure and the torque is increasing. The evaluation point is reached 13 % earlier for PTS Stage A (97 s, without POI: 111.5 s) and 15.2 % for PTS Stage C (30.7 s without POI: 36.2 s) with the post injections compared to the normal operating mode.

Since the total amount of injected fuel is limited by the apparent amount of oxygen, the main injection becomes smaller with the application of a post-injection. This reduces the BMEP initially by 35 % because the post-injection does not contribute to the torque remarkably.

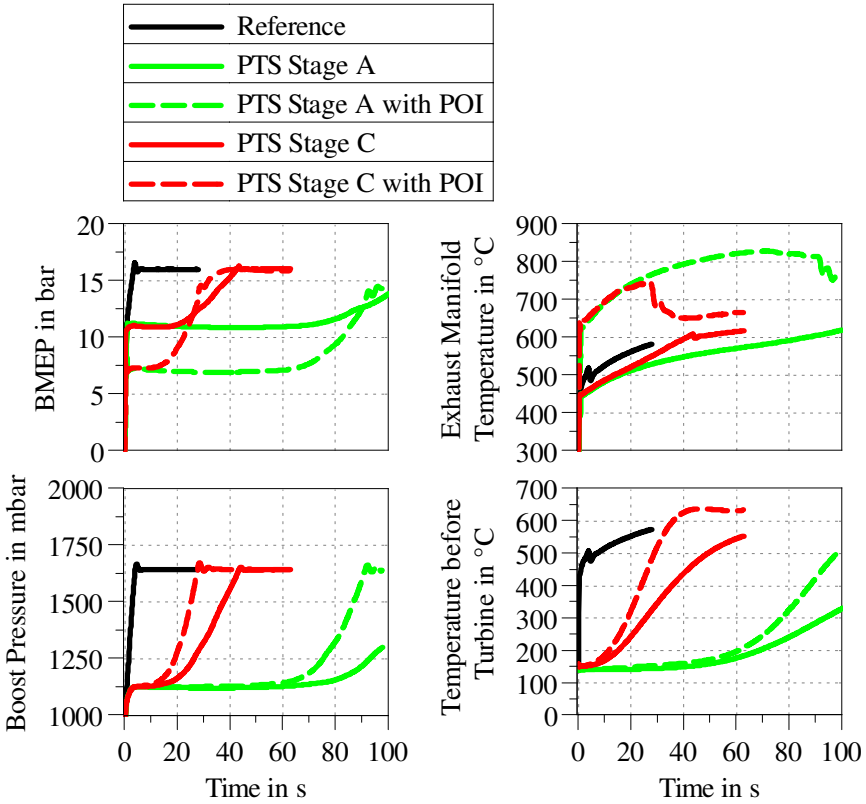

Figure 5.30: BMEP, boost pressure, exhaust manifold temperature and turbine inlet temperature with and without a post-injection for the reference system, PTS Stage A and PTS Stage C

The post-injection reduces the time to reach the evaluation load, and the target load is kept afterwards. However, the delay is still not acceptable, and other transient measures are necessary. It is more a possibility to enhance the heat-up than to reduce the turbo lag. Additionally, until the boost pressure starts to rise, the torque is even lower than without the post injections.

Fuel Injection into the Exhaust Manifold

The fuel injection into the exhaust manifold is only examined with PTS Stage A because a pre-turbine DOC is required for the exothermic oxidation of the fuel, as described in section 4.2.4. Alternatively, a late post injection into the cylinder can be applied that has the same result and does not require an additional injector. In contrast to the early post injection, the main fuel injection mass is not decreased significantly because with lean combustion, enough oxygen for the fuel conversion on the catalytic surfaces is apparent. Hence, the torque does not drop as for the previously shown measure, which can be seen in Figure 5.31 in combination with the boost pressure, DPF outlet temperature and turbine inlet temperature. The effect of fuel injection is visible in the increased cDPF outlet temperature. After 30 s, a remarkable difference between with and without the injection is. Since SCR1 is between the DPF and the turbine, another 20 s pass by until this heat increase reaches the turbine. The boost pressure is rising in accordance with the turbine inlet temperature. The higher boost pressure means that more fuel mass is injected with a constant air to fuel ratio and the torque increases.

With the extra fuel injection, the evaluation load is reached after 90.9 s with PTS Stage A. This is a time reduction of 20.6 s or 18.4 %. This application has two advantages compared to the early POI: The torque does not drop at the beginning of the load step because the main injection stays almost unchanged, and the load step is conducted faster with the late POI. However, the required time is still unacceptable. This measure might be applicable in combination with another transient measure to reduce the time until the turbine provides enough power by itself. One problem of the fuel injection into the exhaust manifold is that the temperature of the pre-turbine catalytic surfaces needs to be high enough to guarantee an effective conversion of the fuel. Otherwise, the tailpipe HC emissions are rising sharply. In any case, this measure causes up to 10 times more tailpipe HC emissions compared to the other measures.

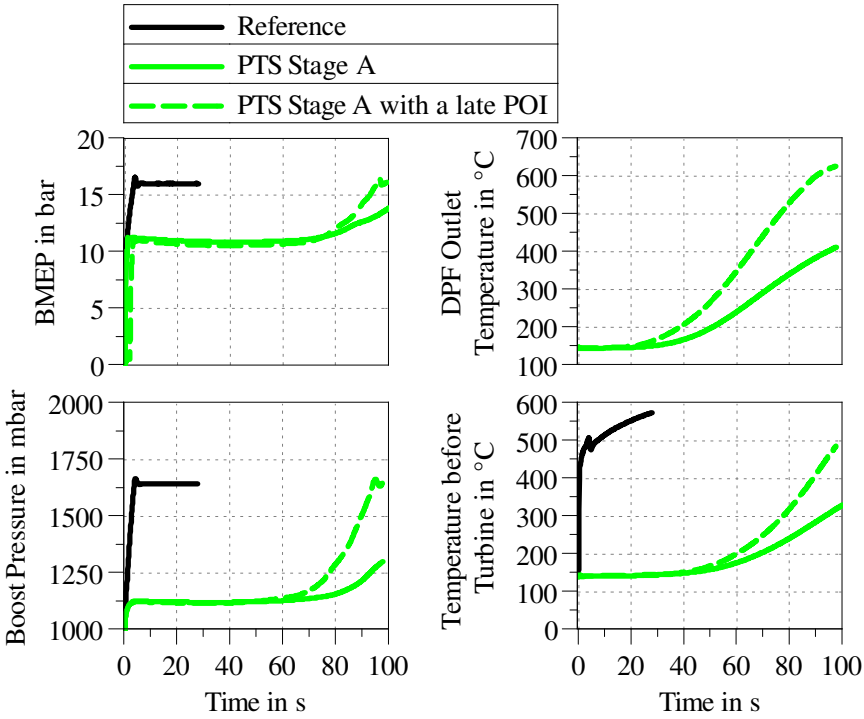

Figure 5.31: Development of the BMEP, boost pressure, temperature after the DPF and turbine inlet temperature during the load step at 1500 rpm with a late post-injection

5.2.2 Shortening of the Catalysts of PTS Stage B

Further examinations are undertaken to analyse the effects of a shortened pre-turbine catalyst. Subranamiam et al. investigated the impact of higher gas density in the pre-turbine position for large diesel engines and concluded that this effect allows a reduction in catalyst volume of up to 70 % [57]. Therefore, the pre-turbine DOC and SCR1 of PTS Stage B are shortened to half of their length, whereas the cell density and cross-sectional area are kept the same. With the shortening, a better dynamic response is expected. The modified

PTS Stage B is examined during the load step at 1500 rpm and the cold start scenario.

Load Step with modified PTS Stage B

The smaller thermal inertia upstream of the turbine requires less time to heat-up, and the higher temperature reaches the turbine faster compared to the standard-length pre-turbine catalysts of PTS Stage B. Thus, the time to reach the target load during the load step of 1500 rpm is remarkably shorter. The BMEP over the time during the load step is shown in Figure 5.32 for PTS Stage B, its modification with the shorter catalysts, and for further comparison, the load step of the reference system and PTS Stage C are added.

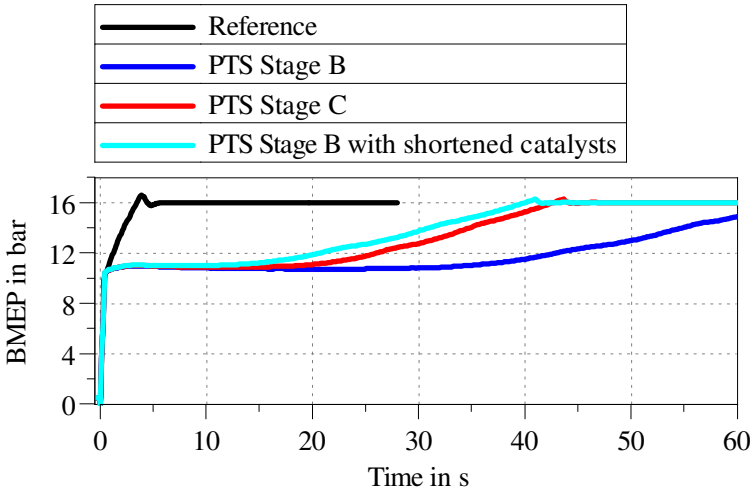

Figure 5.32: BMEP during a load step with shortened pre-turbine catalysts

The modified PTS Stage B has an advantage compared to PTS Stage C regarding the needed time for achieving the assessment point of a BMEP of 14.4 bar, despite the larger pre-turbine volume that is shown in Table 5.4 along with the characteristic values of the load step. For each catalyst, a transition part between the exhaust pipe and the catalyst and a longer pipe section for the

injection and urea decomposition is required. Therefore, the pre-turbine volume of the modified PTS Stage B is larger than that of PTS Stage C.

Table 5.4: Comparison of the characteristics of the reference system and chosen PTS during the load step

System	Pre-turbine volume in l	Required time for load step in s	Required energy with EATC in kJ
Reference	0.87	2.56	
PTS Stage B	4.01	56.8	28.6
PTS Stage C	2.91	36.2	20.5
Modified PTS Stage B	3.23	32.8	16.5

The quantitative comparison between the system with the full-sized catalysts of PTS Stage B and the halved catalysts show that the thermal mass reduction is reflected almost directly in the required time of the load step. Furthermore, the energy for compensating the dynamic disadvantage with the aid of an EATC is nearly halved. With the modified system both values amount to 58 % of the value with the normal PTS Stage B.

Cold Start with modified PTS Stage B

The same comparison is made during the cold start scenario that is described in section 4.6. Figure 5.33 shows the SCR1 and DPF inlet temperatures of the reference system, PTS Stage A and PTS Stage B with the standard catalysts and the shortened DOC and SCR1. Since the DOC inlet temperature is not affected by the shortening of the catalyst, it is not presented.

The DOC has a small cell density and is short compared to SCR1 or the DPF, so its thermal inertia and heat transfer rate are low, and the shortening impact is little. This is visible in the minor deviation of the SCR1 inlet temperature between PTS Stage B with the standard DOC and the shortened DOC that is less than 18 K. The advantage of higher SCR1 inlet temperatures is mainly visible during the first 200 s. Afterwards, both graphs approach each other with

a deviation of less than 2 K. For convenience, the temperatures of PTS Stage A and the reference system are shown.

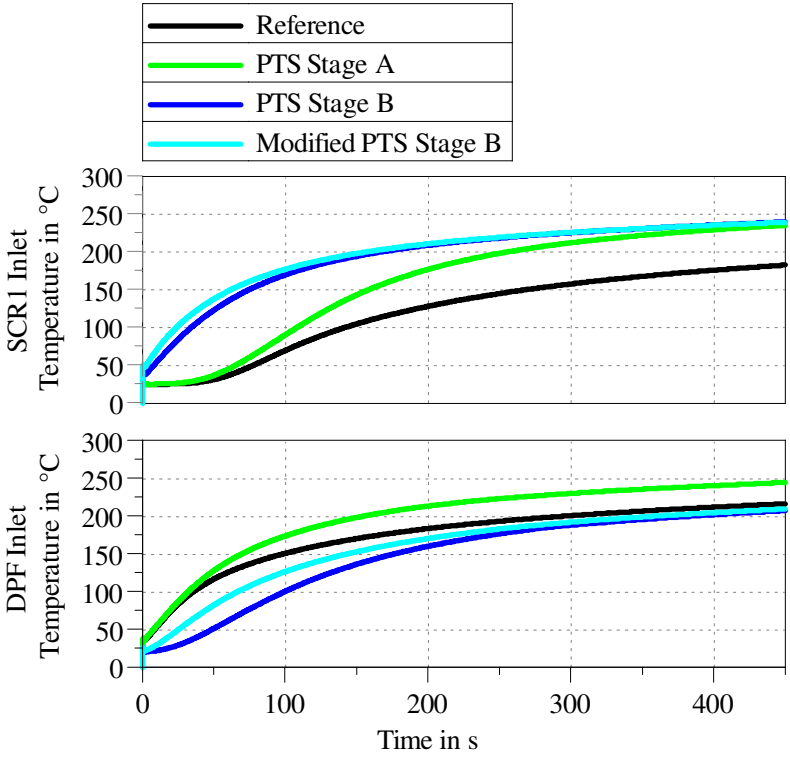

Figure 5.33: SCR1 and DPF inlet temperature development during the cold start scenario with shortened pre-turbine catalysts

From the SCR1 inlet temperature to the DPF inlet temperature, the effect of the shorter SCR1 becomes more apparent. The maximum DPF inlet temperature difference is 32 K. However, the temperature level itself is lower, and the time to reach the same temperature between the two configurations increases: with the short catalysts, the SCR1 inlet temperature reaches 150 °C 12.5 s and the DPF inlet temperature 32 s faster. The deviation of the DPF inlet temperatures of these two variants is after 200 s still greater than 10 K. This implies that a

different thermal mass of a catalyst during the cold start does not necessarily determine the dimension of the downstream temperature gap directly. Moreover, the time to reach a certain temperature level is influenced.

The steady state temperature level, which is achieved after a long time, is only slightly affected by the modifications. After 450 s, the temperature deviation for the DPF inlet temperature is 2 K, and the SCR1 inlet temperature is identical for PTS Stage B and its modification. The source for the difference in the DPF inlet temperature between the reference system and PTS Stage B is the upstream positioned SCR1 that inhibits the temperature rise. The gap between these two systems is mitigated by decreasing the size of the catalysts.

The length of the catalyst at a constant gas velocity determines the resting time of a single gas volume in the catalyst. Thus, it is a magnitude of influence for the conversion rates of the catalyst. The CO and NO_X conversion rates of the EAT systems are plotted in Figure 5.34 during the cold start. From the beginning, the CO conversion rate of PTS Stage B is higher than that of the modification. The entire DOC is heated up quickly with PTS Stages A, B, and the modified PTS Stage B. Thus, the CO conversion rate is almost identical during the first 120 s. The short DOC is disadvantageous in the following, due to the shorter resting time in the catalyst that comes along with lower oxidation rates. After 450 s, the CO conversion rate of the DOC of PTS Stage A and B is 60 %, whereas that of the short DOC is only 40 %. The remaining CO is oxidised by the cDPF.

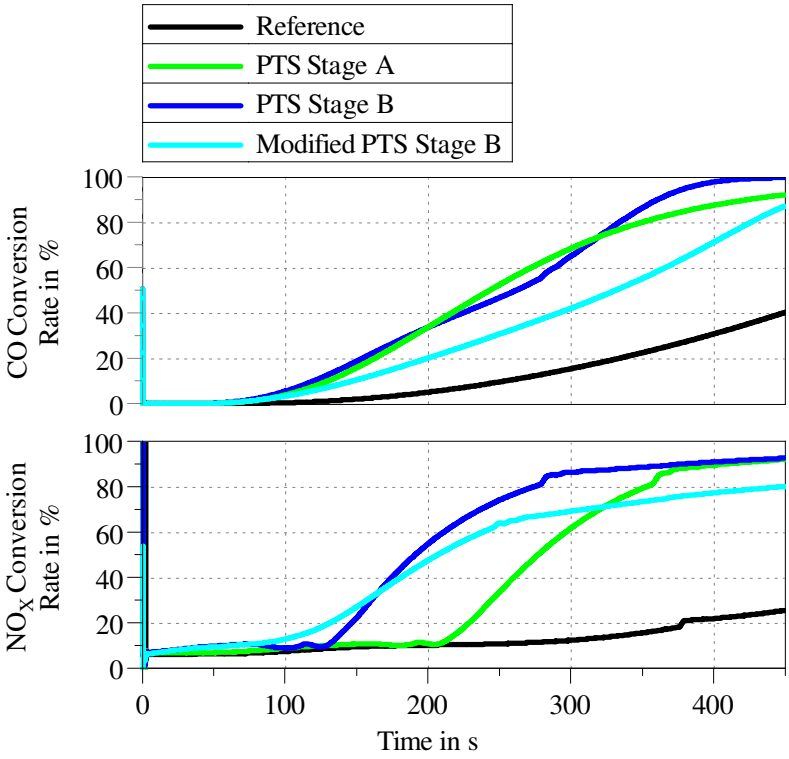

Figure 5.34: CO and NO_X conversion rates during the cold start scenario with shortened pre-turbine catalysts

Since the SCR1 is warmed-up more quickly with a shorter DOC upstream, the urea injection starts 16 s earlier with the modified catalysts. This is visible in the NO_X conversion rate, which increases earlier than that of PTS Stage B. After 170 s, the SCR1 system of PTS Stage B is warm enough to achieve a higher conversion rate with the longer SCR1 system. The higher NO_X conversion rate also has a beneficial effect on the oxidation rates of the downstream positioned cDPF because the NO inhibition is lower. Anyway, the conversion rates are higher than that of the reference system during the entire considered period.

The considered shortening of the catalyst to 50 % of its length is too drastic.

The shortening of the catalyst shows benefits during the load step on the cost of lower conversion rates, even when the temperatures are higher. Very high conversion rates are not achieved due to the shorter resting time within the smaller catalysts. A compromise of the catalyst length might be necessary. However, the optimisation of the length, cross-sectional area and cell density of the pre-turbine catalysts is beyond the scope of this work but might lead to more efficient conversion rates, a faster heat-up and smaller obstruction during the load step scenario. For the following examinations, the modified PTS Stage B is not considered anymore.

5.2.3 Modification of the HP-EGR

At the beginning of the presented cold start simulations in section 5.1.4, the gas temperature after an EAT component remains constant. This demonstrates that the warm-up of a component is not accelerated by increasing the heat transfer between the exhaust gas and the component. The gas temperature and its mass flow rate are the determining. In order to heat-up the pre-turbine EAT components more quickly, the cold start scenario is complemented by another PTS configuration. The high-pressure EGR (HP-EGR) extraction point of PTS Stage A is set after the pre-turbine EAT components, immediately before the turbine. With this modification, the entire exhaust gas mass flow of the HP-EGR passes through the pre-turbine components. Given the same temperature and pressure in the exhaust manifold, the higher mass flow rate also means a higher energetic flow for the components' heat-up.

With the chosen EGR strategy, above an engine speed of 2000 rpm the HP-EGR is active solely. At the examined operating point with a BMEP of 3 bar at an engine speed of 3000 rpm the HP-EGR rate is 33 %. This means that with the modification, the exhaust gas flow through the pre-turbine components is almost 50 % higher compared to the standard HP-EGR extraction point.

Due to the EAT components between the exhaust manifold and the HP-EGR extraction point of the modification, the EGR temperature does not increase immediately. Firstly, the EAT components are heated up. Since the EGR cooler is mostly bypassed, with the standard HP-EGR configuration, the gas temperature in the cylinder inlet is higher. This is also noticeable in the gas

temperature in the exhaust manifold that is up to 10 K above that of the modified system, revealing that the assumption of the same gas temperature in the exhaust manifold is inaccurate. The temperature development of the SCR1 inlet temperature is depicted in Figure 5.35, showing that the higher mass flow rate overcompensates the lower exhaust temperature. An inlet temperature of 150 °C is achieved 30 s faster, but the advantage decreases with the time so that for 200 °C, the lead is 25 s.

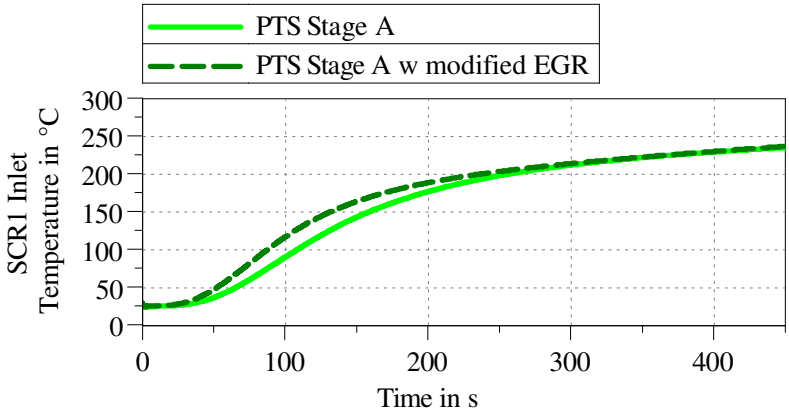

Figure 5.35: Temperature development of PTS Stage A with two different HP-EGR configurations

Additionally, the faster warm-up upstream of the turbine impacts the downstream component as well: The temperature of SCR2 is increased to the same extent as that of SCR1, and a temperature of 150 °C is reached 32 s sooner than with the standard HP-EGR configuration. The fuel consumption shows an enhancement of 0.5 % with the modification, despite higher pumping losses. The reason for this is lower wall heat losses due to lower temperatures in the cylinder.

The modification demonstrates some potential to enhance the heat-up of the EAT even further. This modification is only possible for PTS, increasing their potential regarding cold starts. A high LP-EGR rate might have a similar effect regarding the mass flow rate through the components but with lower temperatures. However, some issues have to be mentioned: The modified

HP-EGR has only benefited at operating points with high HP-EGR rates. With the chosen application, this is mainly above engine speeds of 2000 rpm. Additionally, the modification reduces the pressure difference between the EGR extraction point and the intake manifold. The steady state examinations show that the pressure upstream of the turbine is significantly lower than with the reference system at high engine speeds and high loads. Thus, at these operating points, the modification might lead to impossible HP-EGR rates.

5.3 Driving Cycles

The previously examined synthetic scenarios do not often occur in real driving events, even if it is not impossible. Driving at a constant speed at a flat motorway is an imaginable scenario in which the engine runs in one steady operating point. The load step could correspond to a constant speed drive when the road slope increases. The engine speed stays stable, but the demanded torque increases with the slope of the road. However, these scenarios are mainly suitable for reconstructing extreme driving situations and isolating single effects of the EAT systems. With the following investigations of driving cycles, more ordinary operating conditions are simulated.

5.3.1 Worldwide Harmonised Driving Cycle (WLTC)

The simulation setup of the WLTC is described in section 4.7.1. To keep the number of simulations small, only PTS Stage A is considered without any transient measures. It is the borderline case with the largest pre-turbine mass. The additional components before the turbine of PTS Stage A change the gas flow characteristics through the engine, especially during dynamic driving events. The build-up of boost pressure is strongly delayed due to the extra thermal inertia before the turbine. This also affects fuel consumption. In Figure 5.36, the fuel consumption difference between the reference system and PTS Stage A is visualised (a positive value indicates higher fuel consumption of PTS Stage A). Over the entire cycle, the reference system has an advantage of 0.6 % in fuel consumption.

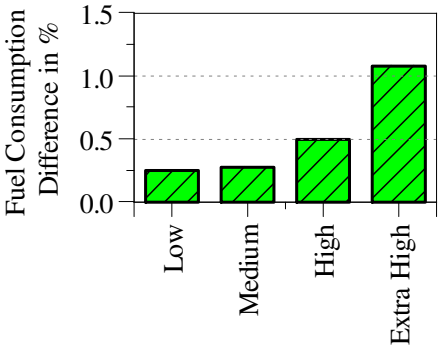

Figure 5.36: Fuel consumption difference during the WLTC split into the single parts (PTS Stage A - Reference)

The slightly higher fuel consumptions during all parts of the WLTC are in contrast to the steady state considerations. These showed the potential of PTS regarding fuel consumption in section 5.1.1 and in the literature [30][57]. The largest efficiency benefits of PTS were observed at high engine speeds. At these, the mass flow rate and the pressure ratio of the turbine are high. Thus, the effect of a lower exhaust manifold pressure due to the positioning of the pressure drops before the turbine is the greatest. This results in lower pumping losses and lowers fuel consumption. During the cycle, the efficiency optimized shifting strategy prevents the operation at high engine speeds, and the effect of lower exhaust manifold pressures is not apparent. Additionally, the PTS deteriorates the dynamic response of the engine. Therefore, it takes longer for a steady state to develop, and the driving situation might change again during this period so that hardly any stationary driving occurs.

The operating area during the entire WLTC is plotted in Figure 5.37, with the most frequent points coloured in red. The left plot shows the operating area with the reference EAT system and the right one with PTS Stage A. It can be seen that only very few points lie above an engine speed of 2000 rpm. Most operating with a positive load happens close to the steady state operating points 1 and 2 from section 5.1.1. At those points, the use of a PTS had a

disadvantage regarding fuel consumption due to the exhaust tract's changed pressure pulsations.

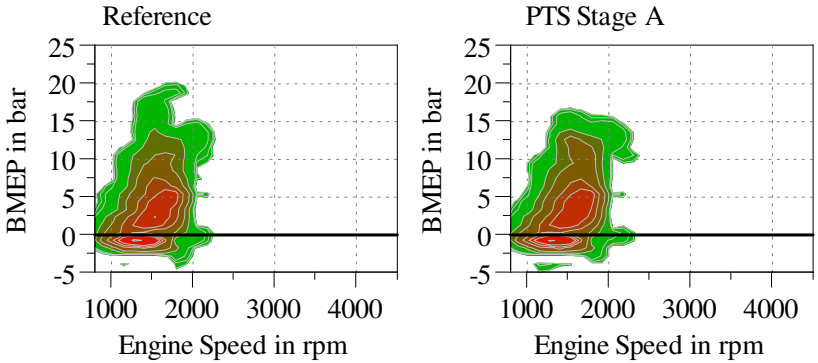

Figure 5.37: Distribution of the engine operating points during the WLTC

When comparing the operating distribution between the two systems, another aspect becomes visible: Without a supporting system, high loads are difficult to achieve due to the missing boost pressure. Thus, the low-end torque is not as high as with the reference system. The time to achieve a high load at these low engine speeds is too long, even at the end of the WLTC, when the pre-turbine EAT components are heated up. However, the operation above the naturally aspirated maximum load is possible, that is a BMEP of approximately 11 bar at 1500 rpm.

The highest difference in fuel consumption is observed during the extra high velocity part. Here the strongest acceleration of the cycle is conducted. In Figure 5.38, some of the characteristic values regarding the turbocharger are plotted for this last acceleration of the cycle. To estimate the intensity of the acceleration, the velocity is plotted additionally.

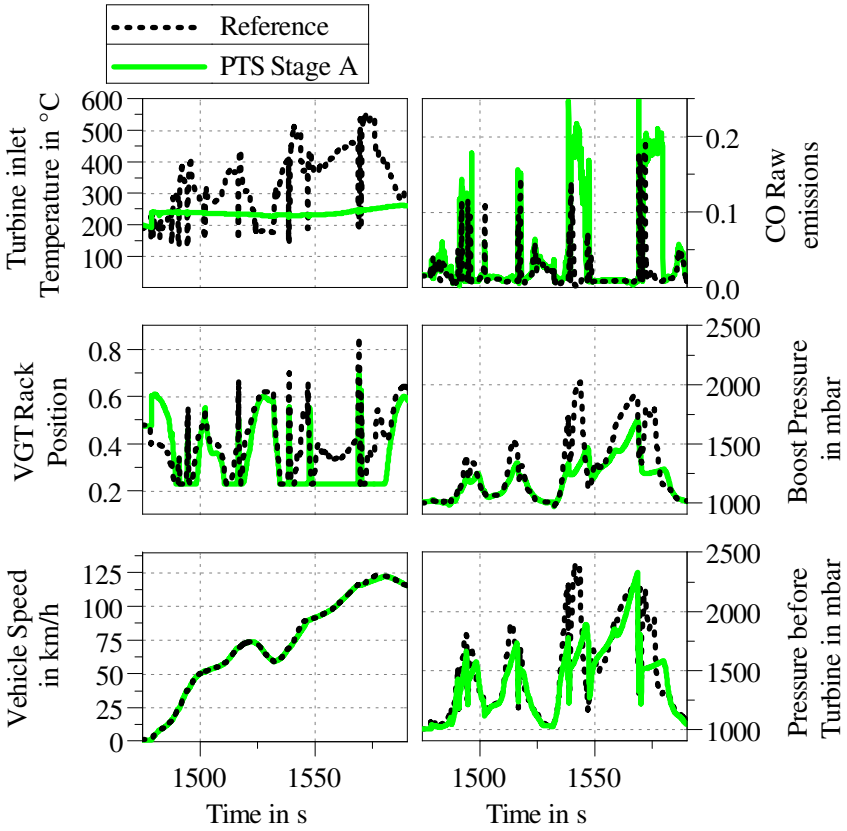

Figure 5.38: Boost pressure, pressure before the turbine, turbine inlet temperature, VGT rack position, and vehicle speed during the extra high velocity part of the WLTC

It is obvious that the boost pressure of the reference system is not achieved with the PTS. This has only a small influence on the vehicle speed since the target speed is almost achieved without a supercharging of the engine. Anyway, the supercharging system influences the combustion: Due to a richer air-fuel mixture in the cylinder, the PTS has lower internal efficiency. Additionally, the fewer mass in the cylinder has a lower thermal capacity and heats up quicker.

This increases the peak temperature during the combustion of the PTS compared to the reference system. The higher temperature increases the wall heat losses.

Another aspect that indicates the higher fuel consumption during the acceleration is the pumping losses. Since the desired boost pressure is not achieved, the VGT rack position is set to the closest position. This first increases the pressure upstream of the turbine before the boost pressure is rising, which results in high pumping losses. Compared to the wall heat losses, the disadvantage of pumping losses is almost twice as high. Even when the pressure upstream of the turbine is at the same level as with the reference system (and thus the pressure ratio of the turbine), the VGT rack position has to be operated at a more closed position because the turbine inlet temperature is lower. The closer VGT position results in lower turbine efficiency and thus higher losses. All the described effects have a negative impact on fuel consumption during strong accelerations.

During the gear change, the rack position is opened suddenly because the target load and target boost pressure decrease to a minimum, for example, after 1550 s. This results in a massive pressure descent before the turbine and in the intake manifold. Afterwards, the pressure levels from before the gear change are not reached for a longer period, and the VGT rack position stays closed again. This shows some potential for improvement in the application for PTS: During gear shifts, the VGT rack position should not change its position drastically in order to keep the pressure levels during the entire acceleration high. With the aid of simulation, this scenario is replicable for many possible applications in order to maintain the best one for the VGT rack position during gear shifts with a PTS.

The previously described supercharging system behaviour of the PTS additionally influences the raw emission formation. Compared to the reference system, the richer combustion of the PTS increases the carbon monoxide (CO) formation rate by approximately 35 % over the entire cycle. Due to the lack of fresh air, more locally rich zones are apparent in the cylinder, in which the combustion efficiency is lower, and the CO is formed. Figure 5.39 shows the CO conversion rate of both systems during each part of the WLTC. Additionally, the difference in CO emissions of the PTS Stage A compared to the reference system are visualised.

Especially during the extra high velocity part – where the already shown strongest acceleration takes place – the CO raw emissions are almost doubled

with the PTS due to the strongest lack of boost pressure during the cycle. Despite a small difference in the conversion rates, the tailpipe CO emissions are 1.5 times higher with the PTS because the raw emissions are too high for PTS to achieve the highest conversion rates. Although the catalyst temperatures are warmer than with the reference system, the tailpipe CO emissions are higher. For the reference system in the extra high velocity part, almost the entire CO is converted because the catalysts achieved the temperature window, where they work efficiently. In the cold phase at the beginning of the cycle, the CO raw emissions are highest in general, and only a small part of it is converted into less harmful CO_2. During the first two parts, the tailpipe CO emissions are 1 % lower with the PTS despite the higher raw emissions. The reason for this is the higher conversion rate due to a faster warm-up of the DOC and cDPF.

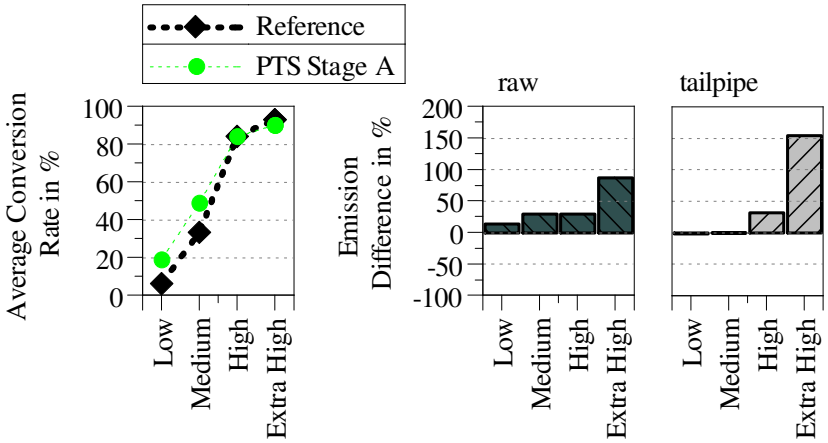

Figure 5.39: CO conversion rates and emissions during the WLTC without transient measures

The increase of the total hydrocarbon (THC) emissions with the PTS compared to the reference has the same root as for CO but is less pronounced with an increase by approximately 10 % over the entire cycle. The difference in raw emissions is equally distributed over all parts of WLTC, which is shown in Figure 5.40. Again, the highest raw emissions are apparent during the warm-up of the engine in the low velocity part. During this phase, the THC is barely

converted by the catalysts resulting in a large amount of tailpipe THC. As time goes by, the catalysts warm up and achieve a remarkable conversion rate of more than 93 % with the PTS compared to 84 % with the reference system. For the THC, the comparison between the reference and the PTS shows an advantage of the PTS in the tailpipe emissions, in particular for the high and extra high part. Here, the catalyst's more elevated temperature of the PTS causes a better HC oxidation and up to 60 % less tailpipe THC emissions. The THC tailpipe emissions of the PTS are approximately 19 % lower compared to the reference system over the entire WLTC.

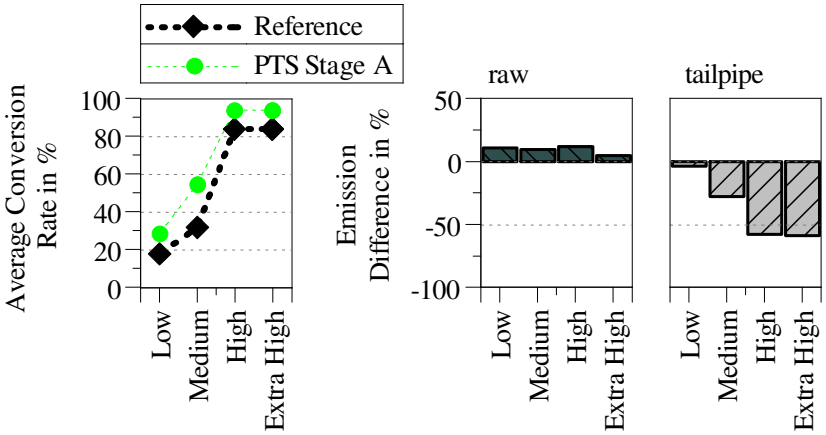

Figure 5.40: THC conversion rates and emissions during the WLTC without transient measures

The applied smoking limit prevents a rich air-fuel mixture, and the global air-fuel equivalence ratio is always greater than a value of 1.05. Therefore, during the entire combustion globally enough oxygen is available for complete combustion. The excess oxygen in combination with high temperatures during the combustion results in strong NO formation rates. Compared to CO and THC, the raw emissions of NO_X do not decrease in the high velocity parts, because during the long and stronger accelerations, the combustion temperature rises and favours NO_X formation. As already described, the PTS causes a lack of boost pressure and increased maximum temperatures due to less mass in

the cylinder. This causes approximately 6 % higher NO_X raw emissions of the PTS compared to the reference system on average. The conversion rates of the SCR systems and the raw and tailpipe emission comparison are depicted in Figure 5.41.

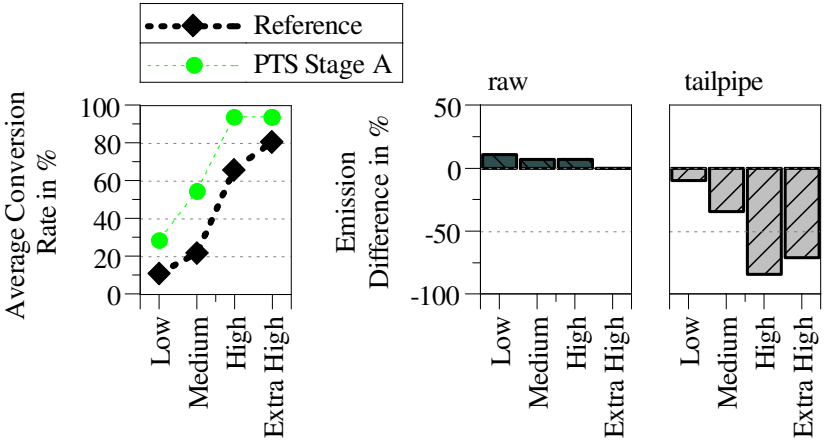

Figure 5.41: NO_X conversion rates and emissions during the WLTC without transient measures

NO_X conversion starts in the high velocity part, where remarkable emission reduction for the reference system is visible. The tailpipe NO_X emissions of PTS Stage A are more than 70 % lower for the last two parts and with 49 mg/km respectively 58 mg/km below the Euro 6d limit of 80 mg/km, without any warm-up strategy. Besides the higher temperature in the SCR1, the second urea dosing system is found to be advantageous. Compared to the reference system, PTS Stage A has the two SCR catalysts more separated. The temperature difference between the two catalysts becomes higher and it is more probable that one of the catalysts operates in the efficient temperature window.

Regarding the NO_X reduction, a clear advantage of PTS Stage A over the entire cycle is visible, resulting in an overall conversion rate of 71.5 % to 50 % with the reference system. For low temperatures, the fast SCR reaction is crucial in the SCR system. A high NO_2/NO_X ratio is necessary to reach high NO_X

conversion rates at low temperatures. During the colder phases in the low velocity parts, the warmer DOC and cDPF of the PTS increase the ratio of NO_2/NO_X by oxidising NO. Thus, a NO_X reduction is already apparent during the first parts of the cycle, when temperatures are still relatively low.

Besides CO, HC, and NO_X, soot was modelled and examined during the WLTC. Figure 5.42 shows the filter loading and DPF average filter temperature during the entire WLTC. The total amount of formed soot in the cylinders is 2 % higher with the reference system. As the reason for this, the higher combustion temperatures with the PTS due to a lower gas mas inside of the cylinder are identified. This increases the oxidation rate of soot particles inside the cylinder. The contradictious effect of less oxygen in the cylinder that favours the soot formation is overcompensated.

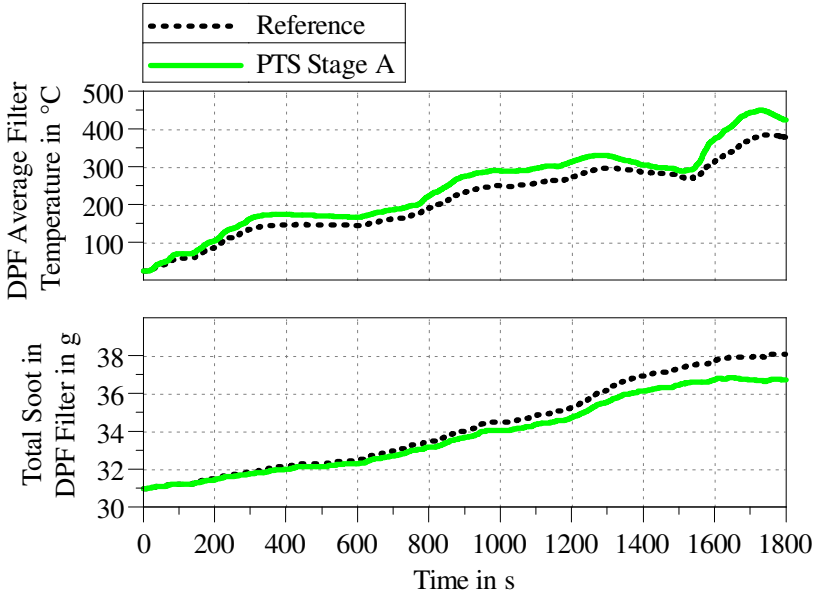

Figure 5.42: DPF average temperature and collected soot mass in the filter during the WLTC

The higher DPF filter temperature favours the passive DPF regeneration. Additionally, the hotter DOC of the PTS oxidises a greater amount of NO into NO_2. For the passive regeneration, the following reaction (10) is dominant, in which the soot reacts with NO_2. As already described, due to higher temperatures in the catalytic coatings of the pre-turbine DOC, the NO_2/NO_X ratio is higher for the PTS. In combination with the higher DPF temperatures (up to 50 K), this results in higher passive regeneration rates. Approximately 15 % less mass of the filtered soot remains in the filter during the entire cycle with the PTS.

The lower DPF loading at the end of the cycle shows potential advantages of a pre-turbine DPF: Firstly, it might increase the triggered active DPF regeneration intervals. The active regeneration is usually triggered by means of high exhaust temperatures that are achieved by fuel post injections. The post injections do not contribute to the engine torque but increase the fuel consumption remarkably. Alternatively, the size of the DPF might be reduced to keep the intervals between the regenerations constant. A smaller DPF usually leads to a lower pressure drop. Another point is the lower pressure drop over a less loaded filter. This might save some fuel in longer driving cycles without an active DPF regeneration. However, the heat released during the active regeneration with a pre-turbine DPF should not get too high to avoid thermal damage at the turbine. This is possibly realised by lower regeneration temperatures and the control of the exhaust gas temperature.

Despite the moderate accelerations in the WLTC, the engine configurations with PTS Stage A could not always follow the target speed perfectly. When the desired torque exceeds the naturally aspirated load, the inertia of the system is too high to provide the target boost pressure immediately. This causes 14 short periods of one second during which the actual vehicle velocity is outside of the tolerance range. This indicates that PTS Stage A is not applicable in passenger cars in series without dynamic support.

As a supplement to the WLTC shown with a cold engine as the initial condition, both systems are examined again in the WLTC, but this time with a warmed-up exhaust system at the start and a more common shifting strategy. At the beginning of the cycle, the entire exhaust tract temperature is set to 200 °C, and the cooling water temperature is 90 °C. The modification of the shifting strategy leads to the same power demand to higher engine speeds. This is visible in

the frequency distribution over the engine map in Figure 5.43 and mitigates the deviation between the reference system and the PTS. With this shifting strategy, even with PTS Stage A, the target velocity profile is followed within the tolerance band.

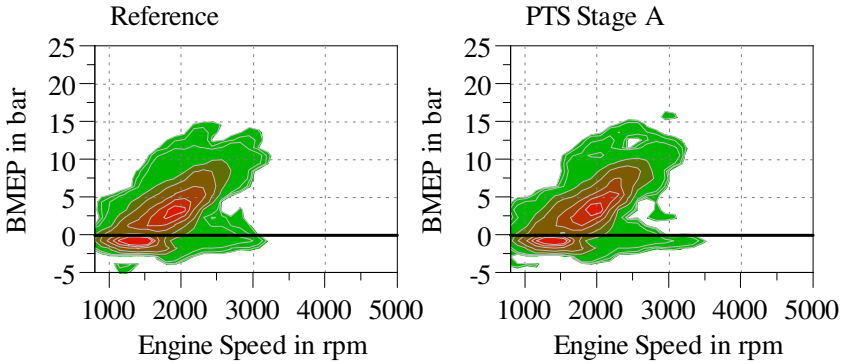

Figure 5.43: Distribution of the operating points during the warm WLTC with modified shifting strategy

The modification of the shifting strategy leads to higher fuel consumption for both configurations. The reason for this is more pumping losses due to larger backpressure at the increased engine speed. Additionally, the engine friction rises with engine speed. The results of the steady state examinations of section 5.1.1 revealed the benefits of the PTS at high engine speeds. It was expected that these results can be transferred to the WLTC. Since the turbine inlet temperature with the PTS increases only slowly and shows hardly any change due to the modified switching strategy, it is during the acceleration still like in Figure 5.38. Compared to the reference system, the lower turbine inlet temperature is compensated by a higher demanded pressure ratio over the turbine. This causes higher backpressure and more pumping losses. Over the entire cycle, the fuel consumption is 1.15 % higher with the PTS. However, the build-up of boost pressure is faster at higher engine speeds, which is in accordance with the investigations of the load steps in section 5.1.2.

Furthermore, the more significant backpressure leads to higher internal EGR rates that favour the soot formation with the PTS. In contrast to the previously shown results of the WLTC, with the modified shifting strategy, the total amount of soot is 6.3 % higher compared to the reference system. Additionally, the maximum DPF filter temperature is more than 100 K lower, although the initial temperature is higher. This is caused by the higher engine speeds during towing, which cool the EAT system more severely. However, the filter loading at the end of the cycle is lower with the PTS compared to the reference system. The higher temperature and a greater NO_2 concentration due to more active DOC and cDPF engage the passive DPF regeneration.

The higher engine speed caused by the shifting strategy also has an impact on the raw emission formation. The NO_X raw emission formation is reduced by 20 % with the reference system and 16 % with PTS Stage A because the engine operation at the low-end torque is avoided, where a strong NO_X formation is observed. Regarding the CO raw emissions, with the reference system, no remarkable change is detected. The faster build-up of boost pressure with the PTS due to the shifting strategy decreases CO formation, in particular during the high and extra high parts. HC emissions are also lower for both systems because great HC formation during the cold start is avoided. Anyway, the raw emissions are still higher with PTS Stage A for all species compared to the reference system. The higher starting temperatures and lower raw emissions lead to increased conversion rates for all considered species, which is depicted in Figure 5.44.

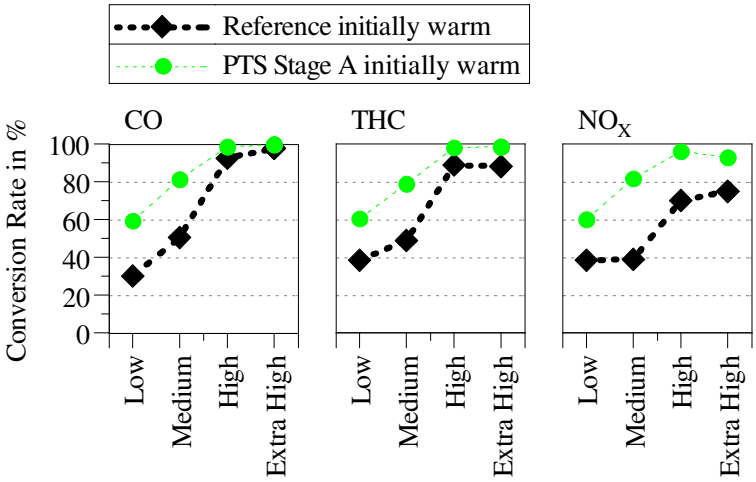

Figure 5.44: Conversion rates during the WLTC with an initially warm EAT and modified shifting strategy

The initial temperature of 200 °C is not efficient to achieve full pollutant reduction. With PTS Stage A, the temperature of the DOC and cDPF is rising faster, which results in a better conversion, especially for the low and medium velocity parts. In the same manner, the PTS affects the NO_X conversion rate, for which the separation into two autonomous SCR system has an additional advantage. Over the entire WLTC with PTS Stage A, 47 % less CO, 48 % less HC and 60 % less NO_X is emitted.

5.3.2 Low-Temperature RDE Cycle

All PTS are examined during a cold RDE driving cycle at an ambient temperature of 0 °C, with respect to section 4.7.2. With the long downhill drive during the slow urban part, the warm-up of the engine is very demanding. No special warm-up measures are applied to outline the differences between the EAT component's position only. The longitudinal vehicle model from section 3.5 is used in combination with an EATC to ensure that the velocity profile is followed

exactly. This also guarantees similar conditions for diesel combustion regarding the air to fuel ratio.

The first examination is conducted with a cold engine at the start of the driving cycle, i.e., all parts have 0 °C, the same temperature as the environment. Due to the long downhill passages, the load requirement is low, and so is the exhaust gas temperature. In the downhill passages, the engine is towed often. During towing, no fuel is injected, but the air is pumped through the air path, which leads to cold exhaust temperatures that let the EAT components cool out quickly. Compared to this, the impact of the cooling out during still stand is small. The EAT barely reaches temperatures during the urban driving, at which a significant conversion takes place and the temperatures in the exhaust tract alternate. For all considered EAT systems, this causes a steady increase and drop of the catalysts temperatures, particularly when positioned as the first component of a pre-turbine system. This is demonstrated by the SCR1 inlet temperature in Figure 5.45 with PTS Stage C.

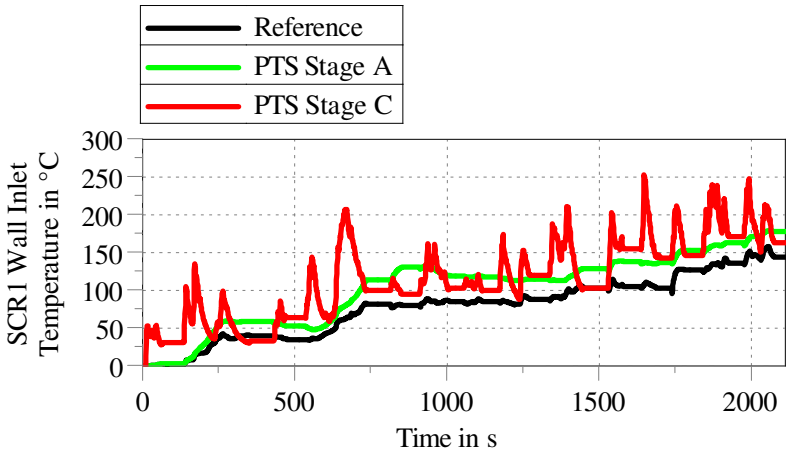

Figure 5.45: SCR1 inlet Temperature development during the urban part of the low-temperature RDE

For convenience, only three curves are shown. Usually, the warm-up is assessed by the time required until a certain temperature or conversion rate is achieved.

Under these conditions, this is strongly dependent on the chosen value, and after achieving it, it might drop again. Thus, reaching a certain temperature or conversion level is not meaningful to assess and compare the EAT systems.

In order to obtain a good overview of the thermal behaviour of the EAT components, some characteristic quantities of the respective configuration are presented in Figure 5.46 for the urban part of the driving cycle (the first 2111 s). The maximum wall inlet temperature of each component and configuration is marked with a cross and the average temperature during these first 2111 s with a circle. Additionally, the temperature range between 20 % and 80 % percentiles is shown with the dashes. These values are chosen arbitrarily to highlight the range in which the components operate most of the time during the urban part.

The maximum temperature is highest in the first component after the cylinders, and the pre-turbine DOC has an up to 32 K higher maximum temperature compared to the reference. However, the wall inlet temperature is for all configurations more than 80 % of the time below 170 °C, which shows that no efficient emission removal is possible. The results are used nevertheless to demonstrate the thermal behaviour of the PTS compared to the reference system and to each other. Since the temperature is too low, exothermic reactions on the catalytic surfaces are negligible. SCR1 best illustrates the impact of the position of a component. The differences in the peak temperatures are the largest because the inlet temperature rises quickly as soon as the engine load increases. After a temperature peak, it drops rapidly during the towing engine, which is visible well in Figure 5.45 for PTS Stage C. Even at the end of the urban part, the SCR1 wall inlet temperature of PTS Stage C drops below that of PTS Stage A. This is why, despite the peak temperature of 251 °C, for less than 6 % of the time, the temperature is above 200 °C.

During towing, previous components do not act as a heat sink as during the load steps or cold starts. Rather, they have the property of a heat source. This is why the 80 % percentile is almost identical to PTS Stage B. The average temperature of the three PTS is at least 25 K higher compared to the reference system. This underlines the improvable underfloor position of the SCR1 in the reference system.

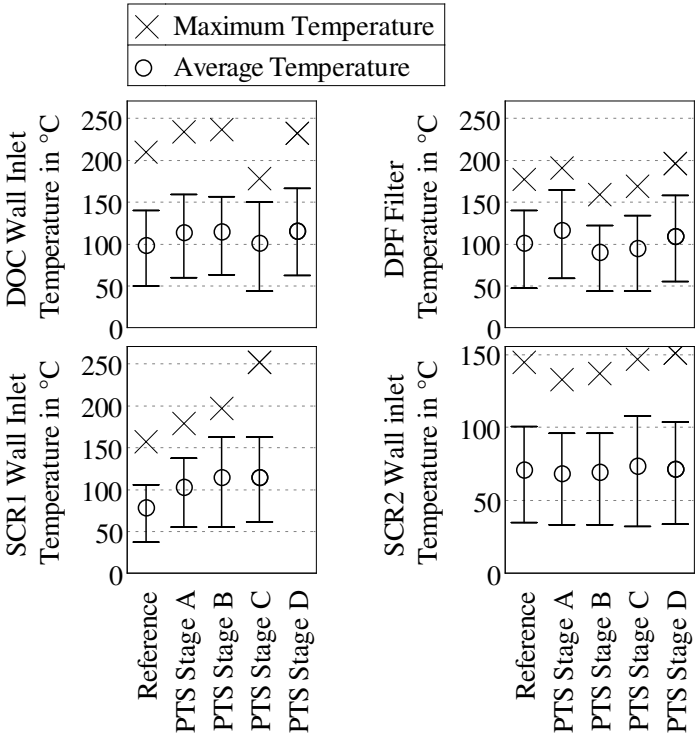

Figure 5.46: The temperature during the urban part of the low-temperature RDE

For the DPF, the pre-turbine position is demonstrated in the higher average and maximum temperatures of PTS Stage A and PTS Stage D, but the absolute differences compared to the reference system are smaller than for the DOC. Besides the number and size of upstream positioned components, their order also influences the apparent temperature. This becomes apparent in the difference of the 80 % percentile and maximum DPF temperature between PTS Stage B and PTS Stage C and also in the temperature differences of SCR2. A larger thermal mass upstream of the turbine keeps its inlet temperature lower. Thus, to achieve the same turbine power, its pressure ratio needs to be increased, which is realised by a more closed VGT rack position. The higher pressure ratio means

a greater expansion of the gas over the turbine, resulting in a larger temperature drop and lower post-turbine temperatures. Therefore, the maximum SCR2 wall inlet temperature of PTS Stage A is the lowest, followed by PTS Stage B. Although PTS Stage D has a large pre-turbine thermal mass, the maximum SCR2 temperature is the highest. The reason for this the elimination of one component, which makes the system more compact.

The more closed VGT rack of PTS Stage A during most of the time of the urban part impacts the temperature of the pre-turbine EAT components. Due to the higher pressure in the exhaust manifold caused by the rack position, the expansion from the cylinder into the exhaust manifold is smaller. This results in a slightly higher gas temperature in the exhaust manifold that is reflected by the higher average DOC wall inlet temperature. Additionally, to the demonstrated results, the urban section of the RDE is considered again with an initially warm EAT. The entire exhaust tract temperature is set to 200 °C. The assessment of these simulations showed that instead of further warming-up, the EAT components cooled out from the initial temperature. The first EAT component has the widest temperature range again and has the warmest and coldest temperature compared to the other components. Except for the first components, the maximum temperature during the urban part is the initial 200 °C.

This demonstrates that the warm-up and keeping warm of the EAT system during the urban part is too demanding without any measures. Anyway, the PTS showed a faster warm-up for the pre-turbine components and higher maximum temperatures. The following rural part of the low-temperature RDE cycle is mainly uphill with higher power demand and fewer towing passages. The starting conditions are that of the end of the urban part and consequently vary slightly between the configurations. For the evaluation, the same procedure as for the urban part is applied to the rural part that starts after 2112 s and ends after 4613 s of the total driving time.

The maximum and average wall inlet temperature of the EAT components are plotted in Figure 5.47. The lower dash marks the temperature, above which the current one is 80 % of the time. Except for the first components, this temperature is above the maximum temperature during the urban part.

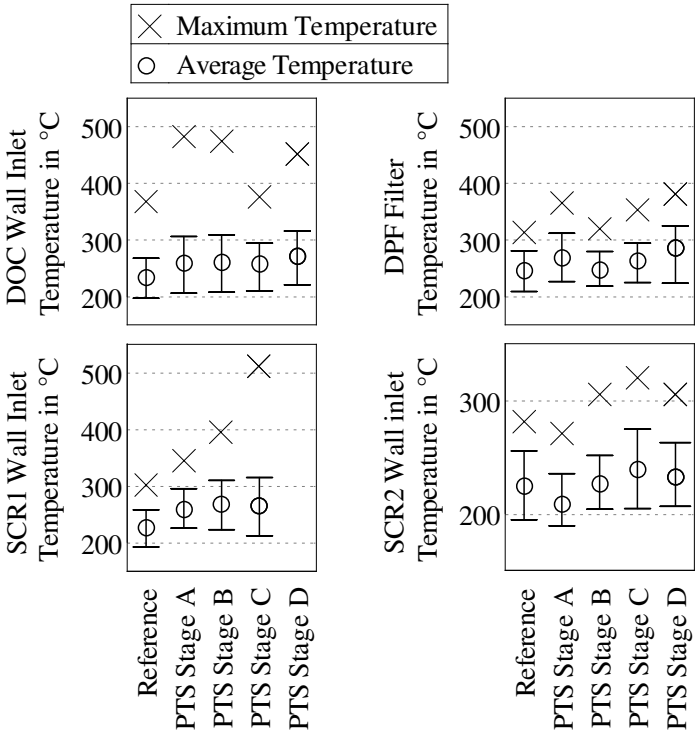

Figure 5.47: The temperature during the rural part of the low-temperature RDE

With the higher temperatures in the DOC and cDPF, remarkable oxidation rates are observed. Their heat release has an impact on the temperature of the downstream components. Thus, for this part, the isolated thermal consideration of the warm-up is not possible anymore. The faster warm-up of the DOC and cDPF reduces CO and HC emissions and accelerates the further warm-up of the components. With PTS Stage C, the wall inlet temperature of SCR1 is above 500 °C, where ammonia oxidation might occur. Thus, the urea injection is deactivated for these high temperature points. The system is heated-up quickly enough that even the SCR2 reaches the temperatures for an efficient NO_X removal quickly. Thus, the too hot conditions of SCR1 are compensated by the second SCR system. Anyway, most of the time, the temperature is within the optimal working range for the SCR1 system. Compared to the reference

system, all PTS have a larger temperature gap between the two SCR systems. Since its temperature range is limited to the high and the low end, this extends the operation field in which an efficient NO_X conversion is possible.

PTS Stage C has the NO_X removal of SCR1 upstream of the DOC and cDPF. This avoids the NO inhibition in these components, leading to higher CO and HC oxidation rates described in section 5.1.4. The same effect is visible with PTS Stage B in the cDPF. This is the reason for the higher SCR2 wall temperature of these configurations. Figure 5.48 summarises the conversion differences of the PTS compared to the reference system.

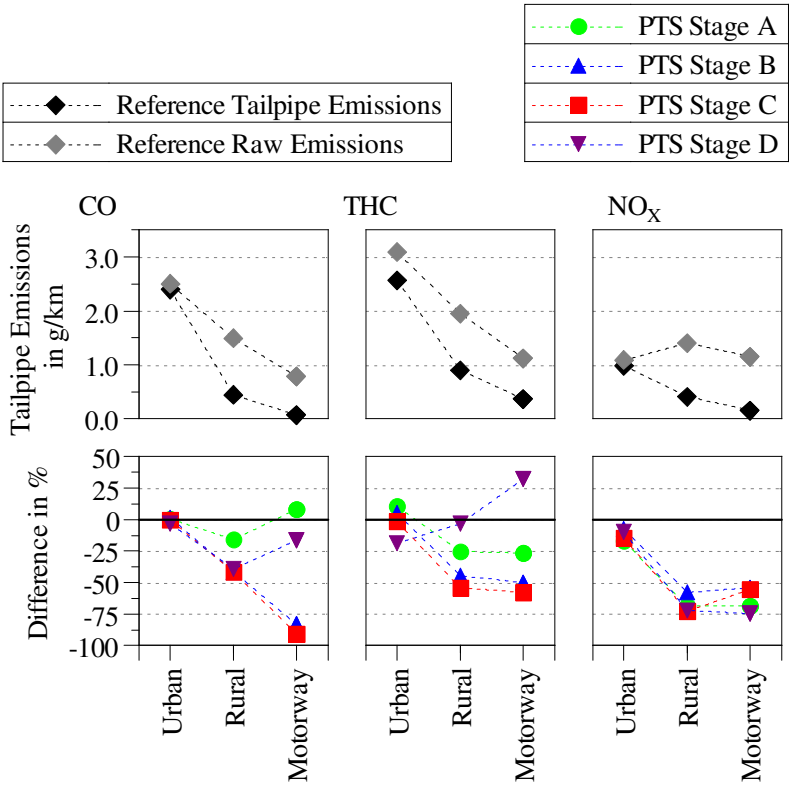

Figure 5.48: Tailpipe emission differences between the reference system and PTS during the low-temperature RDE cycle

The higher CO and HC conversion rates of PTS Stages B and C are clearly visible, in particular, for the last sections of the cycle. For the urban part, the CO tailpipe emissions are the same for all configurations, because no conversion takes place. For the motorway part, the CO tailpipe emissions of the reference system are minimal. Thus, small absolute deviations have an impact on the relative difference.

Regarding HC, PTS Stage D shows lower emissions, because its DOC has a strong HC adsorption characteristic. During the urban part, the HC reduction is completely caused by the HC adsorption. The temperatures of the DOC and cDPF are higher of PTS Stage A. Thus, the desorption of HC starts earlier compared to the other systems, causing 10 % more HC tailpipe than the reference. However, during the rural and motorway part, this PTS reduces more HC than the reference. Due to the higher temperatures in the SCR1 respectively sDPF, all PTS have fewer NO_X tailpipe emissions. During the urban part, the benefit is between 7 % for PTS Stage B, and 16 % for PTS Stage A. The better NO_2 to NO_X ratio of PTS Stage A counteracts the higher SCR1 temperatures of PTS Stage C, that has a benefit of 14 %. In the motorway part, the faster cooling-out of SCR1 during towing passages diminishes the NO_X reduction performance of PTS Stage C compared to PTS Stage A. However, the advantage compared to the reference system is still 55 %.

5.3.3 High Dynamic RDE Cycle

The PTS examinations during a high dynamic RDE drive aim to estimate the energy requirement for the compensation of the dynamic lag within daily driving situations. The details of the driving cycle are explained in section 4.7.3. Two different transient measures are implemented in the simulation model for PTS Stage A: a P2-hybrid, which adds power to the engine shaft before the gearbox and an electrically assisted turbocharger (EATC) that accelerates the turbocharger shaft when required to increase the boost pressure more rapidly. Both measures are only activated when the acceleration pedal exceeds a value of 80 %, and the target boost pressure is not achieved. This application is not optimized regarding fuel consumption, the raw emission formation, or the EAT heating up. The main target is rather to follow the velocity profile with the fewest possible extra energy amount. However, besides the energetic view,

the impact of the transient measures on the emission formation and on the conversion rates of the EAT is part of the evaluation. Only PTS Stage A is assessed during this cycle because it has the largest thermal inertia upstream of the turbine. Thus, the outlined effects are probable to occur for the other PTS as well, in a less distinctive expression. Both variants of PTS Stage A are compared to the reference system. Due to stability issues of the simulations, only the soot formation is considered, but not its filtration or DPF regeneration.

Over the entire driving cycle, the reference system has an average fuel consumption of 48.77 g/km. With PTS Stage A and an EATC, it is 49.51 g/km, which is slightly higher, mainly caused by higher pumping losses. With the chosen strategy for controlling the EATC, the VGT rack position is set to the closest before the electrical support is activated. Even during the boosting of the EATC, this position is held and over the entire cycle, the PTS forces the VGT to a more closed position. This leads to the mentioned increased pumping losses due to higher pressure before the turbine and in the exhaust manifold. A restriction for the closest position of the VGT in combination with an EATC, might lead to achieve higher turbine efficiencies and lower pumping losses. The highest efficiency of the turbine is usually at a half-closed rack position (0.4 – 0.6). The lower pressure ratio over the turbine needs to be compensated by the electrical motor of the EATC. Although the electrical power demand would increase, the total energy requirement is possibly lower. Another aspect that needs to be mentioned is that the shaft inertia of the EATC is 10 % higher compared to the standard turbocharger. This increases the turbo lag and the described higher pumping losses.

With the P2-hybrid, the average fuel consumption is with 45.92 g/km almost 6 % lower compared to the reference system. During the strong accelerations, the injected fuel mass is often lambda-limited by the amount of fresh air. Since the P2-hybrid does not increase the air mass flow rate directly, less fuel is injected. This is compensated by the stronger electrical motor and a higher electrical energy requirement of 1.66 kWh compared to 0.07 kWh with the EATC. For comparison, the PHEV version of the longitudinal vehicle model has a capacity of 13.5 kWh. It has to be mentioned that the energy amounts correspond directly to the mechanical energy; to obtain the energy amount that has to be provided by the battery, an estimation for the electrical efficiencies has to be included.

An overview of the fuel consumption and required boosting energy is given in Figure 5.49, split into the single parts of the driving cycle. The average fuel consumption per kilometre is highest during the urban part for all considered systems due to many acceleration and deceleration manoeuvres at low velocities. Additionally, the engine structure is heated up after the cold start, which requires extra energy that comes from the fuel. The altitude difference between the start and end of this part is 150 m downhill.

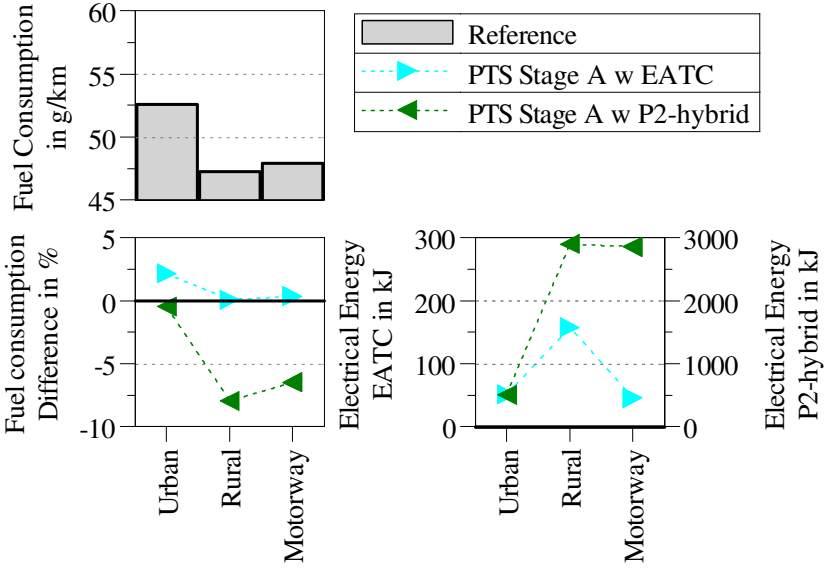

Figure 5.49: Fuel consumption and required electrical energy of the transient measures during the high dynamic RDE cycle

The average fuel consumption per kilometre is lowest during the rural part due to higher velocities and smoother accelerations, although the endpoint lies 100 m above the start. The strong acceleration from still stand to 150 km/h leads to increased fuel consumption in the motorway part. With the EATC, the disadvantage regarding fuel consumption compared to the reference is lowering with time from 2.17 % higher fuel consumption in the urban part to 1.15 % on the motorway. The reason for this is the heating up of the pre-turbine EAT

such that a higher enthalpy rate reaches the turbine, and the pumping losses are reduced with the increase of the turbine inlet temperature and short boosting periods of the EATC.

With the EATC, the highest external energy is required during the rural part because here most strong accelerations are conducted, and the turbine inlet temperature is still not as high as on the motorway. Additionally, the rural part is more than twice as long as the motorway section. During this, the required energy drops to the same value as that of the urban part. One reason for this is the heated-up exhaust tract that shortens the supporting periods. The higher turbine inlet temperature also enables the recuperation mode of the EATC instead of opening the VGT rack position. 51 kJ of mechanical work are recuperated during this section, whereas 88 kJ are required. Taking into account the efficiency of the motor and battery, this nevertheless improves the overall balance to a considerable extent.

The decisive variables that allow recuperation are plotted in Figure 5.50, where several short recuperations take place. It is visible that the acceleration pedal and turbine inlet temperature are strongly connected for the reference system. The turbine inlet temperature with the PTS stays almost constant during the entire time, independent of the pedal position. The target load and target boost pressure depend on the accelerator position. When it drops, the VGT rack is usually opened in order to control the boost pressure. Instead of opening the VTG further and letting the exhaust gas escape unused, energy is recovered via the EATC. As a limit for the rack position, a value of 0.6 is used. Again, it must be mentioned that a coarse controlling strategy for the EATC was chosen that is still improvable: the more closed VTG rack increases the turbine efficiency, and energy is recuperated, but the pressure before the turbine is higher, which implies greater pumping losses. To achieve the highest efficiency, further investigations are necessary. No recuperation was considered during braking with the EATC, which would be possible with a mild hybrid vehicle. However, this shows some potential in the combination of PTS with an EATC that can be fully exploited with the help of the virtual application in the simulations.

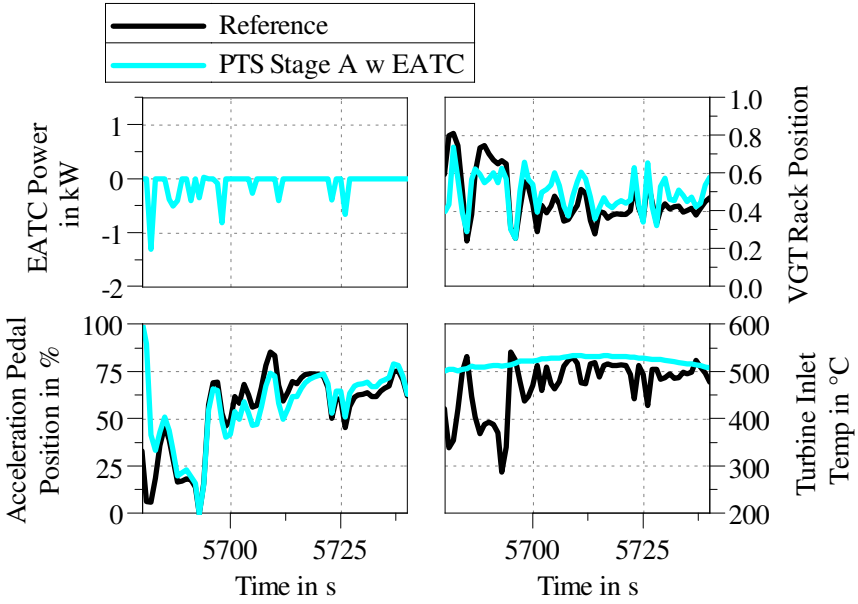

Figure 5.50: EATC power, VGT rack position, turbine inlet temperature and acceleration pedal position during a recuperation period

In contrast to the EATC, with the P2-hybrid for PTS Stage A, fuel consumption is lower than with the reference system in all parts. However, more support energy is required. Particularly in the parts where the consumption advantage is greatest, most energy is required, as shown in Figure 5.49. However, the required external energy is more than 20 times higher than with the EATC. Assuming a total efficiency of 70 % for the battery and the electric motor, the total energy requirement is approximately 1.5 % lower than that with the reference system. However, the effect of the PTS on the P2-hybrid cannot be extracted. Implementing a P2-hybrid with the reference system would have the same effect.

Overall, it is shown that the dynamic disadvantage of the largest PTS can be compensated with relatively limited external energy input. This is clarified again using the example of a stronger acceleration during the RDE cycle, where the required electric support power is particularly high. During the acceleration, the

differences between the configurations are the highest, and the dominant effects are best displayed. In Figure 5.51, an acceleration from 0 to almost 100 km/h is examined for the reference system, the PTS Stage A with an electrically assisted turbocharger, and the PTS Stage A with a P2-hybrid electrical support. The velocity profile is followed well by all three systems.

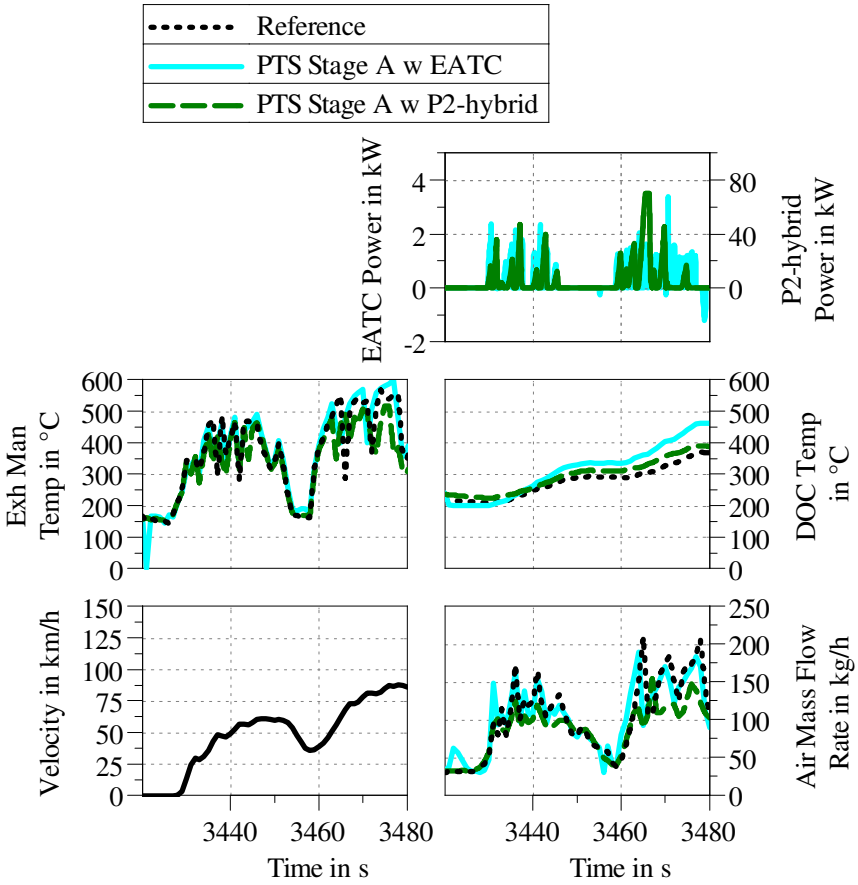

Figure 5.51: Velocity, fresh air mass flow rate, exhaust manifold temperature, DOC wall outlet temperature, and required electrical power for one acceleration during a high dynamic RDE cycle.

During the acceleration event, the required boost power of the two configurations varies strongly: The EATC requires less than 4 kW for a short period, whereas with the P2-hybrid, the extra power reaches 70 kW. The required external energy for the shown acceleration is correspondingly 5.7 times higher with the P2-hybrid compared to the EATC.

The impact of the EATC on the entire engine becomes visible in the higher mass flow rate over a long period. Since the amount of injected fuel is limited by the apparent fuel to air ratio, more fuel is injected with the EATC and the reference system compared to the variant with the P2-hybrid. This is reflected in the higher gas temperatures in the exhaust manifold that are also representing the combustion temperature. During idling, the temperature drops to the same value for all three variants (between 3455 and 3460 s). The higher air mass flow rate combined with the increased exhaust gas temperatures results in a faster heating-up of the EAT components. This is demonstrated by the DOC Temperature that is with the EATC more than 50 K above the one with the P2-hybrid at the end of the section. The same behaviour is observed in the warm-up of the exhaust system at the beginning of the driving cycle: The DOC outlet temperature reaches 200 °C with PTS Stage A and an EATC after only 91 s and with the P2-hybrid 100 s. If one considers the time until the outlet temperature reaches 300 °C, the advantage becomes even more apparent. With the EATC, it is exceeded after 2338 s, the P2-hybrid needs 113 s longer, and the post-turbine DOC of the reference system reaches the outlet temperature of 300 °C after 2928 s. Hence, the EATC does not only help to compensate the dynamic disadvantage of the PTS but also to reduce the warm-up time of the EAT.

Despite the higher boost pressure, the CO raw emissions with the EATC are still higher than for the reference system, which is shown in Figure 5.52. Here the cumulative raw and tailpipe emissions during the acceleration of Figure 5.51 for the two configurations are compared with the reference.

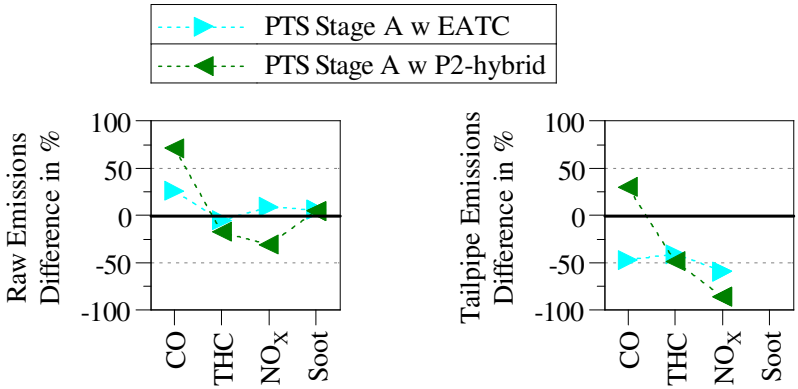

Figure 5.52: The relative difference of raw and tailpipe emissions between the reference system and PTS Stage A with electrical support during one RDE acceleration

A closer look at the configuration with the EATC shows that during the acceleration, there are short periods in which the EATC is not active. In these periods, the CO raw emissions increase due to a richer combustion. This shows some potential for an improvement of the chosen EATC controlling strategy that is beyond the scope of this work. Again, a virtual application by means of 0d/1d simulation seems promising. NO_X and HC raw emissions show fewer differences; higher combustion temperatures with the EATC are indicated by a little warmer exhaust manifold temperature in Figure 5.51 and result in slightly higher NO_X raw emissions. The soot formation is 6 % higher for both PTS configurations. The reasons for this are the same as that of the increased CO raw emissions. Since no filtering is considered, no statement can be made about the tailpipe soot.

With the P2-hybrid configuration, CO raw emissions are remarkably higher compared to the reference system. The P2-hybrid does not intervene in the engine's air path and the boost pressure, and thus the fresh air flow rate is drastically lower. During the acceleration, the maximum load of the combustion engine is demanded, and the fuel injection rate is limited by the amount of apparent oxygen. This is the reason for the higher CO emissions. HC and NO_X raw emissions are lower, though. NO_X formation is temperature driven and

so mitigated by the lower temperatures. In terms of HC emissions, a similar tendency as for the CO raw emissions was expected. As already described, the fresh air flow rate is remarkably lower, and less fuel can be injected to stay above the smoking limit with the air to fuel ratio. The amount of injected fuel is a degree for the possible heat release and exhaust temperatures. The less injected fuel is the reason for the lower exhaust temperatures. Additionally, less fuel also prejudices the likelihood of remaining unburned or partially burned fuel in the form of HC emission.

With respect to the tailpipe emissions, the PTS shows potential with both transient measures. Although the P2-hybrid shows difficulties in converting the higher amount of CO raw emissions, the tailpipe THC (-38 %) and NO_X (-85 %) are reduced remarkably. For both PTS, the SCR1 has an approximately 50 K higher substrate temperature that leads to higher conversion rates. The PTS with the EATC shows a tailpipe emission reduction for all considered emission types. Besides 60 % less tailpipe NO_X, the tailpipe CO reduction by 40 % stands out. This is a result of the faster-rising temperature in the DOC. The effects shown with regard to emission formation are evident over the entire cycle.

Figure 5.53 shows the relative deviation of the raw emissions with PTS Stage A compared to the reference system. CO raw emissions are higher due to the richer combustion. This becomes most clear during the motorway part, where the strongest acceleration is conducted. During this acceleration, the EATC is activated for many short periods that last about one second. The boost pressure rises until its target value is reached. In the following, it drops quickly until the EATC is activated again. This drop of the boost pressure causes rich combustion corresponding with a high CO formation rate. During the other parts with the EATC, the air mass in the cylinder is increased compared to the P2-hybrid configuration. The air to fuel limit is reached more often with the P2-hybrid, which results in higher CO formation rates over the entire cycle.

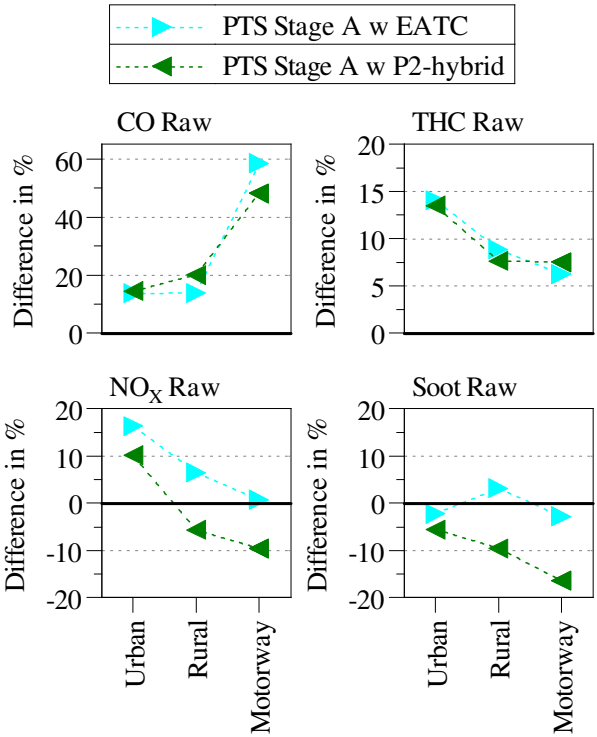

Figure 5.53: Difference between PTS Stage A and the reference system during the dynamic RDE regarding raw emissions

In contrast to the acceleration section presented, the HC raw emissions show a different trend over the entire cycle. With both configurations of PTS Stage A, HC formation is encouraged, in particular during the urban part, where the engine is still cold. The globally lower air to fuel ratio with the PTS in combination with cold combustion temperatures during a large portion of the operation is identified as the cause. This also happens at moderate accelerations, during which the boost pressure build-up is delayed. This overcompensates the explained mechanism of the lower HC raw emissions during strong accelerations, especially during the urban part. For the higher NO_X raw emissions with the PTS during the urban part, no common cause is

identified. The low NO_X level with the reference system in this part makes small deviations seem relatively large, that decrease in the following parts. With the EATC, more NO_X is detected than with the P2-hybrid due to more oxygen and higher combustion temperatures in the cylinder. Regarding the soot formation, only small deviations are observed that correspond to the required fuel mass. Thus, with the P2-hybrid, the total amount of soot is the lowest.

Despite the higher emission formation rates, the end emissions with the PTS are mainly reduced. Figure 5.54 summarises the deviation of the end emissions between the reference system and the two configurations of PTS Stage A. Regarding CO emissions, during the urban part, the faster warm-up of the DOC and cDPF overcompensates the higher raw emissions. For the rural drive, the configuration with the EATC shows the same tendency, with 23 % less CO tailpipe emissions. In this part, the pre-turbine EAT shows better conversion rates due to higher temperatures. The configuration with the P2-hybrid does not compensate the 20.3 % higher CO raw emissions because the warm-up is inferior compared to the EATC configuration. The tailpipe CO emissions are still 17.8 % higher. The reason for this is the lower exhaust gas temperature and mass flow rate during accelerations, as shown in Figure 5.51. The PTS does not compensate the higher raw emissions in the last section, but the disadvantage of 58 % more in-engine CO is reduced to a 4.3 % greater amount of tailpipe CO with the EATC. Especially during the first period of the accelerations, the PTS shows its potential of the faster warm-up and the related thereto improved conversion.

The PTS with P2-hybrid is able to achieve the target velocity during the acceleration more quickly due to the high electrical support torque. During this first period of the acceleration, the raw emissions are highest compared to the other configurations. Since the EAT is not warm enough to achieve the full conversion of CO at this point, the end emissions rise rapidly. Afterwards, the raw and end emissions with the P2-hybrid are lower compared to the EATC. The total CO conversion rate is 89.4 %, similar to the reference system during the motorway part.

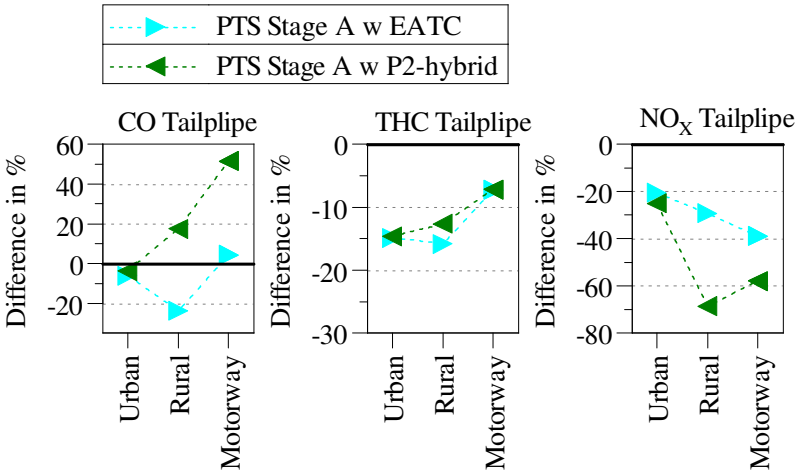

Figure 5.54: Difference between PTS Stage A and the reference system during the dynamic RDE regarding tailpipe emissions

The PTS show an advantage regarding the HC end emissions over the reference system in all parts, in particular during the urban drive. Here, the faster warm-up helps to convert more hydrocarbons within the DOC and cDPF. Additionally, the HC absorption ability of these components plays an important role. At temperatures below 250 °C, the absorbable compounds are stored in the catalyst. At the next temperature rise, they are desorbed and better oxidised with the PTS due to the faster temperature increase. The slower temperature rise at the DOC and cDPF of the reference system lets slip a larger amount of this desorbed HC. This effect overcompensates the higher raw HC emissions during the entire cycle. Between the two transient measures, the difference is relatively small, and both configurations show a similar performance.

The largest deviation between the PTS and the reference system was achieved regarding the NO_X tailpipe emissions. Especially with the P2-Hybrid and its lower raw NO_X emissions, the tailpipe emissions are reduced drastically. In the urban part, the advantage is mainly caused by the faster warm-up of the SCR1 system. Thus, the higher raw emissions are converted better, achieving an averaged conversion rate of 53 % in this section compared to 32 %

with the reference system. In the following sections, the SCR system of all configurations is warm enough to achieve conversion rates of over 80 % with the reference system and almost 90 % with the PTS. The main advantage of the PTS comes here along with the two separated urea injection systems that allow the second SCR (SCR2) to work more efficiently. Its ammonia storage level is controlled more easily and achieves higher values with the PTS. This is especially advantageous in the last period of the driving cycle when urea injection is partly interrupted due to temperatures above 500 °C.

The potential of combining a pre-turbine exhaust aftertreatment with the two considered transient measures is clearly visible. It is possible to compensate the dynamic disadvantage with these measures and control the emission formation and the heat-up of the EAT components. In particular, the chosen P2-hybrid strategy is straightforward and has the target to support the combustion engine only when necessary. However, due to its high power, the possibilities for its strategy are wide. In order to keep the EAT warm during coasting, declutching and switch-off of the engine avoids a cold gas flow through the EAT components. In general, with a more sophisticated activation strategy of the measures, engine operation with high emission formation rates could be avoided. Alternatively, with the aid of the EATC and higher boost pressure, the EGR rate might be increased to reduce the combustion temperature further and thus NO_X formation.

6 Conclusion and Outlook

6.1 Summary

With the help of the calibrated and validated simulation model, different pre-turbine EAT layouts are analysed within developed scenarios. The steady state investigations do not exhibit any noteworthy differences regarding the conversion of the emissions. The temperature of the EAT components is affected by their position in relation to the turbine. The maximum temperature difference between the underfloor SCR of the reference system and the pre-turbine SCR of PTS Stage C is 154 K at the rated power. Pre-turbine components smoothen the gas fluctuations in the entire pre-turbine exhaust tract, but the pulse charge effect on the turbine is small and only apparent at low engine loads. Due to the higher pressure and density upstream of the turbine, the gas velocity is slower, which causes a smaller pressure drop. This decreases the backpressure and consequently the pumping losses for PTS at high mass flow rates dependent on the size and amount of the pre-turbine components.

The impact of PTS on the turbine becomes visible at the sudden load increase with a constant engine speed. SCR1 only upstream of the turbine increases the time to reach 90 % of the full load by 33.6 s compared to the reference system. DOC, cDPF and SCR, the duration is increased by 109.9 s. This demonstrates that a pre-turbine EAT is not applicable to passenger vehicles without transient measures. Not all considered transient measures are sufficient for the compensation of the dynamic lag. Mechanical-pneumatic systems that pump air into the exhaust manifold or cylinder are capable of increasing dynamics for a short period but fail to hold the target load for more than 8 s with the smallest PTS. Post-injections enhance the dynamics only slightly, but the discrepancy to the reference system stays unacceptable. Only electrical measures lift the dynamic response permanent to the level of the reference system. An electrically assisted turbocharger (EATC) and an electrically driven booster help increase the exhaust gas mass flow rate, enhancing the warm-up of the EAT compared to the P2-hybrid. By increasing the boost pressure

further than required, the exhaust gas temperature is lowered, which can help to minimize the thermal stress of the first component.

Starting with a cold structure, PTS show their potential for an accelerated warm-up of the catalysts. The light-off time of the reference system is almost doubled for all emission species at a constant engine operating point compared to the PTS. The cumulative tailpipe emissions are up to 59 % lower than with the reference system. The systems with a pre-turbine SCR upstream of the DOC or cDPF, benefit from a smaller NO inhibition within these components. This positively affects the conversion of CO and HC at low temperatures.

The DPF profits during a triggered active regeneration from the conditions upstream of the turbine. The oxidation rate of the soot burnout is increased compared to the standard positioned DPF. Furthermore, the fuel amount of the applied post-injections for lifting the exhaust gas temperature is lower. To remove the same soot mass from the filter, the examined PTS required 15 % less fuel compared to the reference. Passive regeneration is also higher, which is demonstrated by the results of the WLTC. Besides the raised temperature, more NO_2 favours passive regeneration. The upstream DOC of the PTS is also warmer and oxidises more NO into NO_2. Both aspects cause 15 % less soot within the filter after the cycle. The resulting advantage of lower pressure loss is not reflected in fuel consumption, that is over the entire cycle 0.6 % higher with the considered PTS. In all dynamic scenarios, the thermal inertia of the pre-turbine EAT inhibits the turbine inlet temperature. As a consequence, the VGT rack is permanently in a more closed position. This causes a higher pressure ratio of the turbine, which in the end increases the pumping losses with PTS. The PTS benefits from improving warm-up behaviour during the WLTC. Despite higher raw emissions, HC and NO_X are reduced by 19 %, respectively 70 %. CO emission formation increases by 35 % due to the lack of boost pressure. The fewer amount of oxygen favours the CO formation process.

Without further measures for enhancing the warm-up, the considered PTS exposed no advantage over the reference system. The engine load is low causing exhaust gas temperatures that do not allow any pollutant reduction. Even for the PTS, this part is too demanding for the EAT and measures for increasing the exhaust gas temperature are required. The activity of the catalytic converters is noticeable during the following urban section. However, when

applying measures to lift the exhaust gas temperature, like early post injections, it is expected, that the PTS heat-up quicker with a smaller amount of extra fuel.

The examination of the PTS during the high-dynamic RDE cycle is conducted with the system of the largest pre-turbine thermal mass. The required energy amount for compensating the dynamic lag during the high-dynamic RDE cycle is determined with an EATC and a P2-hybrid. With a simple strategy, the EATC requires 0.07 kWh and the P2-hybrid 1.66 kWh. The capacity of modern PHEV is suitable to provide enough energy to complete the cycle six times in a row. Since the EATC affects the air flow through the engine, it changes the combustion conditions compared to the configuration with the P2-hybrid. Thus, emission formation is affected that is mainly dependent on the air to fuel ratio.

6.2 Conclusion and Outlook

Regardless of the exact configuration, the EAT system should be designed as compactly as possible in order to keep the exhaust backpressure low and minimise fuel consumption. Even a small pre-turbine component decreases the dynamic response drastically. However, the investigations proved, that the disadvantage can be compensated by electrical support systems for the borderline case with the largest pre-turbine mass of all components (PTS Stage A). Thus, when choosing the optimal configuration of a pre-turbine exhaust gas aftertreatment system, the focus can be set on emission reduction and fuel consumption.

Increased activity of the pre-turbo catalysts as in the literature [57] is not found in this work. Instead, the pre-turbine DPF exhibits potential for downsizing due to the increased passive regeneration. With respect to the component arrangement, there is an advantage in preventing NO inhibition in the DOC by prior NO_X reduction. Furthermore, the DOC increases the NO_2 to NO_X ratio, which is advantageous for the SCR during warm-up and for the passive DPF regeneration. For the active DPF regeneration, a DPF position close to the engine is beneficial in order to achieve high temperatures that start the regeneration. Since the DPF has a larger mass compared to the catalysts, the catalysts after the DPF need remarkably longer to heat-up.

When triggering the active DPF regeneration by means of early post injections in the cylinder, an upstream SCR is disadvantageous, because temperatures would be too high for NO_X reduction. To combine all the advantages, it would be conceivable to install two smaller DOCs: one upstream of the turbine and the other downstream. For selective NO_X reduction, the sDPF upstream of the turbine is appropriate, as in the case of PTS Stage D. Finally, the division into two independent, separate SCR systems shows great advantages, as the temperature gap between the two is heightened. The probability that one of the systems is in the temperature range of an effective conversion is increased. The complete system would consist of a pre-turbine DOC and sDPF and a DOC and SCR system after the turbine. An overview of the advantages, disadvantages and challenges of the considered PTS is given in Table 6.1 and Table 6.2.

It is expected, that the amount of hybrid electrified vehicles will further rise in the medium-term to achieve the CO_2 targets. Two possible hybrid vehicle concepts shall be discussed in combination with a PTS: Plug-in hybrid vehicles (PHEV) and a hybrid electric vehicle with a 48 V electrical system and a larger battery compared to conventional vehicles.

A PHEV in the P2-hybrid configuration has usually a strong electric motor, that allows long phases during which the internal combustion engine (ICE) is switched off. When starting the ICE, a fast warm-up of the EAT is desired for which a PTS is beneficial and can reduce the time until a full emission conversion is achieved. The investigation of this work prevailed, that the lack of boost pressure remains with the PTS in combination with a P2-hybrid. This causes a combustion at low equivalence air to fuel ratios ($\lambda < 1.1$) with a large amount of raw emissions and low thermal efficiency. Furthermore, the examinations of the load steps showed, that high internal engine loads are only achieved after a long time. Thus, even with an electric engine on the driveshaft that compensates the dynamic lag, the enhancement of the boosting system is necessary. In addition to increasing dynamics, the required measures can be used to improve raw emissions and heat-up behaviour by controlling the boost pressure. A combination of P2-hybrid with electric turbocharging would increase the scope for reducing raw emissions while increasing heating performance. By regulating the required load of the internal combustion engine, operating at low raw emissions with high exhaust gas temperatures might be targeted preferentially. Additionally, the range for varying boost pressure or the

EGR rate is extendable with the electrified boosting system. Overall, energy consumption must also be taken into account for a holistic consideration. With a balanced combination of PTS and the appropriate use of methods to enhance dynamics, a considerable overall emission reduction amount can be achieved.

The lighter hybrid configuration with the 48 V electrical system and an integrated starter generator (ISG) is not able to provide enough power directly on the crankshaft. During the high dynamic RDE cycle, maximum power of 70 kW is attached to the crankshaft. Therefore, in order to fulfil the dynamic requirements, the ICE has to operate at a high load and an electrified turbocharging system is necessary that has a lower power demand. Consequently, a smaller battery is sufficient and the vehicle mass is smaller compared to a PHEV.

Table 6.1: Summary and evaluation of the investigated pre-turbine systems (part 1)

System	Advantage	Disadvantage	Challenges
PTS Stage A (DOC-cDPF-SCR1-Turbine-SCR2)	• high passive DPF regeneration rate	• highest pre-turbine mass and greatest turbo lag • NO inhibition in DOC • NO_X reduction system is the last component • higher NO_X raw emissions (depends on application) • higher mass inertia of the turbocharger	• compensating the dynamic disadvantage • mechanical reliability of the components
PTS Stage B (DOC-SCR1-Turbine-cDPF-SCR2)	• small DOC in the first position dampens temperature jumps for SCR1 and enhances NO_2 to NO_X ratio	• low passive DPF regeneration; active DPF regeneration more challenging than for reference system	• active DPF regeneration difficult; SCR1 and turbine are between DOC and DPF

Table 6.2: Summary and evaluation of the investigated pre-turbine systems (part 2)

System	Advantage	Disadvantage	Challenges
PTS Stage C (SCR1-Turbine-DOC-cDPF-SCR2)	• fast NO_X light off • avoidance of NO inhibition in DOC + cDPF leads to faster CO and HC light off (best results during cold start)	• high thermal stress for SCR • low passive DPF regeneration; active DPF regeneration more challenging than for reference system	• SCR as the first component in pre-turbine position makes the urea dosing strategy challenging due to quickly changing conditions (temperature and pressure)
PTS Stage D (DOC-sDPF-Turbine-SCR2)	• compact EAT system • high passive DPF regeneration rate	• NO inhibition in DOC • large pre-turbine mass	• compensating the dynamic disadvantage

Bibliography

[1] *Grundlagenuntersuchungen zu Abgasnachbehandlungssystemen vor Abgasturbine*. FVV Final Report, Project Number 1305, 2021.

[2] H. I. Abdel-Shafy and M. S. Mansour. A review on polycyclic aromatic hydrocarbons: Source, environmental impact, effect on human health and remediation. *Egyptian Journal of Petroleum*, 25(1):107–123, 2016.

[3] A. K. Agarwal, D. K. Srivastava, A. Dhar, R. K. Maurya, P. C. Shukla, and A. P. Singh. Effect of fuel injection timing and pressure on combustion, emissions and performance characteristics of a single cylinder diesel engine. *Fuel*, 111:374–383, 2013.

[4] M. AL-Harbi, R. Hayes, M. Votsmeier, and W. S. Epling. Competitive NO, CO and hydrocarbon oxidation reactions over a diesel oxidation catalyst. *The Canadian Journal of Chemical Engineering*, 90(6):1527–1538, 2012.

[5] C. Barba. *Erarbeitung von Verbrennungskennwerten aus Indizierdaten zur verbesserten Prognose und rechnerischen Simulation des Verbrennungsablaufes bei Pkw-DE-Dieselmotoren mit Common-Rail-Einspritzung*. PhD thesis, ETH Zurich, 2001.

[6] V. Bermúdez, J. R. Serrano, P. Piqueras, and Ó. García-Afonso. Analysis of heavy-duty turbocharged diesel engine response under cold transient operation with a pre-turbo aftertreatment exhaust manifold configuration. *International Journal of Engine Research*, 14(4):341–353, 2013.

[7] D. Boruah, P. K. Thakur, and D. Baruah. Artificial Neural Network based Modelling of Internal Combustion Engine Performance. *International Journal of Engineering Research and*, V5(03), 2016.

[8] N. Breuer, T. Hauber, J. K. Schaller, R. Schernewski, S. Stein, and R. Wirth. Abgasnachbehandlung für Dieselmotoren. In K. Reif, editor, *Abgastechnik für Verbrennungsmotoren*, pages 59–78. Springer Fachmedien Wiesbaden, Wiesbaden, 2015.

[9] F. Bunar, E.-M. Moser, F. Inci, and L. Zimmet. Abgasgesetzgebung für Pkw-Dieselmotoren. In H. Tschöke, K. Mollenhauer, and R. Maier, editors, *Handbuch Dieselmotoren*, Springer Reference Technik, pages 819–841. Springer Fachmedien Wiesbaden, Wiesbaden, 2018.

[10] R. D. Burke, A. J. Lewis, S. Akehurst, C. J. Brace, I. Pegg, and R. Stark. Systems optimisation of an active thermal management system during engine warm-up. *Proceedings of the Institution of Mechanical Engineers, Part D: Journal of Automobile Engineering*, 226(10):1365–1379, 2012.

[11] T.-M. Chen, J. Gokhale, S. Shofer, and W. G. Kuschner. Outdoor air pollution: nitrogen dioxide, sulfur dioxide, and carbon monoxide health effects. *The American journal of the medical sciences*, 333(4):249–256, 2007.

[12] F. Chmela, D. Dimitrov, G. Pirker, and A. Wimmer. Konsistente Methodik zur Vorausrechnung der Verbrennung in Kolbenkraftmaschinen. *MTZ - Motortechnische Zeitschrift*, 67(6):468–474, 2006.

[13] C. Dönitz, D. Wabbals, R. Kempny, C. Röhr, and N. Brehm. Responseverbesserung durch Drucklufteinblasung bei aufgeladenen Ottomotoren. In J. Liebl, editor, *Ladungswechsel im Verbrennungsmotor 2016*, Proceedings, pages 129–146. Springer Fachmedien Wiesbaden, Wiesbaden, 2017.

[14] A. J. Feneley, A. Pesiridis, and A. M. Andwari. Variable Geometry Turbocharger Technologies for Exhaust Energy Recovery and Boosting–A Review. *Renewable and Sustainable Energy Reviews*, 71:959–975, 2017.

[15] M. Fleiss, R. Burenius, G. Almkvist, and J. Björkholtz. Das pneumatische Turbolader-Unterstützungssystem PowerPulse. *MTZ - Motortechnische Zeitschrift*, 77(6):10–17, 2016.

[16] B. Ghobadian, H. Rahimi, A. M. Nikbakht, G. Najafi, and T. F. Yusaf. Diesel engine performance and exhaust emission analysis using waste cooking biodiesel fuel with an artificial neural network. *Renewable Energy*, 34(4):976–982, 2009.

[17] J. Gieshoff, A. Schäfer-Sindlinger, P. C. Spurk, J. A. A. van den Tillaart, and G. Garr. Improved SCR Systems for Heavy Duty Applications. In *SAE Technical Paper Series*, SAE Technical Paper Series. SAE International400 Commonwealth Drive, Warrendale, PA, United States, 2000.

[18] J. Girard, G. Cavataio, R. Snow, and C. Lambert. Combined Fe-Cu SCR Systems with Optimized Ammonia to NOx Ratio for Diesel NOx Control. *SAE International Journal of Fuels and Lubricants*, 1(1):603–610, 2009.

[19] T. Günter, J. Pesek, K. Schäfer, A. Bertótiné Abai, M. Casapu, O. Deutschmann, and J.-D. Grunwaldt. Cu-SSZ-13 as pre-turbine NOx-removal-catalyst: Impact of pressure and catalyst poisons. *Applied Catalysis B: Environmental*, 198:548–557, 2016.

[20] M. Han, D. N. Assanis, and S. V. Bohac. Comparison of HC species from diesel combustion modes and characterization of a heat-up DOC formulation. *International Journal of Automotive Technology*, 9(4):405–413, 2008.

[21] J. G. Hawley, F. J. Wallace, A. Cox, R. W. Horrocks, and G. L. Bird. Variable geometry turbocharging for lower emissions and improved torque characteristics. *Proceedings of the Institution of Mechanical Engineers, Part D: Journal of Automobile Engineering*, 213(2):145–159, 1999.

[22] P. Jiao, Z. Li, B. Shen, W. Zhang, X. Kong, and R. Jiang. Research of DPF regeneration with NOx-PM coupled chemical reaction. *Applied Thermal Engineering*, 110:737–745, 2017.

[23] V. Joergl, P. Keller, O. Weber, K. Mueller-Haas, and R. Konieczny. Influence of Pre Turbo Catalyst Design on Diesel Engine Performance, Emissions and Fuel Economy. *SAE International Journal of Fuels and Lubricants*, 1(1):82–95, 2009.

[24] B. Kaal and M. Sosio. Instationäre Emissionsmodellierung am Dieselmotor. *Frankfurt am Main: Forschungsvereinigung Verbrennungskraftmaschinen se.V*, (Vols. 1062 – 2015), 2015.

[25] P. Kožuch. *Ein phänomenologisches Modell zur kombinierten Stickoxid- und Rußberechnung bei direkteinspritzenden Dieselmotoren*. PhD thesis, Universität Stuttgart, 2004.

[26] M. Krüger and S. Fischer. Entstehung von Dieselschadstoffen und innermotorische Reduktionsmaßnahmen. In H. Tschöke, K. Mollenhauer, and R. Maier, editors, *Handbuch Dieselmotoren*, Springer Reference Technik, pages 863–880. Springer Fachmedien Wiesbaden, Wiesbaden, 2018.

[27] M. Lapuerta, J. J. Hernandez, and F. Oliva. Strategies for active diesel particulate filter regeneration based on late injection and exhaust recirculation with different fuels. *International Journal of Engine Research*, 15(2):209–221, 2014.

[28] G. A. Lavoie, J. B. Heywood, and J. C. Keck. Experimental and Theoretical Study of Nitric Oxide Formation in Internal Combustion Engines. *Combustion Science and Technology*, 1(4):313–326, 1970.

[29] J. Liebl, editor. *Mercedes-Benz E-Klasse: Entwicklung und Technik des W213*. ATZ-MTZ-Typenbuch. Springer Vieweg, Wiesbaden, 2017.

[30] J. M. Luján, V. Bermúdez, P. Piqueras, and Ó. García-Afonso. Experimental assessment of pre-turbo aftertreatment configurations in a single stage turbocharged diesel engine. Part 1: Steady-state operation. *Energy*, 80:599–613, 2015.

[31] J. M. Luján, J. R. Serrano, P. Piqueras, and Ó. García-Afonso. Experimental assessment of a pre-turbo aftertreatment configuration in a single stage turbocharged diesel engine. Part 2: Transient operation. *Energy*, 80:614–627, 2015.

[32] W. A. Majewski and M. K. Khair. *Diesel emissions and their control*. Number SAE-R-303 in SAE-R. SAE International, Warrendale, Pa., 2006.

[33] M. Masoudi. Pressure drop of segmented diesel particulate filters. In *SAE Technical Paper Series*, SAE Technical Paper Series. SAE International400 Commonwealth Drive, Warrendale, PA, United States, 2005.

[34] C. S. McEnally, L. D. Pfefferle, B. Atakan, and K. Kohse-Höinghaus. Studies of aromatic hydrocarbon formation mechanisms in flames: Progress towards closing the fuel gap. *Progress in Energy and Combustion Science*, 32(3):247–294, 2006.

[35] G. P. Merker, editor. *Grundlagen Verbrennungsmotoren: Simulation der Gemischbildung, Verbrennung Schadstoffbildung und Aufladung ; mit 31 Tabellen*. Praxis. Vieweg + Teubner, Wiesbaden, 4., überarb. und aktualisierte aufl. edition, 2009.

[36] G. P. Merker. *Grundlagen Verbrennungsmotoren*. Springer Fachmedien Wiesbaden, 2019.

[37] P. S. Metkar, V. Balakotaiah, and M. P. Harold. Experimental study of mass transfer limitations in Fe- and Cu-zeolite-based NH3-SCR monolithic catalysts. *Chemical Engineering Science*, 66(21):5192–5203, 2011.

[38] G. Najafi, B. Ghobadian, T. Tavakoli, D. R. Buttsworth, T. F. Yusaf, and M. Faizollahnejad. Performance and exhaust emissions of a gasoline engine with ethanol blended gasoline fuels using artificial neural network. *Applied Energy*, 86(5):630–639, 2009.

[39] H. J. Oelschlegel. Dieselmotorische Verbrennung. In H. Tschöke, K. Mollenhauer, and R. Maier, editors, *Handbuch Dieselmotoren*, Springer Reference Technik, pages 91–116. Springer Fachmedien Wiesbaden, Wiesbaden, 2018.

[40] A. Pant and S. J. Schmieg. Kinetic Model of NOx SCR Using Urea on Commercial Cu−Zeolite Catalyst. *Industrial & Engineering Chemistry Research*, 50(9):5490–5498, 2011.

[41] C. A. Piantadosi. Diagnosis and treatment of carbon monoxide poisoning. *Respiratory care clinics of North America*, 5(2):183–202, 1999.

[42] G. Pirker, F. Chmela, and A. Wimmer. Simulation for DI Diesel Engines Based on Sequential Combustion Mechanisms. In *SAE Technical Paper Series*, SAE Technical Paper Series. SAE International400 Commonwealth Drive, Warrendale, PA, United States, 2006.

[43] R. Prasad and V. R. Bella. A Review on Diesel Soot Emission, its Effect and Control. *Bulletin of Chemical Reaction Engineering and Catalysis*, 5(2), 2011.

[44] H. Pucher. Ladungswechsel und Aufladung beim Dieselmotor. In H. Tschöke, K. Mollenhauer, and R. Maier, editors, *Handbuch Dieselmotoren*, Springer Reference Technik, pages 43–87. Springer Fachmedien Wiesbaden, Wiesbaden, 2018.

[45] J. A. Raub, M. Mathieu-Nolf, N. B. Hampson, and S. R. Thom. Carbon monoxide poisoning — a public health perspective. *Toxicology*, 145(1):1–14, 2000.

[46] K. Reif, editor. *Dieselmotor-Management*. Vieweg+Teubner Verlag, Wiesbaden, 2012.

[47] K. Reif. Innermotorische Emissionsminderung. In K. Reif, editor, *Dieselmotor-Management*, pages 342–363. Vieweg+Teubner Verlag, Wiesbaden, 2012.

[48] D. Rether, A. Schmid, M. Grill, and M. Barargende. Quasidimensionale Simulation der Dieselverbrennung mit vor- und Nacheinspritzungen. *MTZ - Motortechnische Zeitschrift*, 71(10):742–748, 2010.

[49] M. Rößler, T. Koch, C. Janzer, and M. Olzmann. Mechanisms of the NO2 Formation in Diesel Engines. *MTZ worldwide*, 78(7-8):70–75, 2017.

[50] A. Russell and W. S. Epling. Diesel Oxidation Catalysts. *Catalysis Reviews*, 53(4):337–423, 2011.

[51] C. S. Sampara, E. J. Bissett, and M. Chmielewski. Global Kinetics for a Commercial Diesel Oxidation Catalyst with Two Exhaust Hydrocarbons. *Industrial & Engineering Chemistry Research*, 47(2):311–322, 2008.

[52] P. M. Schaber, J. Colson, S. Higgins, D. Thielen, B. Anspach, and J. Brauer. Thermal decomposition (pyrolysis) of urea in an open reaction vessel. *Thermochimica Acta*, 424(1-2):131–142, 2004.

[53] J. W. A. Schlangen, G. W. Neuhaus, M. Madani, and W. F. Maier. Unterschiede in der Totaloxidation organischer Verbindungen an

heterogenen Platin- und Palladiumkatalysatoren. *Journal für Praktische Chemie/Chemiker-Zeitung*, 334(6):465–473, 1992.

[54] J. R. Serrano, V. Bermúdez, P. Piqueras, and E. Angiolini. On the impact of dpf downsizing and cellular geometry on filtration efficiency in pre- and post-turbine placement. *Journal of Aerosol Science*, 113:20–35, 2017.

[55] M. Shelef and R. McCabe. Twenty-five years after introduction of automotive catalysts: what next? *Catalysis Today*, 62(1):35–50, 2000.

[56] Z. Skaf, T. Aliyev, L. Shead, and T. Steffen. The State of the Art in Selective Catalytic Reduction Control. In *SAE Technical Paper Series*, SAE Technical Paper Series. SAE International400 Commonwealth Drive, Warrendale, PA, United States, 2014.

[57] M. N. Subramaniam, C. Hayes, D. Tomazic, M. Downey, and C. Bruestle. Pre-Turbo Aftertreatment Position for Large Bore Diesel Engines - Compact & amp; Cost-Effective Aftertreatment with a Fuel Consumption Advantage. *SAE International Journal of Engines*, 4(1):106–116, 2011.

[58] N. Terdich. *Impact of electrically assisted turbocharging on the transient response of an off-highway diesel engine*. PhD thesis, Imperial college London, 2140.

[59] M. Thiel, R. Werner, R. Brück, S. Kröger, N. Zaldua-Moreno, K. Augsburg, R. Horn, P. Hirth, B. Hu, and C. Schorn. Katalysatorträgerdesigns für die Abgasnachbehandlung zur Einhaltung der gesetzlichen Grenzwerte. In T. Roß and A. Heine, editors, *Der Verbrennungsmotor - ein Antrieb mit Vergangenheit und Zukunft*, pages 409–446. Springer Fachmedien Wiesbaden, Wiesbaden, 2018.

[60] F. V. Tinaut, A. Melgar, B. Giménez, and M. Reyes. Prediction of performance and emissions of an engine fuelled with natural gas/hydrogen blends. *International Journal of Hydrogen Energy*, 36(1):947–956, 2011.

[61] D. R. Tree and K. I. Svensson. Soot processes in compression ignition engines. *Progress in Energy and Combustion Science*, 33(3):272–309, 2007.

[62] H. Tschöke, K. Mollenhauer, and R. Maier, editors. *Handbuch Dieselmotoren*. Springer Reference Technik. Springer Fachmedien Wiesbaden, Wiesbaden, 2018.

[63] S. E. Voltz, C. R. Morgan, D. Liederman, and S. M. Jacob. Kinetic study of carbon monoxide and propylene oxidation on platinum catalysts. *Product R&D*, 12(4):294–301, 1973.

[64] H. E. Wichmann, C. Spix, T. Tuch, G. Wölke, A. Peters, J. Heinrich, W. G. Kreyling, and J. Heyder. Daily mortality and fine and ultrafine particles in erfurt, germany part i: role of particle number and particle mass. *Research report (Health Effects Institute)*, (98):5–86; discussion 87–94, 2000.

[65] V. W. Wong and S. C. Tung. Overview of automotive engine friction and reduction trends–Effects of surface, material, and lubricant-additive technologies. *Friction*, 4(1):1–28, 2016.

[66] Q. Yang. *A quasi-dimensional Charge Motion and Turbulence Model for Combustion and Emissions Prediction in Diesel Engines with a fully Variable Valve Train*. PhD thesis, Universität Stuttgart, 2020.

[67] W. K. Yap, T. Ho, and V. Karri. Exhaust emissions control and engine parameters optimization using artificial neural network virtual sensors for a hydrogen-powered vehicle. *International Journal of Hydrogen Energy*, 37(10):8704–8715, 2012.

[68] S. D. Yim, S. J. Kim, J. H. Baik, I.-S. Nam, Y. S. Mok, J.-H. Lee, B. K. Cho, and S. H. Oh. Decomposition of Urea into NH 3 for the SCR Process. *Industrial & Engineering Chemistry Research*, 43(16):4856–4863, 2004.

[69] M. Yu, D. Luss, and V. Balakotaiah. Regeneration modes and peak temperatures in a diesel particulate filter. *Chemical Engineering Journal*, 232:541–554, 2013.

[70] Y. B. Zeldovich. *Oxidation of Nitrogen in Combustion and Explosions*. Princeton University Press, Princeton, 1992.

Appendix

A.1 Summary of the Transient Countermeasures

For convenience, a brief overview of the advantages and disadvantages of the considered transient measures shall be given in Table A1.1 and Table A1.2. All measures are able to increase the dynamic response of the PTS. However, the load step investigations showed that only the electrical support systems (EATC, EDB, P2-Hybrid) are capable of compensating the dynamic disadvantage of the PTS over a long period. Thus, they are the measures of choice for the later examined driving cycles.

Table A1.1: Summary of considered the transient countermeasures (part 1)

Countermeasure	Advantage	Disadvantage
EATC	• ready for series production • target load is achieved and retainable • EAT warm-up is accelerated • no changes on the inlet side are required • recuperation mode	• higher NO_X raw emissions (depends on application) • higher mass inertia of the turbocharger
EDB	• ready for series production • target load is achieved and retainable • EAT warmup is accelerated	• additional component
P2-Hybrid	• high boosting power • recuperation potential during deceleration	• requires most energy of electrical support systems • rich combustion conditions
Air injection into the cylinder	• increased mass flow through EAT components • tank is filled during towing (no external energy required)	• torque is not retained • only a short boosting period • complex system; additional valve in the cylinder head is required

Table A1.2: Summary of considered the transient countermeasures (part 2)

Countermeasure	Advantage	Disadvantage
Air injection into the exhaust manifold	• relatively simple	• torque is not retained • increased pumping losses • only a short boosting period
Early post-injection for higher exhaust enthalpy	• no extra components required	• torque is not retained • lower torque during the naturally aspirated period • PTS are not able to conduct load step as quick as the reference system
Late post-injection for conversion in the pre-turbine DOC	• no extra components required	• torque is not retained • high tailpipe HC emission • Oxygen required for oxidation in catalyst • PTS are not able to conduct load step as quick as the reference system

A.2 Input Parameters for the Neural Network

The following parameters are used as input parameters for determining the raw emissions by means of the neural network:

- Engine speed
- IMEP 360
- Effective Lambda
- Percent incoming EGR
- MFB 50
- Burn duration
- Railpressure
- Injected mass per cycle
- Maximum temperature
- Exhaust temperature